DRAG CHARACTERISTICS OF A HISTORICAL BRIDGE PIER

A THESIS SUBMITTED TO
THE GRADUATE SCHOOL OF NATURAL AND APPLIED SCIENCES
OF
MIDDLE EAST TECHNICAL UNIVERSITY

MEHMET MERT BÜLBÜL

IN PARTIAL FULFILLMENT OF THE REQUIREMENTS
FOR
THE DEGREE OF MASTER OF SCIENCE
IN
CIVIL ENGINEERING

JANUARY 2017

Approval of the thesis:

DRAG CHARACTERISTICS OF A HISTORICAL BRIDGE PIER

submitted by **MEHMET MERT BÜLBÜL** in partial fulfillment of the requirements for the degree of **Master of Science in Civil Engineering Department, Middle East Technical University** by,

Prof. Dr. GÜLBİN DURAL ÜNVER _____
Dean, Graduate School of **Natural and Applied Sciences**

Prof. Dr. İSMAİL ÖZGÜR YAMAN _____
Head of Department, **Civil Engineering**

Prof. Dr. NURAY DENLİ TOKYAY _____
Supervisor, **Civil Engineering Department, METU**

Examining Committee Members:

Prof. Dr. MUSTAFA GÖĞÜŞ
Civil Engineering Department, METU _____

Prof. Dr. NURAY DENLİ TOKYAY
Civil Engineering Department, METU _____

Prof. Dr. AYŞE BURCU ALTAN SAKARYA
Civil Engineering Department, METU _____

Assist. Prof. Dr. ASLI NUMANOĞLU GENÇ
Civil Engineering Department, ATILIM UNIVERSITY _____

Assist. Prof. Dr. MELİH ÇALAMAK
Civil Engineering Department, TED UNIVERSITY _____

Date: _____

I hereby declare that all information in this document has been obtained and presented in accordance with academic rules and ethical conduct. I also declare that, as required by these rules and conduct, I have fully cited and referenced all material and results that are not original to this work.

Name, Last Name: MEHMET MERT BÜLBÜL

Signature :

ABSTRACT

DRAG CHARACTERISTICS OF A HISTORICAL BRIDGE PIER

BÜLBÜL, Mehmet Mert
M.S., Department of Civil Engineering
Supervisor : Prof. Dr. NURAY DENLİ TOKYAY

January 2017, 96 pages

The construction of river bridge requires placement of bridge piers within the river. These piers obstruct the flow and may cause an increase in water level on the upstream side of the bridge. This increase in water level has a negative impact on the stability of bridge and may be responsible for scouring action around the bridge pier. The shape of the bridge pier is an important factor. Since 20th century on, streamlined shapes for bridge piers are being used. It is also known that for the first time in history, Mimar Sinan has used streamlined shapes for bridge piers in 16th century. However, there is a historical bridge in Diyarbakır, called Ongözlü Bridge which was built in 1065, that has streamlined shaped piers on Tigris River. In the present work, the characteristics of the shape of piers of Ongözlü Bridge is studied numerically using Flow 3D computational fluid dynamics (CFD) sofware. Pier of Ongözlü Bridge is compared with the drag characteristics of the other shapes that have been used as piers in the literature.

The results show that even at 11th century, the hydraulic works in Anatolia were ahead of its time, and the first bridge with a streamlined shape was built 3-4 centuries before Mimar Sinan.

Keywords: Bridge, Afflux, Drag Force, Flow 3D

ÖZ

TARİHİ KÖPRÜ AYAKLARININ SÜRTÜNME KARAKTERİSTİKLERİ

BÜLBÜL, Mehmet Mert
Yüksek Lisans, İnşaat Mühendisliği Bölümü
Tez Yöneticisi : Prof. Dr. NURAY DENLİ TOKYAY

Ocak 2017 , 96 sayfa

Köprü inşaası, köprü ayaklarının nehir içerisinde yerleştirilmesini gerektirir. Bu ayaklar nehrin akışına engel oluşturur ve köprünün memba tarafında suyun yükselmesine sebep olur. Su seviyesindeki bu artış, köprünün rijitliğinde olumsuz bir etki yaratır ve köprü ayakları etrafında oyulmalara sebep olabilir. Köprü ayaklarının şekli önemli bir faktördür. 20. yüzyıldan itibaren, akım çizgilerine uygun köprü ayakları kullanılmıştır. Tarihte ilk olarak akım çizgilerine uygun köprü ayaklarının Mimar Sinan tarafından 16. yüzyılda kullanıldığı bilinmektedir. Buna rağmen, Diyarbakır da bulunan ve Ongözlü Köprü olarak adlandırılan tarihi bir köprüde, köprü ayaklarının akıma uygun bir şekilde tasarlandığı durumu değerlendirilmektedir. Dicle nehri üzerinde yer alan bu köprü 1065 yılında inşa edilmiştir. Bu çalışmada, Ongözlü Köprü ayaklarının şekil karakteristikleri Flow 3D hesaplamalı akışkanlar dinamiği programı kullanılarak nümerik olarak çalışılmış, farklı şekillerdeki köprü ayakları kullanılması durumu sürtünme karakteristikleri bakımından karşılaştırılmıştır.

Sonuçlar, 11. yüzyılda bile Anadolu da yapılan hidrolik çalışmaların çağının ilerisinde olduğunu göstermekle birlikte, ilk olarak akıma uygun köprülerin Mimar Sinan'dan 3-4 yüzyıl önce inşaa edildiğini göstermektedir.

Anahtar Kelimeler: Köprü, Akış, Sürtünme Kuvveti, Flow 3D

To my family

Hürriyet BÜLBÜL,Işıl Merve BÜLBÜL,Mehmet BÜLBÜL, Dilara PAMUKÇİ

ACKNOWLEDGMENTS

I wish to express my sincere gratitude to my supervisor Prof.Dr. Nuray Denli Tokyay for providing me with this thesis project. I sincerely thank to Dr. Tokyay for her criticism, encouragements and guidance throughout the study.

I would also thank to Asst.Prof.Dr. Talia Ekin Tokyay Sinha for supporting my studies with very beneficial information about 'Computational Fluid Dynamics' concept. This is great honor for me to work with these instructors.

Lastly I would like to special thank my family for their motivation, understanding and support. I also want to thank Dilara for her endurance.

TABLE OF CONTENTS

ABSTRACT v

ÖZ vii

ACKNOWLEDGMENTS x

TABLE OF CONTENTS xi

LIST OF TABLES xiv

LIST OF FIGURES xv

LIST OF ABBREVIATIONS xix

CHAPTERS

1 INTRODUCTION 1

1.1 A BRIEF INFORMATION ON HYDRAULICS OF BRIDGE PIERS 1

1.2 LITERATURE REVIEW 5

1.2.1 PREVIOUS EXPERIMENTAL STUDIES 5

1.2.2 PREVIOUS CFD STUDIES 6

1.3 HISTORICAL BACKGROUND OF ONGOZLU BRIDGE . 7

1.4 THE MODEL OF ONGOZLU BRIDGE 9

1.5 AIM OF THE PRESENT STUDY 12

2 METHODOLOGY 13

2.1 PREPROCESSING 14

2.1.1 FLOW DOMAIN 15

2.1.2 BOUNDARY CONDITIONS 17

2.1.2.1 INLET BOUNDARY CONDITIONS . 18

2.1.2.2 WALL BOUNDARY CONDITIONS . 19

2.1.2.3 SYMMETRY BOUNDARY CONDITIONS 21

2.1.2.4 OUTFLOW BOUNDARY CONDITIONS 21

2.1.3 MESH GENERATION 22

2.1.4 GRID DEPENDENCY CHECK 25

2.2 GOVERNING EQUATIONS 27

2.3 VOLUME OF FLUID METHOD 30

2.4 TURBULENCE CLOSURE - RNG K-ε MODEL 32

2.5 DRAG CALCULATION USING FLOW 3D 34

2.5.1 NUMERICAL MODEL IMPLEMENTATION . . 35

2.5.1.1 GRID GENERATION 35

2.5.1.2 INITIAL AND BOUNDARY CONDITIONS 42

2.5.1.3 PHYSICS 43

2.5.1.4 MATERIAL PROPERTIES 46

2.5.1.5 SOLVER OPTIONS 48

3 RESULTS 51

3.1 EFFECT OF SHAPE OF THE PIER ON DRAG (FLOW 3D) 51

3.2 DRAG FORCE ON CIRCULAR PIER FOR DIFFERENT DISCHARGE A COMPARISON BETWEEN FLOW 3D AND FLUENT 59

3.3 TRIANGULAR NOSE AND TAIL CASES ASPECT RATIO EFFECT 69

3.4 SIMULATION OF FLOW AROUND ONGÖZLÜ BRIDGE 74

4 CONCLUSIONS 89

5 FUTURE STUDIES 91

REFERENCES 93

LIST OF TABLES

TABLES

Table 2.1 C_f formulas for different flow types 26

Table 3.1 F_d (N) values attained from simulations 58

Table 3.2 Grid dependency for Flow 3D simulations 63

Table 3.3 F_d values for three different grid dependency taken from TecPlot . . 65

Table 3.4 C_d values 68

Table 3.5 Comparison of C_d values 68

Table 3.6 F_d (N) values attained from simulations 70

Table 3.7 Hydraulic characteristics of free surfaces 73

Table 3.8 Values of back water rise calculation 74

Table 3.9 Froude number calculation of numerical model 75

Table 3.10 Froude similarity between model and prototype 76

Table 3.11 F_d (N) values attained from simulations for Ongözlü Bridge 78

Table 3.12 Geometrical specification of Ongözlü Bridge pier 79

Table 3.13 Calculations of flood discharge of Tigris River 84

LIST OF FIGURES

FIGURES

Figure 1.1 Horseshoe and wake vortices around a cylindrical pier (Dowding et al.,1994) 1

Figure 1.2 Schematic profile of the river flow obstructed due to the bridge . . . 2

Figure 1.3 Plan view of the pier 3

Figure 1.4 Profile view of the pier 4

Figure 1.5 Ongözlü Bridge (Aral, T., 2012) 8

Figure 1.6 Plan view of Ongözlü Bridge 9

Figure 1.7 Profile view of Ongözlü Bridge 9

Figure 1.8 Details of Ongözlü Bridge 9

Figure 1.9 The model of Ongözlü Bridge 10

Figure 1.10 Scaled bridge pier 10

Figure 1.11 Flow 3D component view (xyz) 11

Figure 1.12 AutoCAD 3D components labels (top view) 12

Figure 2.1 General solution method for an incompressible flow (Flow 3D general training class-2013) 14

Figure 2.2 Steps of CFD analysis 15

Figure 2.3 Ongözlü Bridge pier 16

Figure 2.4 Description of general boundary conditions (Versteeg et al., 1995) . 17

Figure 2.5 Inlet (u) boundary condition (Versteeg et al., 1995) 18

Figure 2.6 Inlet (v) boundary condition (Versteeg et al., 1995) 19

Figure 2.7 Wall (v) boundary condition (Versteeg et al., 1995) 20

Figure 2.8 Symmetry boundary condition (Versteeg et al., 1995) 21

Figure 2.9 Outlet (u) boundary condition (Versteeg et al., 1995) 22

Figure 2.10 Grid system for Flow 3D (Flow 3D advanced hydraulic training-2012) 23

Figure 2.11 Object definition (left) and object created (right) (Flow 3D documentation release 10.1.0-2012) 24

Figure 2.12 Control volume representation in Flow 3D (Flow 3D general training class-2013) 30

Figure 2.13 Sharp interface of fluid fraction (Flow 3D advanced hydraulics training-2013) 31

Figure 2.14 y^+ 36

Figure 2.15 Outline view 36

Figure 2.16 Mesh view 37

Figure 2.17 Mesh detail view 37

Figure 2.18 Representation of T=4 s, T=6 s and T=10 s 38

Figure 2.19 Representation of T=15 s, T=30 s and T=60 s 39

Figure 2.20 Output tab 41

Figure 2.21 Boundary conditions 42

Figure 2.22 Gravity tab 44

Figure 2.23 Turbulence tab 45

Figure 2.24 Fluids tab 47

Figure 2.25 Numerics tab 49

Figure 3.1 Water surface elevation z (m) for circular bridge pier 52

Figure 3.2 Elevation of free surface at T=12 s 53

Figure 3.3 Elevation of free surface at T=60 s 54

Figure 3.4 Side view of the water surface elevation at T=60 s 55

Figure 3.5 Three dimensional streamlines (yellow) and two dimensional streamlines at a surface 0.05 m away from the channel floor at T=60 s 56

Figure 3.6 Out of plane vorticity 3D streamlines 57

Figure 3.7 Drag force on rectangular pier, square pier and rectangular pier with curved ends for six discharge values 58

Figure 3.8 Drag force on rectangular pier with triangular nose and tail, rhombus pier, circular pier and elliptical pier for six discharge values 59

Figure 3.9 Comparison of values of drag force from Flow 3D and Fluent simulations 60

Figure 3.10 Comparison of values of drag force from simulations to ones from experiments of Agarwal et al. (2014) 61

Figure 3.11 Water surface levels both upstream and downstream sides during the steady state conditions (Fluent) 62

Figure 3.12 F_d values for three different grid dependency attained from simulations (Flow 3D) 64

Figure 3.13 Water surface levels both upstream and downstream sides for three different grid dependency during the steady state conditions (Flow 3D) . . 66

Figure 3.14 Approximations of pressure distribution 67

Figure 3.15 Representation of upstream and downstream measuring points . . . 68

Figure 3.16 The range of Reynolds number ranges from 6.96 x 10^3 to 7.68 x 10^3 (subcritical flow conditions) 70

Figure 3.17 Drag force on rectangular piers with triangular nose and tail with constant contraction ratio of 0.4 and length of 4, 6, 12 and 16 cm simulated for five different discharge values 71

Figure 3.18 Comparison of values of drag force from simulations to ones from experiments of Agarwal et al. (2014) 71

Figure 3.19 Upstream and downstream free surfaces 73

Figure 3.20 One pier of Ongözlü Bridge at T=180 s under discharge of 5.06x10^{-4} 77

Figure 3.21 Geometrical representation of Ongözlü Bridge pier 78

Figure 3.22 Ongözlü Bridge at T=300 s 80

Figure 3.23 Profile view of Ongözlü Bridge at T=300 s 81

Figure 3.24 Time of change of drag force for abutments and piers of Ongözlü Bridge 82

Figure 3.25 Representation of Ongözlü Bridge at 10 s, 35 s and 120 s 83

Figure 3.26 Ongözlü Bridge at T=180 s (flood case) 85

Figure 3.27 Time of change of drag force for abutments and piers of Ongözlü Bridge (flood case) 86

Figure 3.28 Representation of Ongözlü Bridge at 5 s, 20 s and 120 s (flood case) 87

LIST OF ABBREVIATIONS

A	The cross-sectional area of the channel, m^2
A_p	Projected area of pier, m^2
b	Width of the channel, m
B_p	Width of the pier, m
C_d	Coefficient of Drag
D_e	Hydraulic Radius
e	Percent Error, $\%$
F_d	Drag Force, (N/m)
F_r	Froud Number, $V/\sqrt(gy)$
g	Acceleration due to gravity, m/s^2
h	Flow depth, m
h_d	Downstream flow depth, m
h_u	Upstream flow depth, m
L	Length of pier, m
P	Pressure, Pa
p	Wetted Perimeter
Re	Reynold's Number, VL/ν
S	Bed slope
u	Velocity component of x-direction, m/s
$u_\star$	Shear Velocity, m/s
V	Fluid Velocity, m/s
v	Velocity component of y-direction, m/s
V_d	Downstream velocity, m/s
V_u	Upstream velocity, m/s
y	Distance to the wall boundary
y^+	Dimensionless distance to the wall boundary
${y_1}^+$	Dimensionless distance from center of adjacent cell to the wall boundary
Y	Global Coordinate, Y

Z	Global Coordinate, Z
X	Global Coordinate, X
Q	Discharge, m^3/s
q	Specific discharge, m^2/s
w	Velocity component of z-direction, m/s
α	Contraction ratio
γ	Specific Weight, N/m^3
ν	Kinematic Viscosity, μ/ρ
ρ	Density of fluid, kg/m^3

CHAPTER 1

INTRODUCTION

1.1 A BRIEF INFORMATION ON HYDRAULICS OF BRIDGE PIERS

Piers and abutments are the integral parts of the bridge since they handle the deck of the bridge. The geometric characteristic of the bridge pier which affects the stability of bridge defines the amount of support it supplies, especially during the flood. The rise of water on the upstream side of the pier brings about the negative effect on bridge in terms of pressure and it also creates scouring action. In Figure 1.1, perspective and plan views of bridge under scouring action is shown. Stagnation points which have zero velocity occur on the upstream side of pier. Additionally, vortex formations which create scouring around pier are shown in Figure 1.1.

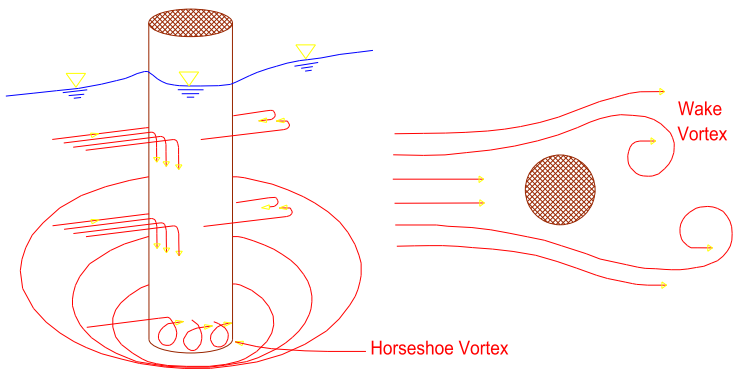

Figure 1.1: Horseshoe and wake vortices around a cylindrical pier (Dowding et al.,1994)

Use of piers through the channel is necessary in order to build bridge structures. The obstruction due to bridge piers and abutments creates an increase in the level of water on the upstream side of the bridge. The amount of obstruction is a function of the geometric characteristics of the pier itself, location of the piers in the channel, the amount of flow, and contraction ratio of channel. Contraction ratio can be defined as ratio between pier width, b and channel width, B. Hydraulic effects are critical in the design of the bridge structures. Several studies with respect to the hydraulic impacts of the bridge pier have been conducted to make designs correctly (L.W. Zevenbergen et al., 2012), (Department of Transport and Main Roads, 2013), (Rene Garcia, P.E., 2016).

In Figure 1.2, water level of upstream and downstream of the bridge is shown. Blue line which is the real profile of river represents swelling on the upstream side of the bridge. At the cross section of bridge, level of water decreases and velocity of water increases due to the contraction. Y1 and Y4 symbolize upstream and downstream water levels, respectively. Red dashed line represents undisturbed water level (without bridge case). Energy grade line and head loss can also be seen in Figure 1.2.

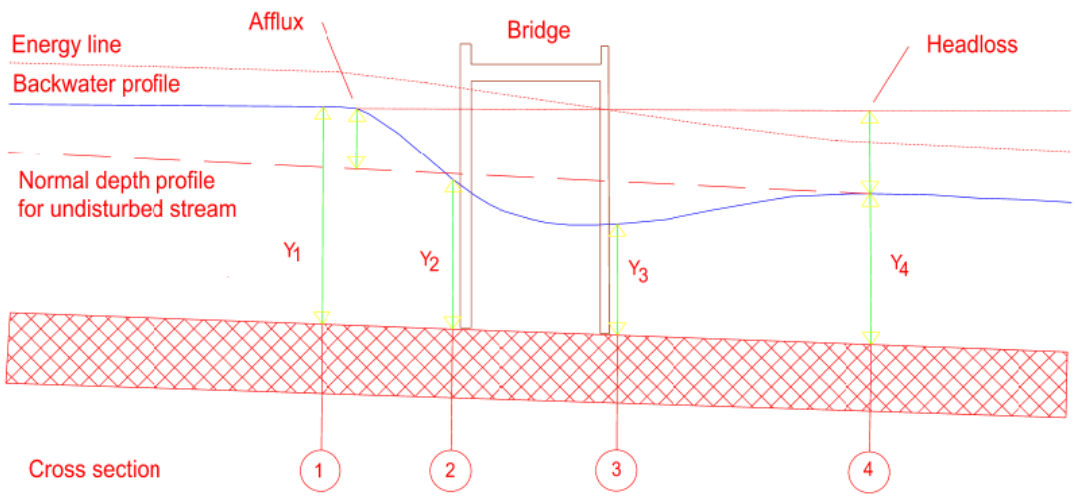

Figure 1.2: Schematic profile of the river flow obstructed due to the bridge

In the present study, hydraulic effects are taken into consideration for Ongözlü Bridge piers. Since the bridge is historical and it has no defects with respect to hydraulic aspect, it is selected for this numerical work. The simulations in the study are developed by using the computational fluid dynamics (CFD) software.

The plan view of the pier, flow direction, channel geometries and position of the pier in the channel are shown in Figure 1.3. In this figure B and b/2 stand for the channel width and the distance between wall and pier, respectively. Pier is placed in a rectangular channel symmetrically. In simulations, symmetrical pier position is used, and the contraction ratio is defined as ratio between pier width and channel width.

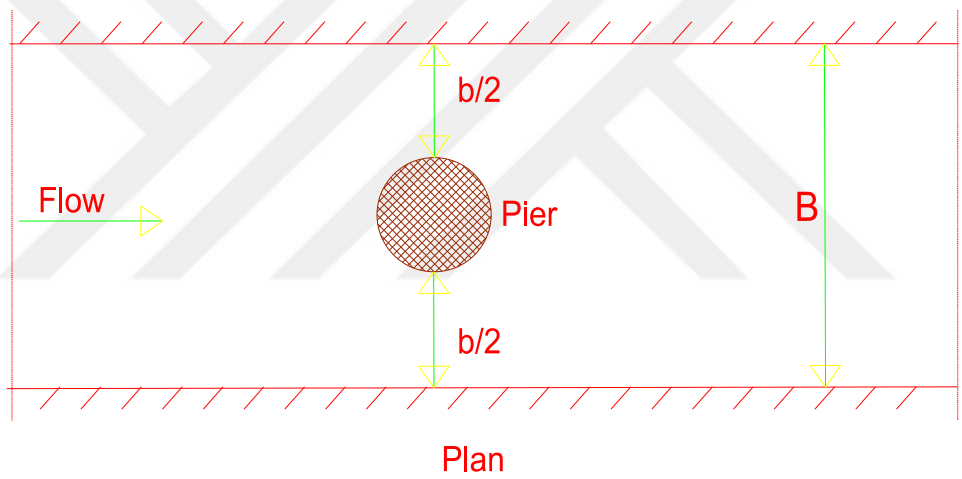

Figure 1.3: Plan view of the pier

Numerical investigations are carried out in drag characteristics of the bridge pier. The experimental studies conducted by and which are 'Backwater Rise and Drag Characteristics of Bridge Piers Under Sub-critical Flow Conditions' Suribabu et al.(2011) and 'Determination of Shape Co-efficient and Drag Co-efficient of Triangular Piers under Sub-Critical Flow Conditions' Agarwal et al. (2014) respectively are used for comparison. The thesis also summarizes the interaction between bridge piers and comparisons between abutments and piers in terms of drag characteristics. Flow 3D

CFD software (Flow 3D from Flow Science, CFD. www.flow3d.com) is used in the numerical simulations. Drawings and solid works are designed via the AutoCAD (Autodesk, Inc., www.autodesk.com) in three dimensions. Additionally, the geometric characteristics of piers (triangular, rectangular, elliptical etc.) are studied with the model and compared using with previous findings.

In Figure 1.4., profile view of the pier in the channel is shown. Y1 and Y3 symbolize upstream and downstream water levels, respectively. Y2 is the lowest point of the water level. Value of Y2 is greater than the critical depth. This situation presents the subcritical flow condition.

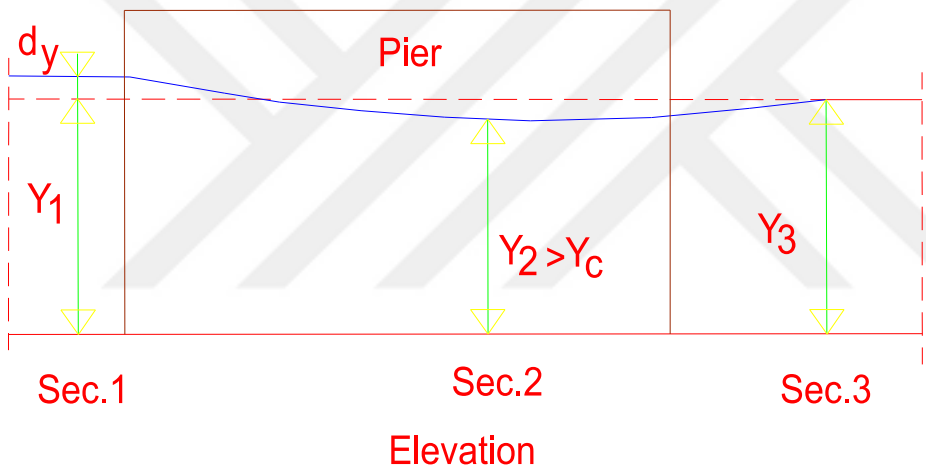

Figure 1.4: Profile view of the pier

1.2 LITERATURE REVIEW

1.2.1 PREVIOUS EXPERIMENTAL STUDIES

As it is mentioned before, the rise in the water level caused by piers and abutments, is supposed to happen as contraction of flow starts upstream of the piers. Due to the drag forces acting on the piers, energy dissipation in the flow occurs and the flow condition creates the rise in the level of water upstream of piers. The magnitude of the drag force over the flow is equal to the force on the pier but it's in the opposite direction. Moreover, the drag force includes the friction drag and the pressure drag. By utilizing the equation of momentum, one can find the total drag force. Abundant number of studies has been conducted regarding the drag characteristics and bridge piers. Charbeneau and Holley (2001) carried out laboratory experiments on the bridge piers and drag characteristics. Suribabu et al. (2011) studied the drag characteristics of different geometry of pier structures, which have 0.33 and 0.4 contraction ratios for the subcritical flow conditions. Agarwal et al. (2014) conducted an experimental study on drag characteristics of cylindrical piers with different slot-collars derivatives.

Some of these studies are directly related to the scope of our study and they are briefly summarized next. Charbeneau and Holley (2001) studied backwater effects, drag forces and water level changes both upstream and downstream side of the bridge piers. In their experimental work, different sizes of bridge piers simulated in the laboratory under subcritical flow conditions. Changes are observed over the water levels and subsequently on drag characteristics on piers. They calculated the drag coefficient of piers and investigated the scaling effect by comparing laboratory and prototype conditions. They compared their experimental outputs with the previous studies and then they improved their proposed formula according to the water level variation and Froude number. The study showed that a formula for backwater can be used for calculating water level.

Suribabu et al. (2011) evaluates the drag characteristics of different shaped piers, which have the same projected area. They examined the piers with two different contraction ratios under subcritical flow conditions. They measured discharges and calculated drag forces, drag coefficients and the changes related to the Froude num-

ber. Circular, elliptical, rectangle with curved ends, rectangle with triangular nose and tail (with 2.5 cm and 3.5 cm), rectangular, square and rhombus shapes were considered and their hydraulic data were measured. They also used mentioned shapes for measuring the effect of contraction ratios of 0.33 and 0.40. Backwater effects were investigated and then compared with Yarnell's (1934) backwater equation. The backwater formulation was tried to be enhanced.

Agarwal et al. (2014), likewise carried out experiments on the triangular piers under subcritical flow conditions to determine the coefficient of drag and shape coefficient. Rectangular model with triangular nose and tail shaped piers were considered with the different aspect ratios. The channel, where the experimental study was realized, had a constant contraction ratio of 0.4. They considered 4 different aspect ratios for rectangular piers with triangular nose and tail. These piers had same thickness (6 cm), however; they have various length of rectangular portion (4; 6; 12; 16 cm). The results show that drag coefficient depends on the aspect ratios of pier. The increase in the discharge changes the backwater level on the upstream side. They also compared their experimental outputs with Yarnell's formula.

1.2.2 PREVIOUS CFD STUDIES

Adhikary et al. (2009) investigated the drag forces, lift forces, and scour around bridge piers during the flood, which is essential to detect the risk. They simulated the scour-hole formation, sediment transport due to the storming flow conditions, by using computational fluid dynamics (CFD). Researchers studied on open channel turbulent flow to detect the final features of scour-hole. Extending the previous 2-D simulation, Reynolds Averaged Navier Stokes (RANS) equations and a k-ε turbulence closure model are used in the 3-D model.

Elapolu et al. (2012) aimed to improve and to apply a 3-D model to examine scour–hole formation around a cylindrical bridge piers. They used STARCCM+ software. Python and Java Macros programs have been used in the study for creating a computational methodology. The model uses RANS equations and k-ε turbulence model. The numerical study is based on the experimental lab-scale tests at the Offshore Center Danmark. The study also tries to analyse single phase transient for all of the flow fields

around the pier and bed shear stress.

In the study of Tulimilli et al. (2010), the aim of the study was to model scour-pit for open channel turbulent flows through flood. They also used RANS equations. They used a methodology called slip-flat-top surface. They compared their results to simulate scouring with other empirical critical shear stress correlations and bed roughness values sediment removal is characterized.

Tănase et al. (2014) investigated flow around an immersed cylinder. Their study is concerned with experimental and numerical investigations. Aim of the study is to compute free surface geometry and flow pattern of the cylinder. 2D channel is simulated under sub-critical flow conditions with Reynolds and Froude numbers in ranges between 5000 and 10000, Fr < 1, respectively. Numerical solutions for the flow are obtained with standard k-ε and RNG k-ε turbulent models and the free surface geometry is calculated by the VOF model available in Fluent code. The aim of the study was to research the interaction between the free surface and the wake developed downstream the separation points.

1.3 HISTORICAL BACKGROUND OF ONGOZLU BRIDGE

Streamlined shapes for bridge piers have been used widely. It is also known that for the first time in our history, Mimar Sinan has used streamlined shapes for bridge piers on 16th century. However, there is a historical bridge on Tigris River in Diyarbakır, called Glorious Ongözlü Bridge which has streamlined shaped piers.

Ongözlü Bridge, which is also called as Tigris Bridge, Mervani Bridge, and Silvan Bridge. The bridge was destructed and then repaired for many times because of the war of conquests. In 974, the last destruction was happened by Byzantine Emperor called Juannes Tzimiscez. After the destruction, the bridge was repaired by Emevi Calif Hisam. It is thought that the bridge was constructed in the era of Nizamuddin Nasr and then other sides of bridge repaired in time, according to the tablets located on the first three eyes. By the years of 1065-1067, the bridge was constructed and repaired lastly. Due to the commands of the Mervanoglu Nizamuddevle Nasr, the bridge survived until today. (Valiliği, D., 2016)

It is understood that the bridge was destructed and rebuilt for many times according to the antic era on the soil of the bridge. As it is mentioned many times in the report, the bridge has the total length of 160 m, and a width of 8.3 m. The railings of the bridge which are covered with prepared in cut ranged side by side and linked with triangular roof shaped stones. Between the first three eyes, the tablet of the bridge is located. A turned right lion teazling exists in a frame, which was designed at the end of the tablet on the same row. The lion figure has some little signs and stones. Thanks to the river streams large and straight flooring, the bridges length was kept long.

Figure 1.5: Ongözlü Bridge (Aral, T., 2012)

Since 20th century, streamlined shapes for bridge piers are being used. It is also known that for the first time in history, Mimar Sinan has used streamlined shapes for bridge piers in 16th century. However, this historical bridge in Diyarbakır has streamlined shaped piers which was built in 10th century. This fact took our attention to study this bridge in detail.

1.4 THE MODEL OF ONGOZLU BRIDGE

Technical drawings of the bridge are taken from General Directorate of Highways, Republic of Turkey. Plan and profile of Ongözlü Bridge, details of the piers and abutments are given as hard copy. The 3-D model was created using AutoCAD and used in the simulations.The plan, profile and detail drawings of the bridge are given in Figures 1.6, 1.7 and 1.8, respectively.

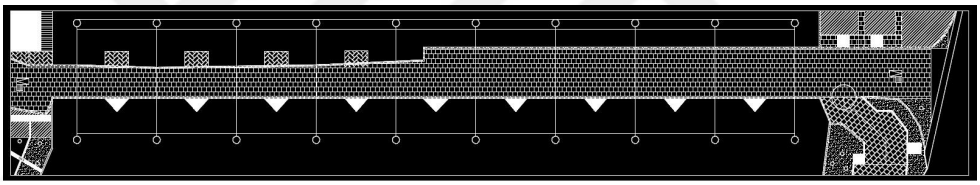

Figure 1.6: Plan view of Ongözlü Bridge

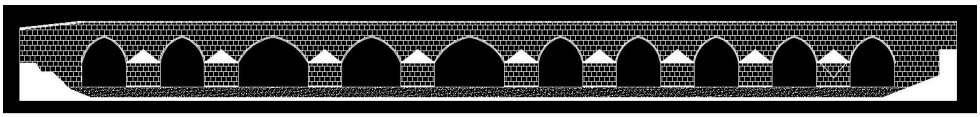

Figure 1.7: Profile view of Ongözlü Bridge

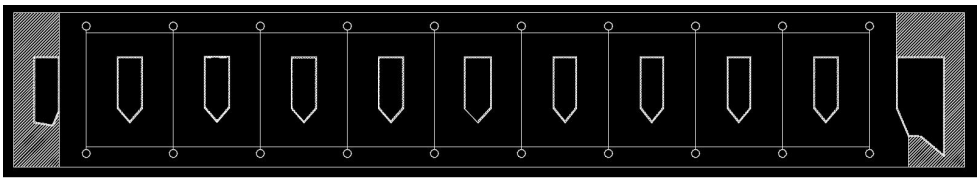

Figure 1.8: Details of Ongözlü Bridge

However, before simulating the flow around the whole bridge, single piers are studied. In the first part of the study, rectangular shape pier with triangular nose and tail of constant contraction ratio of 0.4 are used for 4, 6, 12 and 16 cm length (parallel to flow). Numerical investigation was carried out in a hydraulic flume of 4 m length, 0.15 m width. The flume has rectangular cross section. Subcritical flow condition was

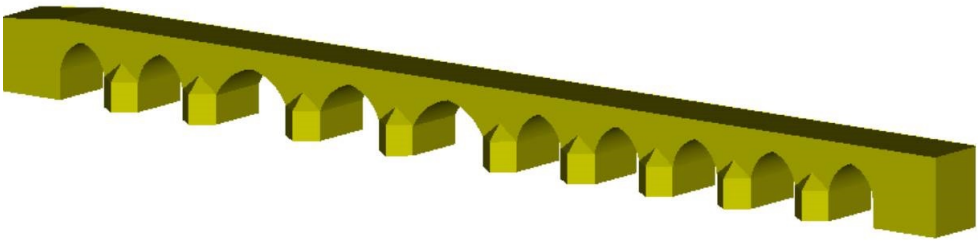

Figure 1.9: The model of Ongözlü Bridge

created for all cases. The numerical results obtained from this part is compared to the experimental ones from the study of Agarwal et al. (2014). To make a comparison, one of the Ongözlü Bridge pier is scaled. The scale factor is selected such that the scaled pier matches with the pier in the experimental study of Agarwal et al. (2014). The scale factor is 6/500 (1/83.33). In Figure 1.9, the model of Ongözlü Bridge is shown. One pier of Ongözlü Bridge is given in Figure 1.10.

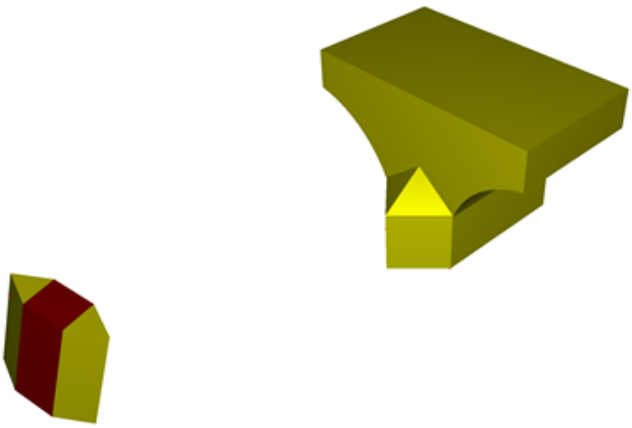

Figure 1.10: Scaled bridge pier

In the second part, the effect of the shape of the pier is investigated by considering isolated pier in various shapes.

As for the final part of the study, Ongözlü Bridge was simulated as a whole. Additionally, same scale factor (1/83.33) is used for Ongözlü Bridge. To make a comparison, discharges, channel slope, simulation setup and measurement techniques are used similar to the initial part of the study. Such that, inflow conditions are similar to single pier case where we keep flow depth and average inflow velocity as a constant.

Piers are taken as separate components for the final part of the numerical investigation. Aim of the research is to measure the drag forces on piers separately. In Figure 1.11, 9 piers and 2 abutments are one by one defined in Flow 3D and their coordinates are adjusted to match the original position of Ongözlü Bridge.

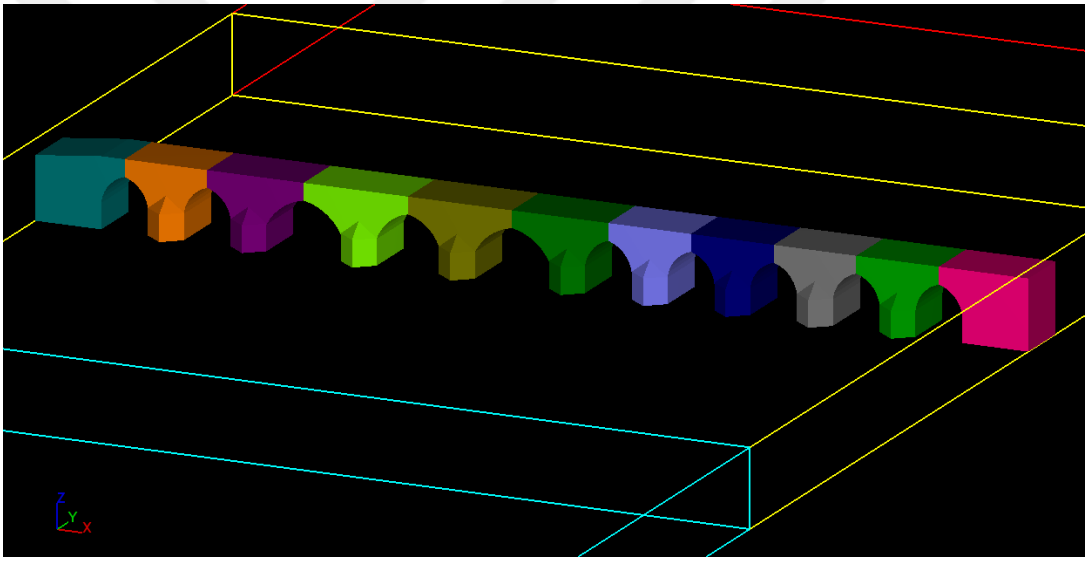

Figure 1.11: Flow 3D component view (xyz)

Ongözlü Bridge is modeled as a whole, components and position of bridge are shown in Figure 1.11. Details about the component configuration such as flow direction, labels of abutments and piers are described in Figure 1.12.

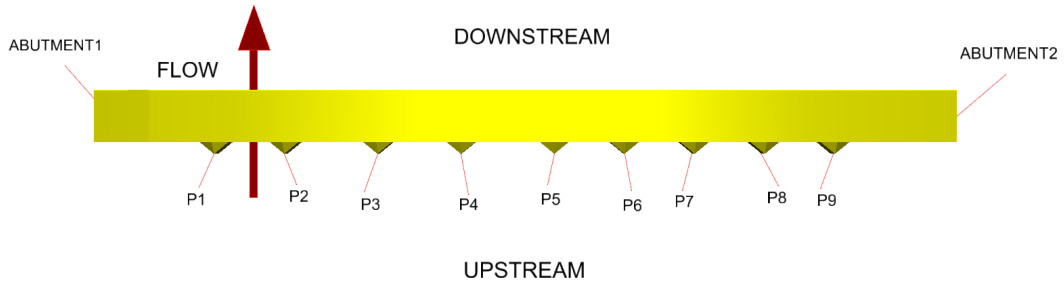

Figure 1.12: AutoCAD 3D components labels (top view)

1.5 AIM OF THE PRESENT STUDY

In the present work, the characteristics of the shape of piers of Ongözlü Bridge is studied numerically and the obtained results are compared with the drag characteristics of the other shapes that have been used as piers and given in literature. The results may show that even in 11th century, the hydraulic works in Anatolia were ahead of its time, and first bridge with a streamlined shape was built 3-4 centuries before Mimar Sinan.

In the study, the force of drag with respect to pier shape is evaluated using the CFD code. Subsequently, comparison of experimental values of drag forces and drag characteristics of different pier shapes are studied and discussed.

CHAPTER 2

METHODOLOGY

Computational fluid dynamics (CFD) is a field of fluid mechanics which consists of numerical methods and algorithms to evaluate and simulate the fluid flow problems. Almost all CFD software are based on solving equations of Navier Stokes and continuity. Users can monitor and examine the results. Data of numerical model must be obtained and used to define flow features of numerical investigation. Thus, analysis of numerical models must be validated with existing experimental results is a must.

All computational fluid dynamics approaches consist of three main procedures as follows;

i. Pre-processing;

• The geometry is identified.

• The mesh generation is defined and then volume of fluid is occupied in cells. The mesh generation can be uniform or non-uniform.

• The physical model is defined.

• Boundary conditions which consist of features of fluid are defined.

ii. The simulation is figured as a steady-state or transient.

iii. Postprocessor begins to analyze the outputs.

Many commercial CFD software are available. These packages offer many advantages to the users about visualization of preprocessing, post-processing, validation of results. Post-processing includes vectors, contours, surface plots, streamlines, geometry, and text data results.

The steps of a CFD study are given in the flow chart in Figure 2.1;

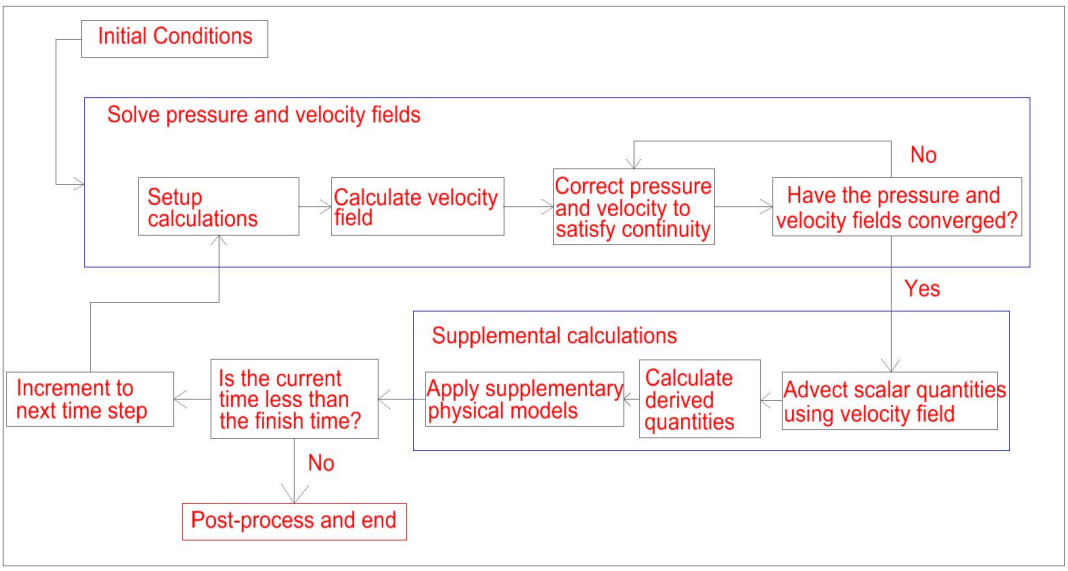

Figure 2.1: General solution method for an incompressible flow (Flow 3D general training class-2013)

2.1 PREPROCESSING

The preprocessing has two basic functions. First, it is used for mesh generation. Second function is to detect basic errors, specifications in defined geometry, mesh generated, boundary conditions and other features of CFD constraints. This feature of the simulation helps saving time, since it prevents some possible mistakes before running the simulation. It also ensures an accurate set up. User can easily check outputs of preprocessor simulation and change conditions before starting the full run.

Preprocessing includes four main steps which are geometry construction and import; mesh generation with structured and unstructured elements; mesh quality examination; and definition of boundary zones handled in Figure 2.2.

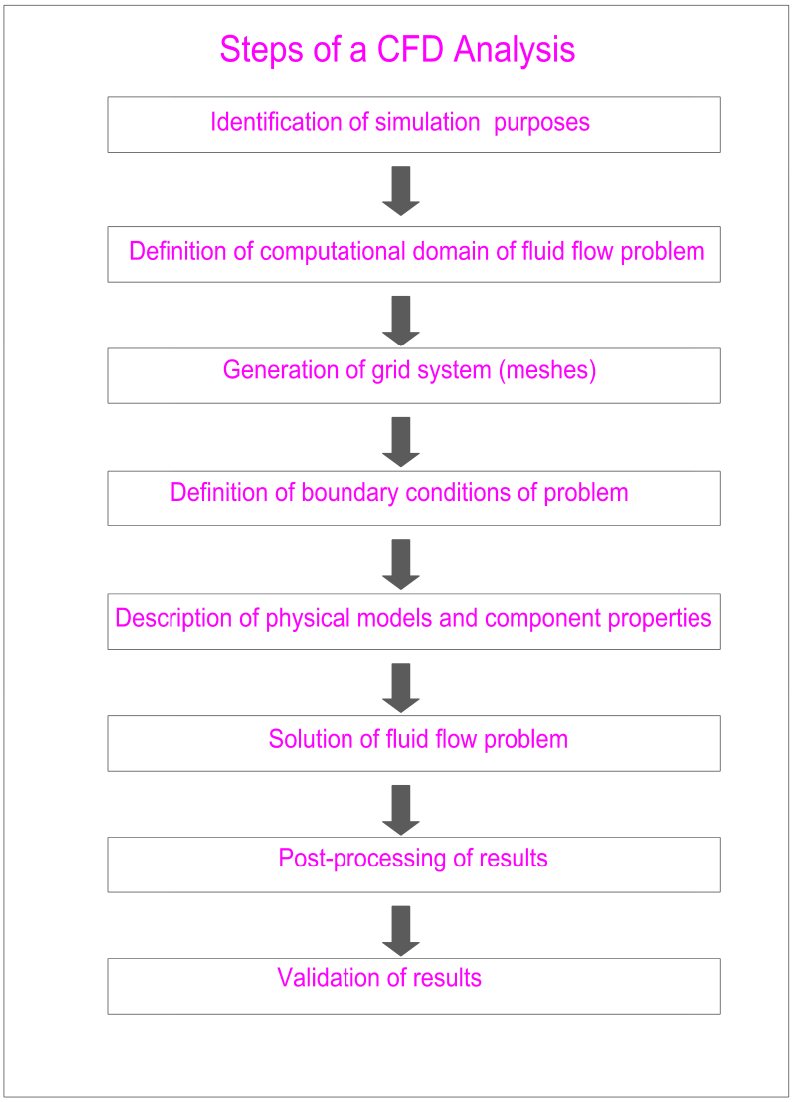

Figure 2.2: Steps of CFD analysis

2.1.1 FLOW DOMAIN

The study includes three main parts. In the first part, different shapes of bridge piers are analysed. In the second part, aspect ratios of bridge piers with rectangular body and triangular nose and tail are examined. In the final part of the study, Ongözlü Bridge is modelled. After simulating Ongözlü Bridge piers, the results are compared with first and second part of the study.

Previously mentioned bridge piers are drawn by AutoCAD-3D modelling tool. Solid geometries are created using AutoCAD-3D modelling tool and imported into the CFD software. The geometric representation of one of the bridge pier is shown in Figure 2.3.

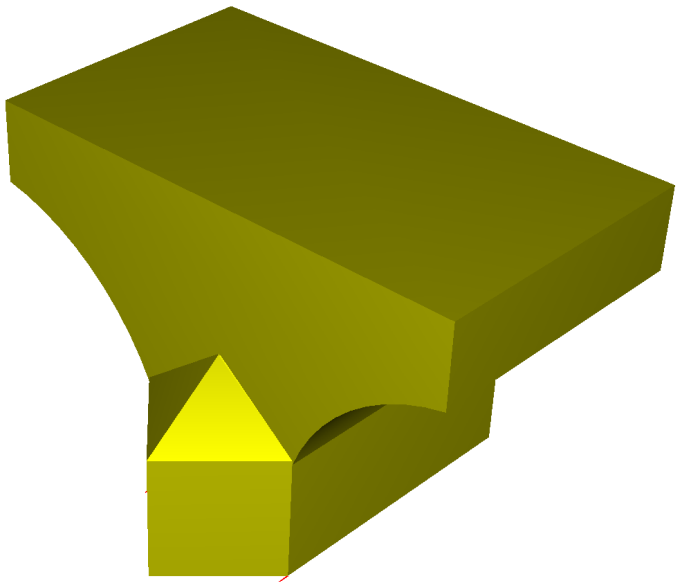

Figure 2.3: Ongözlü Bridge pier

After importing outputs into the CFD software, flow domain is created around the bridge pier. In all simulations, 4 m long, 0.15 m wide, 0.20 m high computational domain is created by utilizing mesh blocks. Cartesian coordinate system is used in all mesh blocks for the numerical models. The flow domain is constrained by mesh of fixed rectangular cells. The flow domain is not related with the geometry of piers. Thus, the geometry and flow domain are unconnected. The connection is made by Volume of Fluid (VOF) definition, which is described in Section 2.3.

2.1.2 BOUNDARY CONDITIONS

Some initial and boundary conditions must be determined for all computational fluid dynamics problems. For execution of these boundary conditions, staggered grid is constructed, and one more node next to the physical boundary is added to handle;

- Nodes which are located close to the outside of the inlet are appointed the inlet conditions.
- The physical limitations can collide with the volume of scalar control limitations. Boundary conditions are defined accordingly for nodes which are close to the boundary.

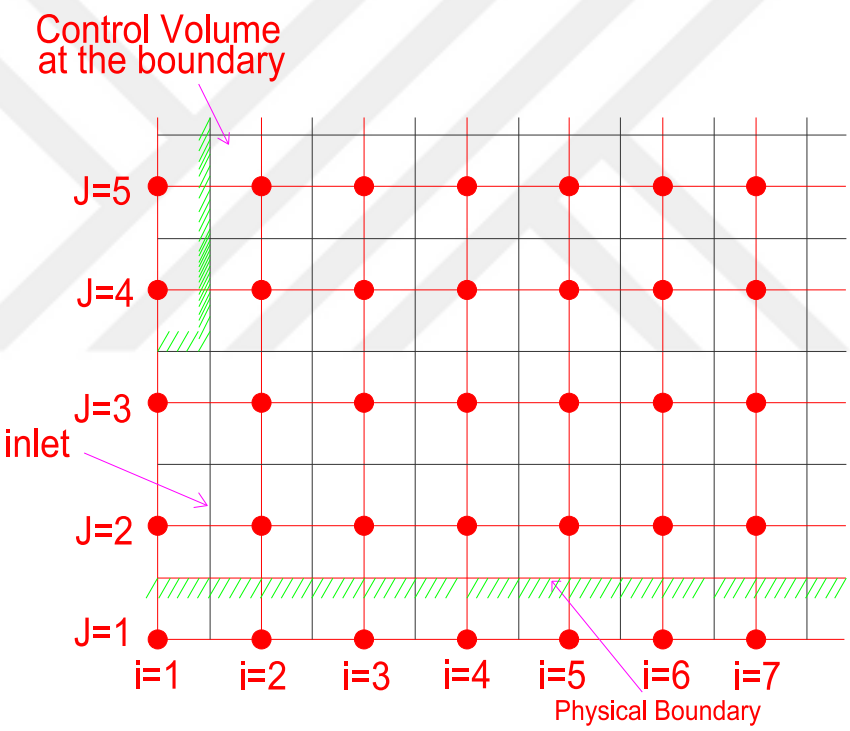

Figure 2.4: Description of general boundary conditions (Versteeg et al., 1995)

The additional nodes enclosing the physical boundary is given in Figure 2.4. Two remarkable properties of the adjustment are the physical boundaries coincide with the scalar boundaries of control volume and the nodes just out the inlet, such as $(i, j) = (1, 1)(1, 2), (1, 3)$ are existing to store the inlet conditions.

Boundary conditions used in CFD simulations are as follows;

-Inlet boundary conditions

-Wall boundary conditions

-Symmetry boundary conditions

-Outflow boundary conditions

2.1.2.1 INLET BOUNDARY CONDITIONS

It is assumed that the inlet is perpendicular to the x-direction.

-For the first cell, velocity components in x and y directions u and v respectively, are linked to neighbouring nodes that are active, so there is no need of any modifications to discretion equations.

-At one of the inlet node absolute pressure is fixed, this is taken as reference pressure hence pressure correction at that node is zero.

-Generally computational fluid dynamics codes estimate k and ε with an approximate formula based on turbulent intensity between 1 and 6 percent and length scale.

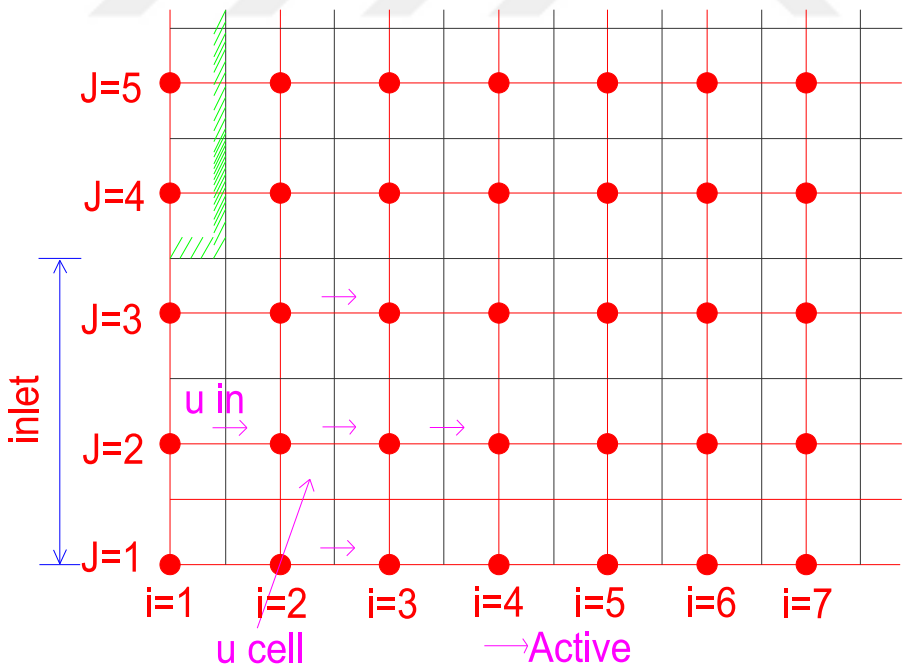

Figure 2.5: Inlet (u) boundary condition (Versteeg et al., 1995)

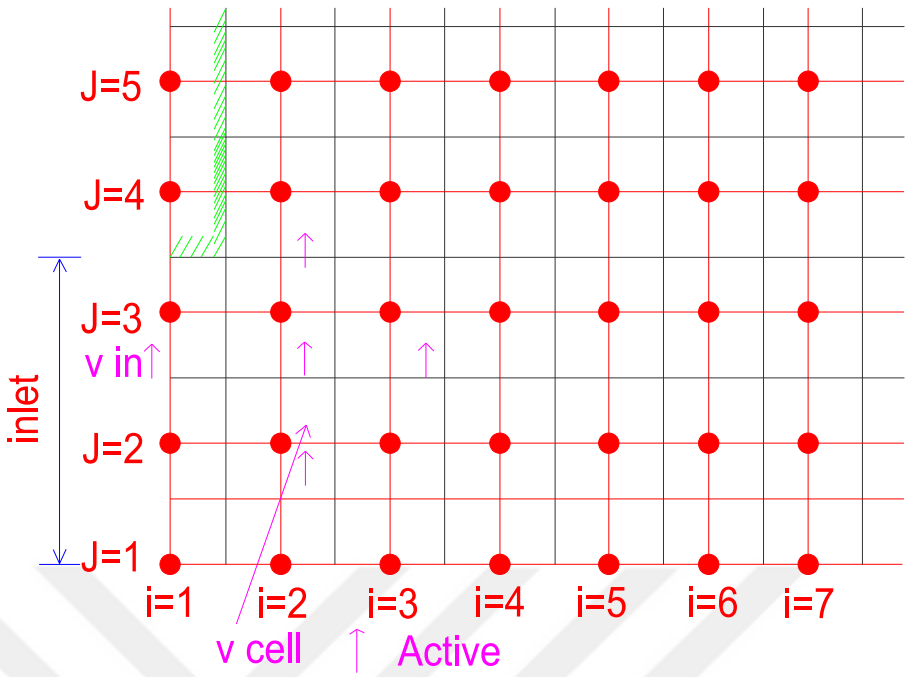

Figure 2.6: Inlet (v) boundary condition (Versteeg et al., 1995)

Figure 2.5 and 2.6 illustrate the grid adjustment in the immediate surround of an inlet for u and v momentum. The direction of flow is supposed to be from the left to the right in the figures.

2.1.2.2 WALL BOUNDARY CONDITIONS

For a solid wall parallel to the x-direction, assumptions made and relations considered are as follows:

-The near wall flow is considered as laminar and the velocity varies linearly with distance from the wall

-No slip condition at the wall: $u = v = 0$.

-"Wall Functions" are applied when the proper conditions satisfied.

In Figure 2.7, details of grid are given in the near wall region for the component of v velocity (perpendicular to the wall). The no-slip condition $(u = v = 0)$ is the convenient condition for the velocity components at solid walls.

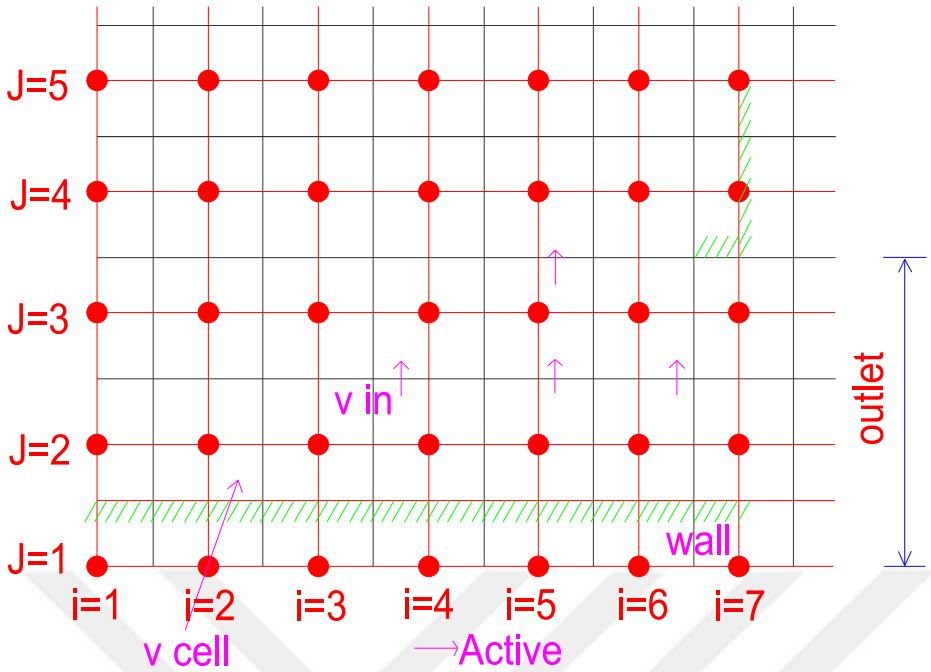

Figure 2.7: Wall (v) boundary condition (Versteeg et al., 1995)

$$y^+ = \frac{u_\star y}{\nu} \,,$$

where y^+ dimensionless distance to the wall, $u_\star = \sqrt{(\frac{\tau_w}{\rho}}$ is the shear velocity, τ_w is the wall-shear stress, ρ is the density of the fluid, y is the distance to the nearest wall and ν is the kinematic viscosity of the fluid.

Turbulent flow is assumed for:

$y^+ > 11.63$

in the log-law region of a turbulent boundary layer.

Laminar flow is assumed for:

$y^+ < 11.63$

Important points for applying wall functions:

-The velocity is constant along parallel to the wall and varies only in the direction normal to the wall.

-No pressure gradients in the flow direction.

-High Reynolds number

-No chemical reactions at the wall

2.1.2.3 SYMMETRY BOUNDARY CONDITIONS

If flow across the boundary is zero:

-Normal velocities are set to zero

Scalar flux across the boundary is zero:

-In this type of boundaries values of properties just adjacent to the boundary at the nearest node just inside the domain are taken as values at the symmetry boundary.

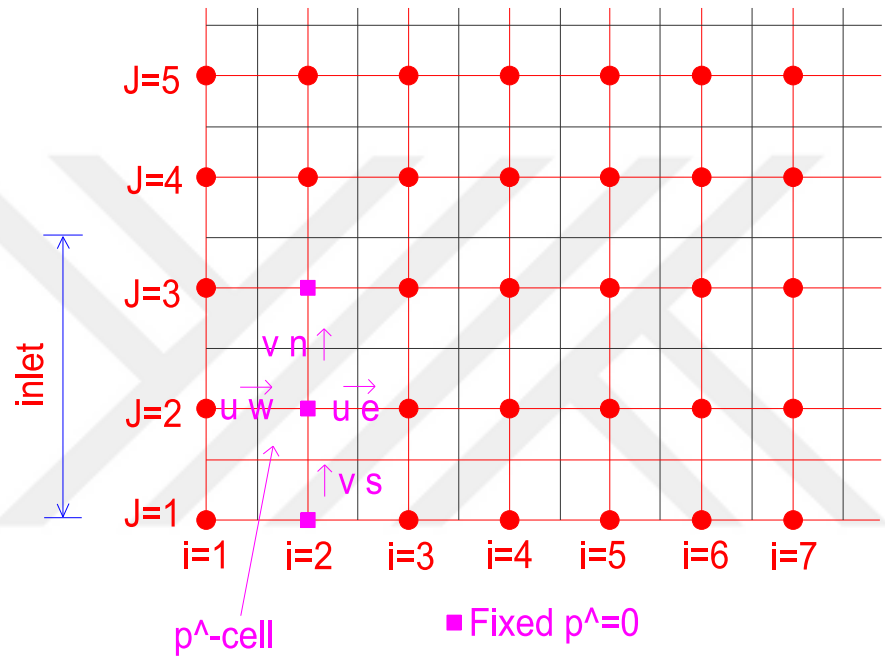

Figure 2.8: Symmetry boundary condition (Versteeg et al., 1995)

2.1.2.4 OUTFLOW BOUNDARY CONDITIONS

Considering the case of an outlet perpendicular to the x-direction;

-In fully developed flow no changes occurs in flow direction, gradient of all variables except pressure are zero in flow direction.

-The equations are solved for cells up to, where NI is outside the domain values of flow variables are determined by extrapolation from the interior by assuming zero gradients at the outlet plane.

The outlet plane velocities with the continuity correction can be defined as:

$$U_{NI,J} = U_{NI-1,J} / \frac{M_{in}}{M_{out}} \tag{2.1}$$

where $U_{NI,J}$ and $U_{NI-1,J}$ neighbour velocities in x direction, M_{in} and M_{out} are total flux of inlet and outlet, respectively.

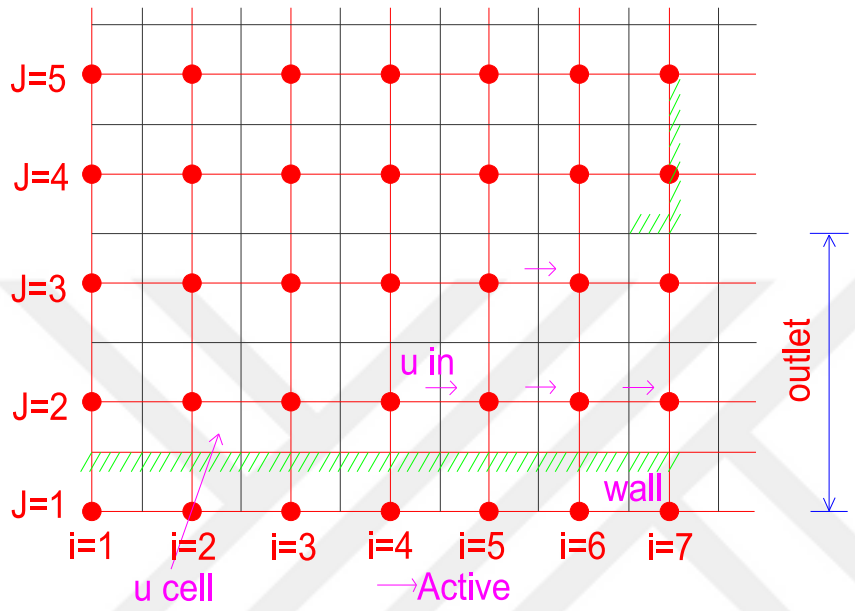

Figure 2.9: Outlet (u) boundary condition (Versteeg et al., 1995)

Figure 2.9 illustrates the grid adjustment near such an outlet boundary. Figure 2.9 which defines case of velocity component u shows that all connections are active for these variables so their discretized equations can be solved using Equation 2.1.

2.1.3 MESH GENERATION

Mesh generation is an exercise on creating a polygonal or polyhedral mesh which approximates a geometric region. The mesh generation is possible using sources such as CAD, STL(file format) or a point cloud. The mesh generation can be done in CFD software.

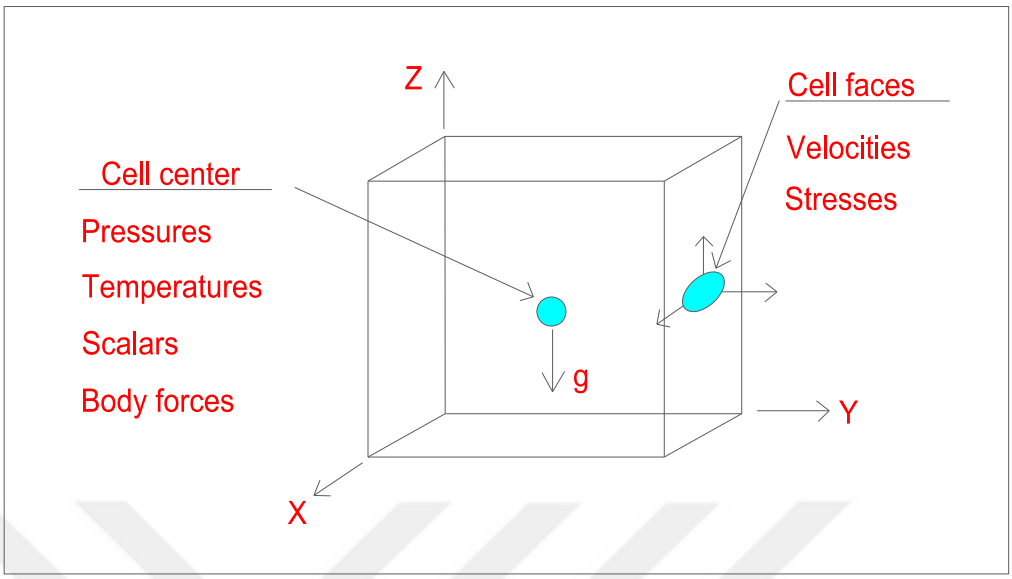

Figure 2.10: Grid system for Flow 3D (Flow 3D advanced hydraulic training-2012)

Flow 3D governs the finite-volume method to solve the RANS equations. Cells which are consist of rectangular grids are established subdividing the computational domain. Rectangular grids are very easy to create due to the regular character of rectangular mesh system. The analysis is implemented based on a unit cell after the computational domain is subdivided by rectangular grids. The computational cells are defined in direction of x (i), direction of y (j) and direction of z (k). Scalar quantities are solved at the cell centers whereas vector and tensors are solved at the cell faces. The grid system for Flow 3D is given in Figure 2.10.

In staggered configuration mentioned earlier in boundary conditions, some flow variables are defined at the center of the cell and some are defined at the cell surface as shown in this figure.

Mesh blocks are placed on geometry to cover a flow domain.

-Mesh blocks examine all around flow field.

-Individual mesh blocks can be located in specific domains for getting better resolution.

-Mesh blocks can be intimated for complicated flow

domains to create meshing which resolves areas of interest efficiently.

-The mesh resolution decides how correctly the geometry is defined.

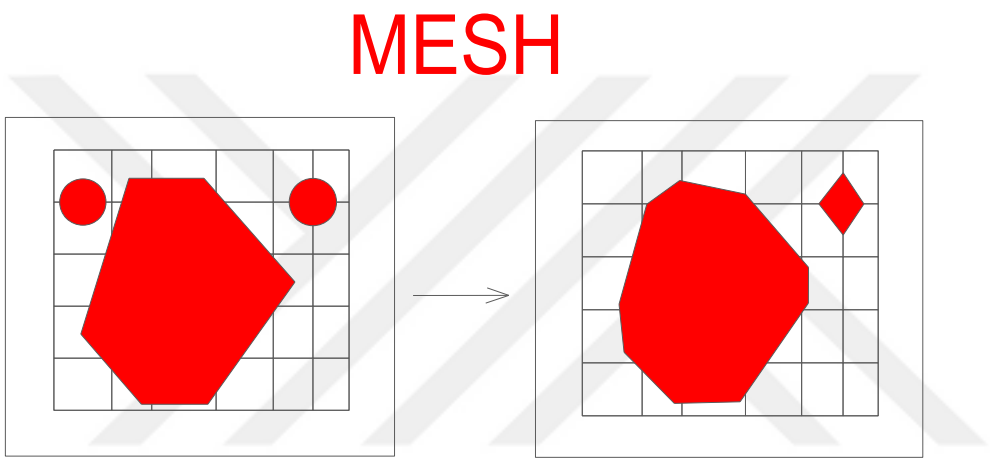

Figure 2.11: Object definition (left) and object created (right) (Flow 3D documentation release 10.1.0-2012)

It is possible that the geometry may coincide a cell face several times for some geometries and mesh resolutions. In this circumstance the corresponding cell edge is supposed to be both fully inside the object and fully outside, as shown in Figure 2.11.

2.1.4 GRID DEPENDENCY CHECK

Near-wall mesh and Reynolds number affect the global mesh resolution parameters. That's why it is important to check grid dependency.

There are two main options for near wall modeling strategy;

i. Viscous Sublayer

-Vicous sublayer option is for high priority impacts near a wall-bounded region. These can be adverse pressure gradients, pressure drop, heat transfer, aerodynamic drag. Viscous Sublayer includes the full resolution of the boundary layer.
-Viscous Sublayer should use a suitable low-Reynolds number turbulence model.
-The height of grid neighbour to a wall should be have a y^+ of the order of O(1).

ii. Wall Function Grid

-It includes the boundary layer and utilizes the log-law wall function. It is appropriate for some cases, where impact of flow near to the wall-bounded region is secondary. This approach is suitable for flow that undergoes geometry-induced separation, such as modern automobile design.
-The height of grid neighbouring the wall should reside in the log law region. It is necessary to estimate the height of first cell during the preprocessing step. With choosing the height, hydrostatic head will be in the estimated interval. In some cases, first cell height will change along the wall. Thus, in complicated regions, the mesh should be designed with high sensitivity.
-This approximation can be used in all turbulence models.

At first, Reynolds number and hydraulic radius should be calculated;

$$R_e = \frac{\rho U D_e}{\mu} \tag{2.2}$$

$$D_e = \frac{4A}{p} \tag{2.3}$$

where, U is the free stream velocity, ρ and μ are the fluid density and viscosity respectively, and D_e is the hydraulic radius.

Estimated y^+ value and fluid properties are known and the shear velocity need to be calculated ($U_\star$), which is stated on page 20.

$$\tau_w = \frac{1}{2} C_f \rho U^2 \tag{2.4}$$

The near wall mesh size in term of wall units could be calculated based on an empirical formula for external flows which estimates a skin friction coefficient C_f (Schlichting, 1979). This coefficient is used for finding the wall shear stress based on far stream velocity, U. Based on the Reynolds number and far stream velocity of flow, the y_+ value is estimated using below formula.

Table2.1: C_f formulas for different flow types

Flow Type	**Empirical Estimate**
Internal Flows	$C_f = 0.0079 * Re^{0.25}$
External Flows	$C_f = 0.058 * Re^{0.2}$

With those of known values, Δy_1 can be easily estimated from equations.

In case of simple flows and simple geometry, it is necessary to find this correlation accurately. However, complicated flow and complex geometries may require refinement to get the desired value. To get the target value of the y^+, re-mesh option of CFD model can be used.

2.2 GOVERNING EQUATIONS

Definition and mathematically expression of turbulent flow is quite difficult to solve. Reynolds–Averaged-Navier–Stokes equations (RANS), are regarded as the most satisfactory definition of turbulent flows (Martin, 2010). Irregularity, three dimensionality and rotationality are the predominant nature of turbulent flow. Turbulent flow is also diffusive and dissipative. Because of these conditions, internal energy of flow is increased by viscous shear stress. This energy increases the momentum rates.

Conservation of mass is described in Equation 2.6. Conservation of momentum is given in Equation 2.7.

$$\frac{\partial \rho}{\partial t} + \frac{\partial}{\partial x_i}(\rho u_i) = 0 \tag{2.5}$$

$$\rho \frac{\partial u_i}{\partial t} + \frac{\partial \rho u_i u_j}{\partial x_j} = -\frac{\partial p}{\partial x_i} + \frac{\partial}{\partial x_j}(2\mu S_{ij}) \tag{2.6}$$

S_{ij} is the strain-rate tensor and described in Equation 2.8, where μ is the dynamic viscosity term.

$$S_{ij} = \frac{1}{2}[\frac{\partial u_i}{\partial x_j} + \frac{\partial u_j}{\partial x_i}] \tag{2.7}$$

Reynolds equations were simplified. The simplified version is called Reynolds-Averaged Navier-Stokes (RANS) equations. Reynolds equations are decomposed the flow properties into time-averaged and fluctuating parts as follow;

$$u_i = U_i + u_i' \tag{2.8}$$

$$p = P + p' \tag{2.9}$$

where capital terms represent the time-averaged values and primed values are the fluctuating part. The terms u_i and P are the instantaneous velocity and pressure, respectively.

In time averaging process the averaged values of primed values become zero, that is;

$$\overline{u_i} = U_i \qquad , \qquad \overline{u_i'} = 0 \tag{2.10}$$

$$\overline{p} = P \qquad , \qquad \overline{p'} = 0 \tag{2.11}$$

Nguyen (2005) defined RANS equations for incompressible flows such as;

$$\frac{\partial U_i}{\partial x_i} = 0 \tag{2.12}$$

$$\rho \frac{\partial U_i}{\partial t} + \rho \frac{\partial}{\partial x_j}(U_i U_j) = -\frac{\partial p}{\partial x_i} + \frac{\partial}{\partial x_j}(2\mu S_{ij} - \rho \overline{u_i' u_j'}) \tag{2.13}$$

S_{ij} , which is the mean strain-rate tensor, can be defined as;

$$S_{ij} = \frac{1}{2}(\frac{\partial U_i}{\partial x_j} + \frac{\partial U_j}{\partial x_i}) \tag{2.14}$$

The final form of RANS equation is achieved by consolidating these expressions, which is given in Equation 2.16;

$$\frac{\partial U_i}{\partial t} + U_j \frac{\partial U_i}{\partial x_j} = -\frac{\partial p}{\partial x_i} + \nu \frac{\partial^2 U_i}{\partial x_i \partial x_j} - \frac{\partial \overline{u_i' u_j'}}{\partial x_j} \tag{2.15}$$

By using unsteady RANS equations, velocity field is obtained. Volume of fluid model is used for free surface modelling. Details are given in the next section. When the simulation is observed to reach a steady state, it is finalized. The latest data is used in calculation of drag force. Due to presence of piers the water level on upstream side of bridge increases. The water level increases due to drag forces by piers. The situation causes energy loss in the channel. Drag forces have three main parts which are form, surface, and wave drag.

The geometry of the pier, reattachment points at the downstream side and location of separation affects the form drag. By assuming that the velocity distribution is uniform in all cross section, additionally, neglecting channel slope and boundary friction in the channel, the drag calculations can be done using Equations 2.17;

$$F_d = \frac{1}{2} C_d \rho V^2 A_p \tag{2.16}$$

where F_d is the drag force due to friction, C_d is the drag coefficient, V is the average velocity, A_p is the projected area of pier.

The difference between high pressure on the upstream side at stagnation zone and low pressure on the turbulent wake region in the downstream side creates the form drag. The increase in pressure on the upstream side of the pier occurs because of the conversion of kinetic energy to potential energy at stagnation point. Linear momentum equation along the flow direction is;

$$P_1 - P_2 - F_d = \rho Q (V_2 - V_1) \tag{2.17}$$

In open channel flows the state of flow is important with respect to Froude Number, F_r. When F_r <1 the flow is called a subcritical flow. When F_r >1, the flow is characterized as supercritical flow. Moreover, when F_r =1 , the flow is called a critical flow. For rectangular cross sections, the Froude number is;

$$F_r = \frac{V}{\sqrt{(gy)}} \tag{2.18}$$

Reynolds number of the pier is given by;

$$Re_{pier} = \frac{VB_p}{\nu} \tag{2.19}$$

where V and y represent the average velocity and the depth of flow, respectively. B_p is the width of the pier and ν is the kinematic viscosity of fluid.

2.3 VOLUME OF FLUID METHOD

The volume of fluid (VOF) method is a free-surface modelling technique which is using in computational fluid dynamics. Eulerian methods are used in VOF method. It is qualified by a mesh which is stationary or moving in a significant volume to accommodate the progressing form of the interface. VOF method does not only solve flow algorithm, but also user can track the position and shape of the interface. The flow motion is described by using the Navier-Stokes equations.

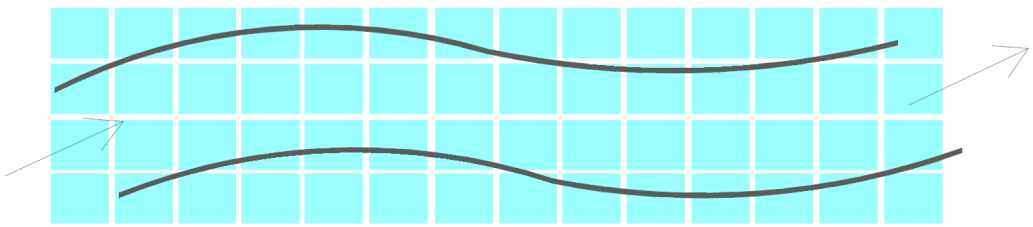

Figure 2.12: Control volume representation in Flow 3D (Flow 3D general training class-2013)

A computational mesh must effectually discretize the physical space. During the operation of integration, it is assumed that the cell is little enough that the flow variables do not vary significantly at this scale. The free surface is calculated using TruVOF. The control volume figuration of Flow 3D is given in Figure 2.12.

The VOF method is based upon the opinion of called 'fraction function' F. F is described as the integral of fluids feature function in the volume of a computational grid cell. In principle, F is zero when computational grid cell is blank with no flow motion inside. On the other hand, F is equal to 1 when control cell is full. When value of F is between 0 and 1, interface interrupt the cell. F is a function of non-continuous and its valuation changes between 0 and 1 when the fluid moves into volume. (Flow 3D Lecture Notes, Hydraulics Training Class, 2013)

F which is called the fraction function is a scalar function. Fluid particles generate the identity of flow domain, when these particles move with velocity vector ($\overrightarrow{v}$= $(u(x,y,z), v(x,y,z), w(x,y,z))$ in 3D space.

A VOF method should contain an algorithm for after then the sharp interface between the void and fluid. The presentation of sharp interface of fluid fraction in Flow 3D is given in Figure 2.13.

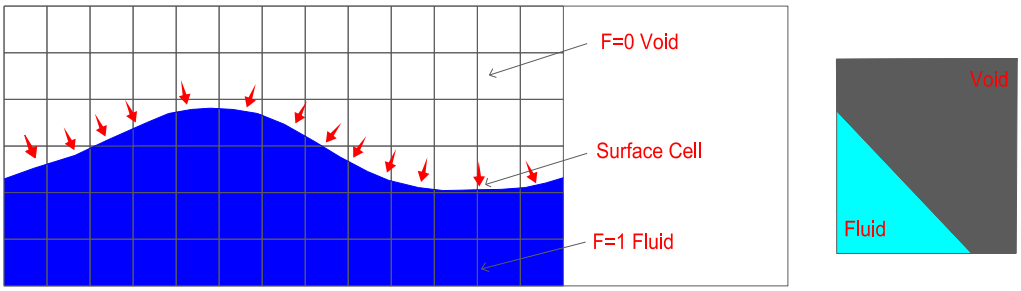

Figure 2.13: Sharp interface of fluid fraction (Flow 3D advanced hydraulics training-2013)

2.4 TURBULENCE CLOSURE - RNG K-ε MODEL

Closure problem

The continuity and RANS equations generate a complex set of four equations with four unknowns which are the velocity components u, v, w and the pressure p. Time-averaging term of the momentum equations which involves the instantaneous fluctuations is discarded. Consequently, six extra unknowns, Reynolds stresses are obtained in the time averaged equations of momentum. Likewise, time average transport equations have additional terms. The confusion of turbulence generally make impossible for ordinary formula for the additional stresses and turbulent terms. It is the base task of turbulence modelling to enhance computational method of adequate accuracy and generalization for engineers to foresee the Reynolds stresses and the transport terms. For this purpose in numerical modelling, turbulence modelling is necessary. (Yakhot et al., 1992)

Turbulence models

Turbulence model is computational method to solve of flow equations derived for all unknowns. In many engineering problems it is no need to solve the details of the turbulence fluctuations but instead, the influences of the fluctuations on the average flow are mostly sought. The following one-equation models are the ones which are mostly used;

- Prandtl's one-equation model
- Spalart-Allmaras model
- Baldwin-Barth model

In the two-equation models, k-ε and k-ω models are the most widely used ones. There are also three kinds of k-ε model. The main equations are the k-ε equations, alternative two equations are refinement or developments to this main model.

Five different turbulence models exist in Flow 3D. Turbulence models are Prandtl's model, one and two equation k-ε, Large Eddy Simulation (LES) and Renormalization Group Method (RNG) model.

Renormalization Group Method (RNG) was improved by Yakhot et al. (1992) to renormalize the RANS equations to calculate for the influences of smaller volumes of motion. The eddy viscosity is specified using a single turbulence length scale in the standard k-ε model. The Renormalization Group Method (RNG) approximation which can be used to multiply turbulence model is a mathematical procedure. This model is similar to the k-ε.

In this thesis Model of Renormalization Group Turbulence (RNG) is used as a turbulence model. RNG and k-ε model solve the RANS equations. However, turbulent equations constants which are found using empirical equations in k-ε model are derived in the RNG model. RNG model usually has extended applicability than other turbulence models. RNG turbulence model describes low intensity turbulence flows and flows having strong shear regions more accurately (Flow 3D Lecture Notes).

2.5 DRAG CALCULATION USING FLOW 3D

In this study, Flow 3D (Flow 3D from Flow Science, CFD. www.flow3d.com) is used as a CFD software. Flow 3D ensures a powerful sofware for complicated fluid modelling topics. Flow 3D allows high degree of precise simulations of free surface flows via TruVOF, an improved version form of the Volume of Fluid (VOF) technique. Flow 3D CFD Software solves the RANS (Reynolds-Averaged Navier-Stokes) equations in three dimensions (x,y,z) to simulate the fluid flow equations together with the continuity equations and some advection equations for the turbulence quantities for turbulence closure.

Flow 3D ensures relieve of accessing to the instructions and menus. In the base window of user-interface, following tools were placed to ensure easy access.

a) File:In this tab, it is probable to conduct several options for simulations, and workspaces, which acts as a container guide.
b) Diagnostics: This tab proposes many options about the simulation such as creation report, computing errors and taking messages about the simulation.
c) Preference: This tab ensures options about the configuration of the program.
d) Utilities: This tab where the licensing and file abbreviation can be controlled.
e) Simulate: This tab permits conducting simulation process.
f) Materials: This tab ensures material data base to export material features directly to the model.
g) Help: This tab ensures accessing to the help file folders.

Navigation tab ensures other options for the simulation file folders. In the model tab setup numerical model is realized. In simulate tab, simulation command can be given and several data about the simulation can be monitored such as average velocity, time step, fluid forces etc. In analyze tab, it is probable to manage post simulation research. Display tab increases the experience by images. In Figure 2.20 you may see these tabs. Model setup is the base part for forming the numerical model. Subsections were listed and explained as follows;

a) General: This subsection permits arrangement compressibility, finish time, simulation units etc.

b) Physics: This subsection the main physical dynamics which are gravity and turbulence models were defined.
c) Fluids: In this subsection, fluids can be identified and features of fluids can be arranged.
d) Meshing and Geometry: In this subsection where geometry of domain is formed and meshing is handled.
e) Boundaries: In this subsection user can be set boundary conditions.
f) Initial: This tab provides the simulation to improve by introducing initial conditions.
g) Output: The output file can be placed in this subsection.
h) Numerics: Numerical methods can be defined in this subsection.

2.5.1 NUMERICAL MODEL IMPLEMENTATION

2.5.1.1 GRID GENERATION

The most essential step to take reliable results with the CFD problems is grid generation. After importing the STL which is called as solid geometries to Flow 3D, grid generation can be created for CFD simulations. Flow 3D uses two types of mesh generation which are Cartesian coordinate systems and cylindrical coordinate systems. In this study, Cartesian coordinate systems are used. Flow region is defined by cells which have the same geometrical properties and volume. To have realistic results, it is necessary to choose suitable mesh size. It also affects the results of the simulation model. Choosing mesh size depends on the many factors listed below;

- Grid Dependency
- Distance from wall boundary to adjacent cells
- Computation time
- Solid geometric quality

Grid Dependency Check requires y^+ calculations in details (Chapter 2.1.4). Grid dependency is calculated and then y^+ value is founded as 81.61 in this study.

The value should be bigger than 5 or 11 to have an accurate CFD simulation with RNG model. Thus our CFD simulations satisfy this condition. In Figure 2.14, y^+ representation of flow is given.

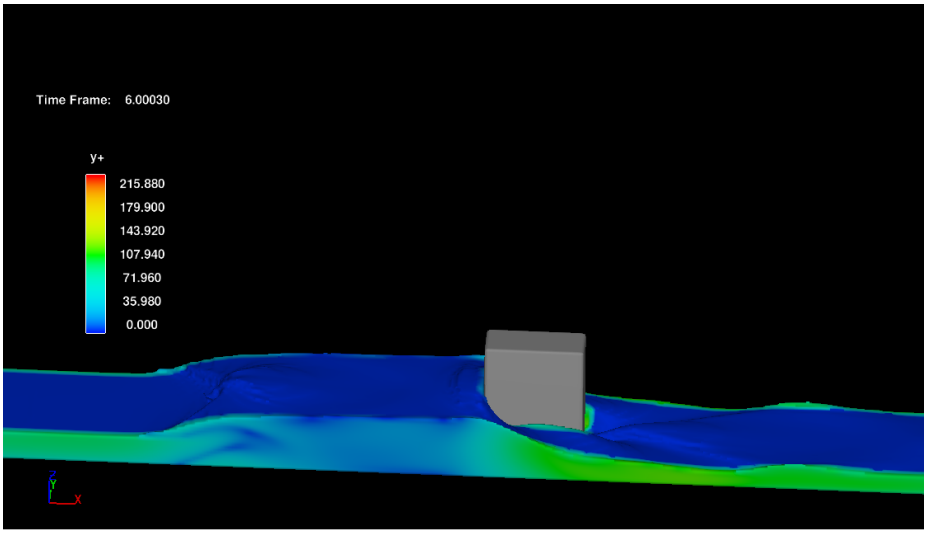

Figure 2.14: y^+

The origin value of cell size is calculated with empirical formulas. Additionally, grid dependency is checked according to the results which have three different cell sizes. After comparing these results, it is deduced that the Flow 3D simulation which have different mesh sizes give similar results. Then results are compared with experimental analysis, it is observed that they have similar outputs. In Figure 2.15, outline view of flow domain is given.

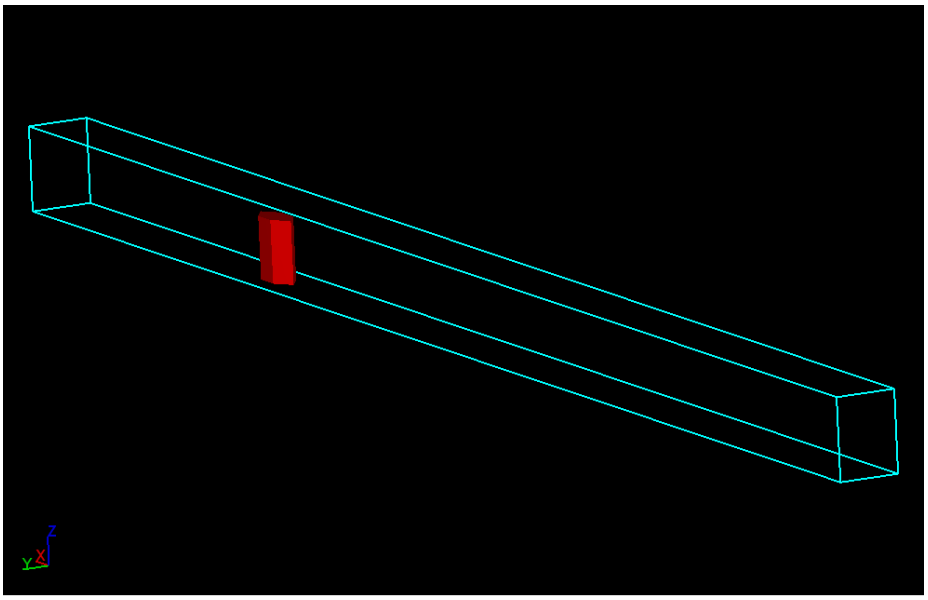

Figure 2.15: Outline view

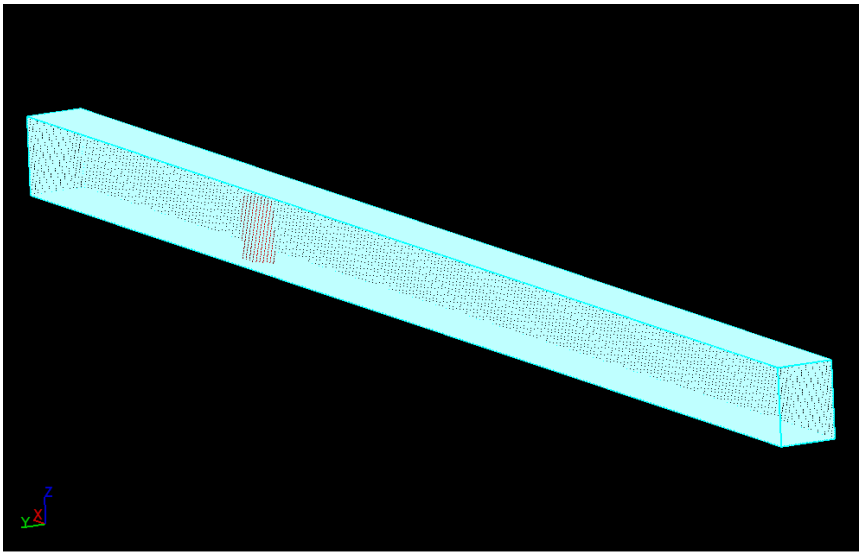

Figure 2.16: Mesh view

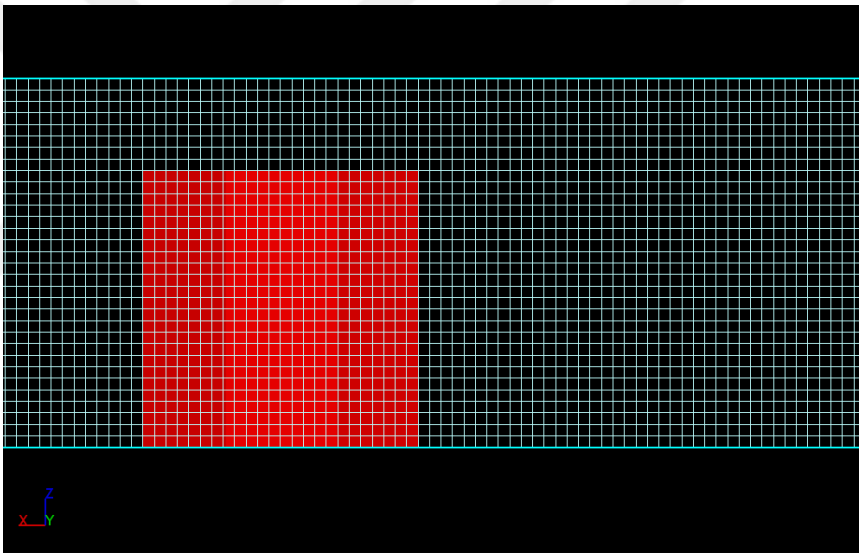

Figure 2.17: Mesh detail view

The computation time is important for completing the analysis and for specifying steady state conditions. It is observed that calculations of inflow discharge and outflow discharge are the same and net flux is zero. It is also observed that surge formation is completed before computation time is finished. Surge formation increases upstream water level. After completing surge formation, it is realized that the drag force values are constant. In Figure 2.16 and 2.17, represent the mesh generation of flow domain.

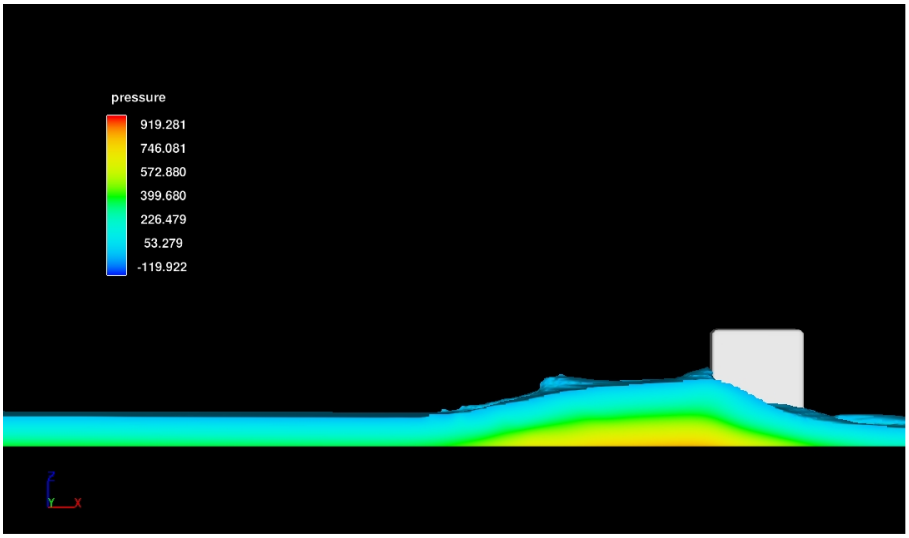

T = 4 s

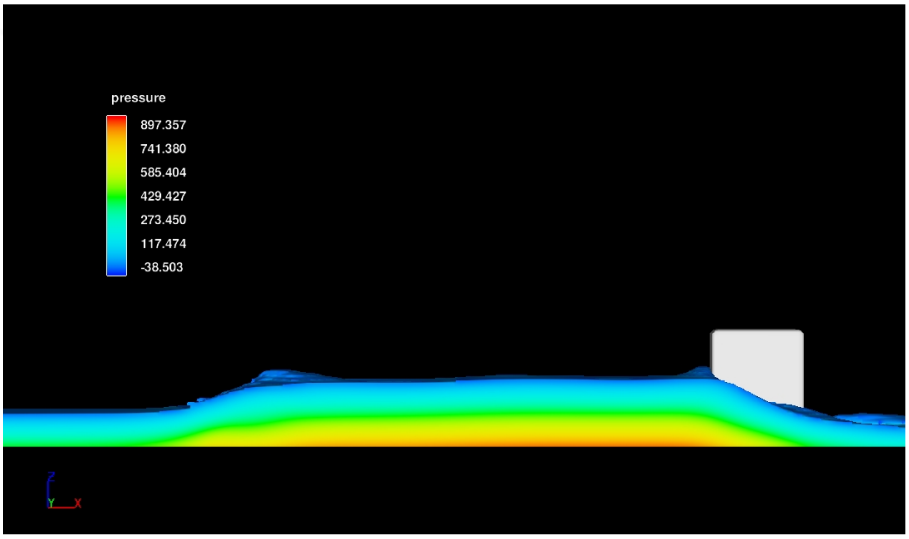

T= 6 s

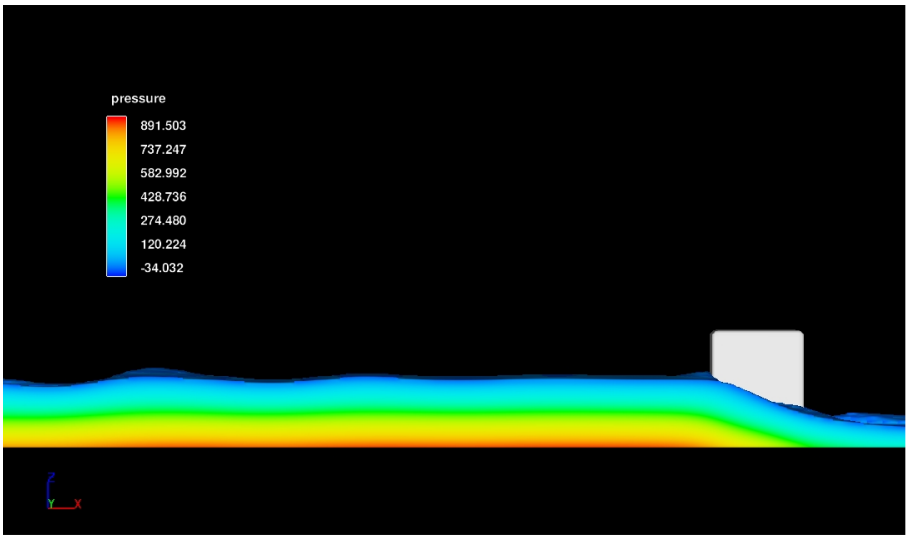

T = 10 s

Figure 2.18: Representation of T=4 s, T=6 s and T=10 s

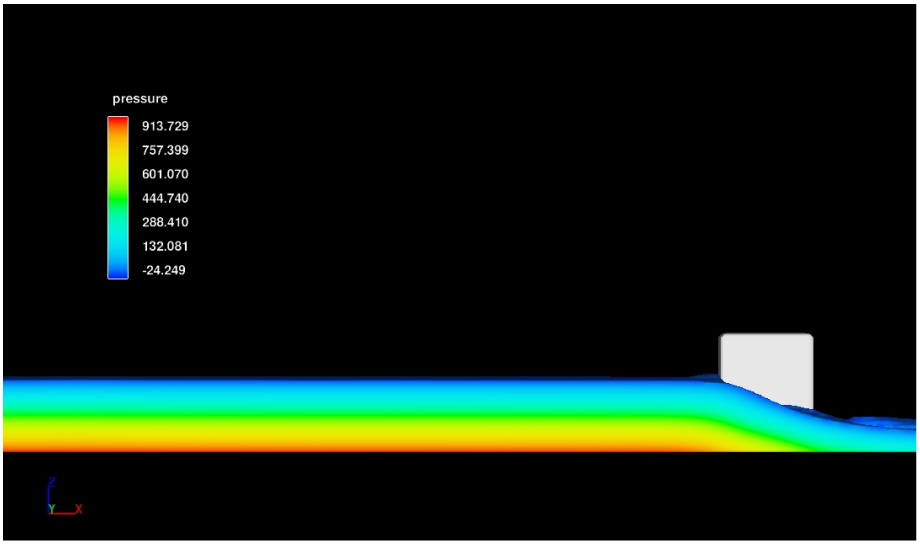

T = 15 s

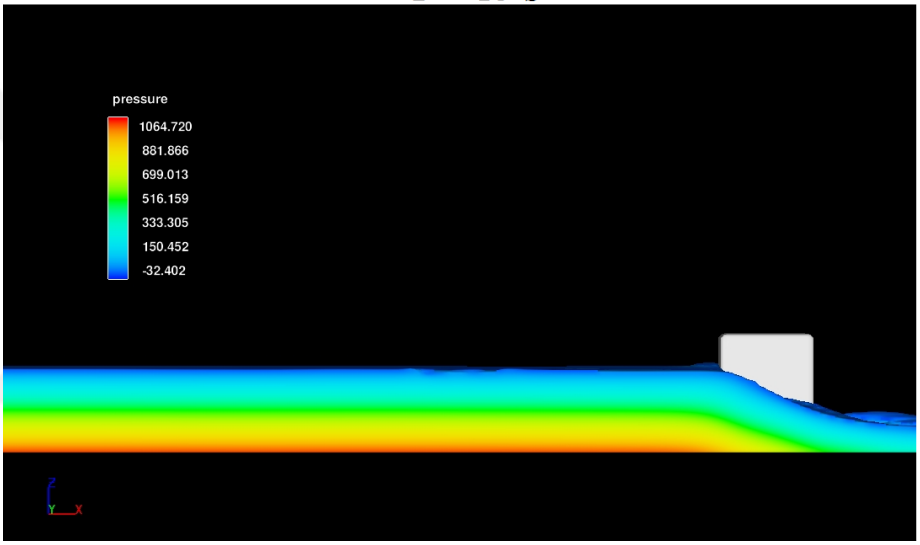

T = 30 s

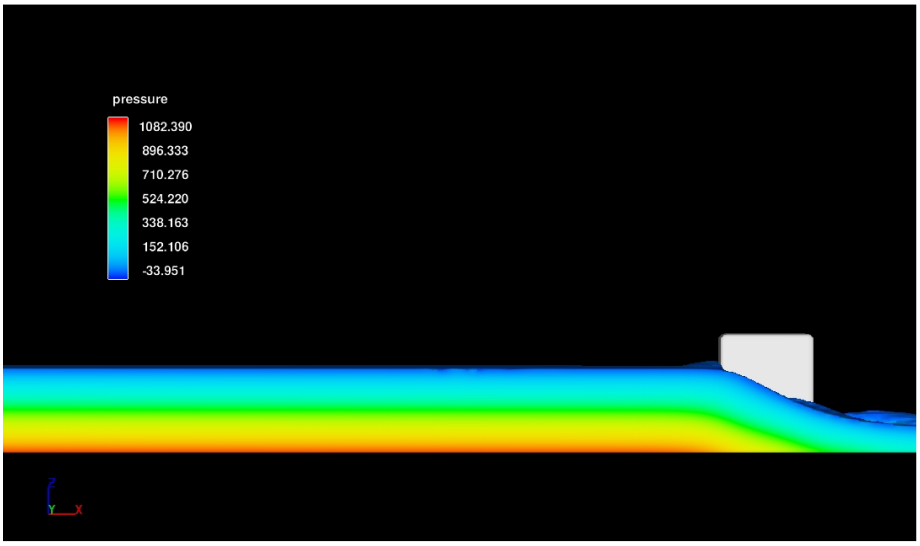

T = 60 s

Figure 2.19: Representation of T=15 s, T=30 s and T=60 s

In Figure 2.18 and 2.19, unsteady flow around pier is shown in the open channel. Time of 4 s, 6 s, 10 s, 15 s, 30 s and 60 s are captured from simulation. Time of change of water level and surge formation are also shown in given figures.

The solid geometry step is also important component which affects the CFD simulations. To have an accurate CFD simulation results, solid geometry should be drawn carefully. The coordinates and rotations of solid geometry should be also defined according to analysis in the flow domain.

In this study, drag force acting on piers is investigated. In this respect, pressure and shear force outputs are activated in the 'mesh and geometry' tab. This tab shows fluid force magnitudes on x, y, z directions and their combinations acting on solid geometry. In Figure 2.20, 'Meshing and Geometry' tab is given.

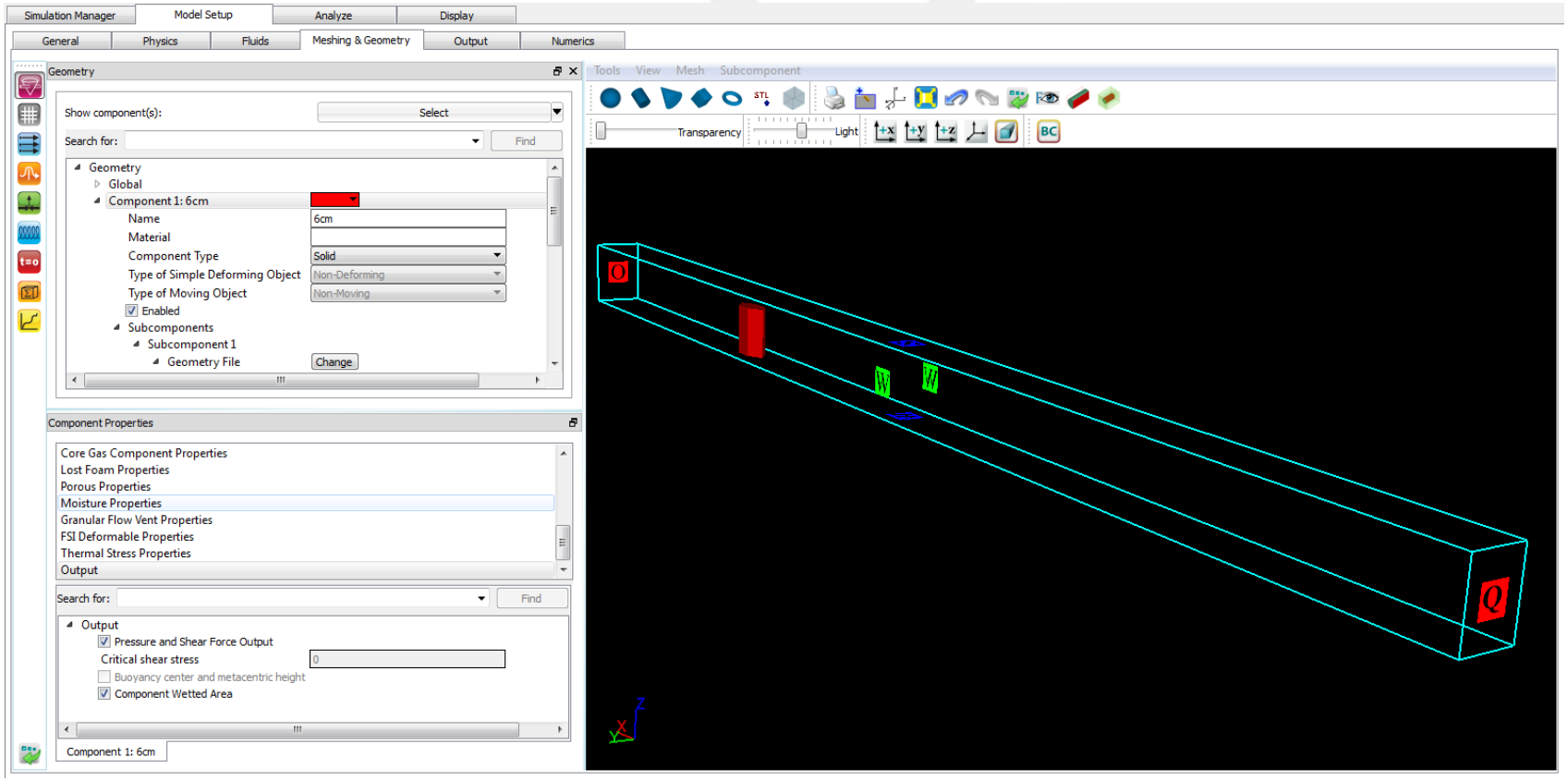

Figure 2.20: Output tab

2.5.1.2 INITIAL AND BOUNDARY CONDITIONS

For accurate numerical analysis, definition of boundary conditions is an important step in the simulation setup. Definition of boundary conditions generate flow characteristic with physical conditions. In this study, six boundary conditions described in the rectangular prism. Defined boundary conditions are as follows:

Upstream boundary : Volume Flow Rate boundary condition
Downstream boundary : Outflow boundary condition
Bottom Boundary: Wall boundary condition
Top boundary: Symmetry boundary condition
Side boundary : Wall boundary condition

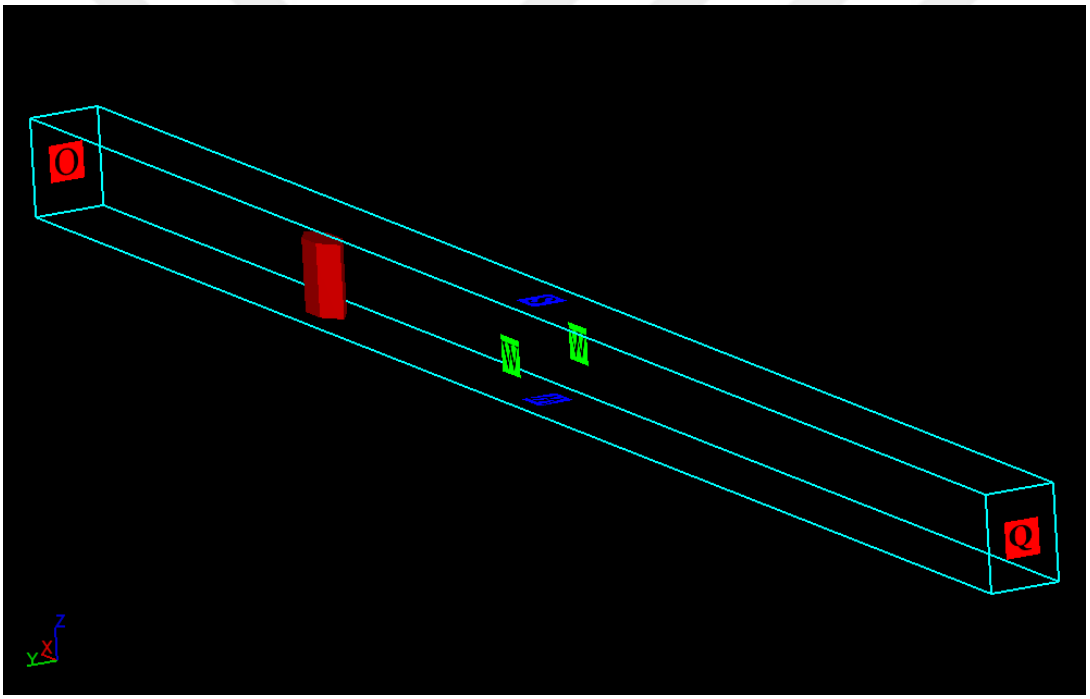

Figure 2.21: Boundary conditions

2.5.1.3 PHYSICS

Physical parameters are defined using physics tab shown in Figure 2.22 in Flow 3D CFD software. For modelling incompressible and 3D flow conditions, in physics tab 'gravity and non-inertial reference frame' and 'viscosity and turbulence' tabs activated. According to the Flow 3D coordinate system, z component of the gravitational acceleration is defined 9.81 m/s^2 with using 'gravity' tab. 'Active non-inertial reference frame' tab is not activated because this tab does not relevant for this numerical investigation.

Flow is defined as 'viscous flow' via 'viscosity and turbulence' tab. 'Renormalized group (RNG) model' has been selected for turbulence model. Additionally for turbulence model 'dynamically computed' method is defined in the turbulent mixing length tab. 'No-slip boundary conditions' is assumed for flow conditions and activated using 'viscosity and turbulence' tab as shown in Figure 2.23.

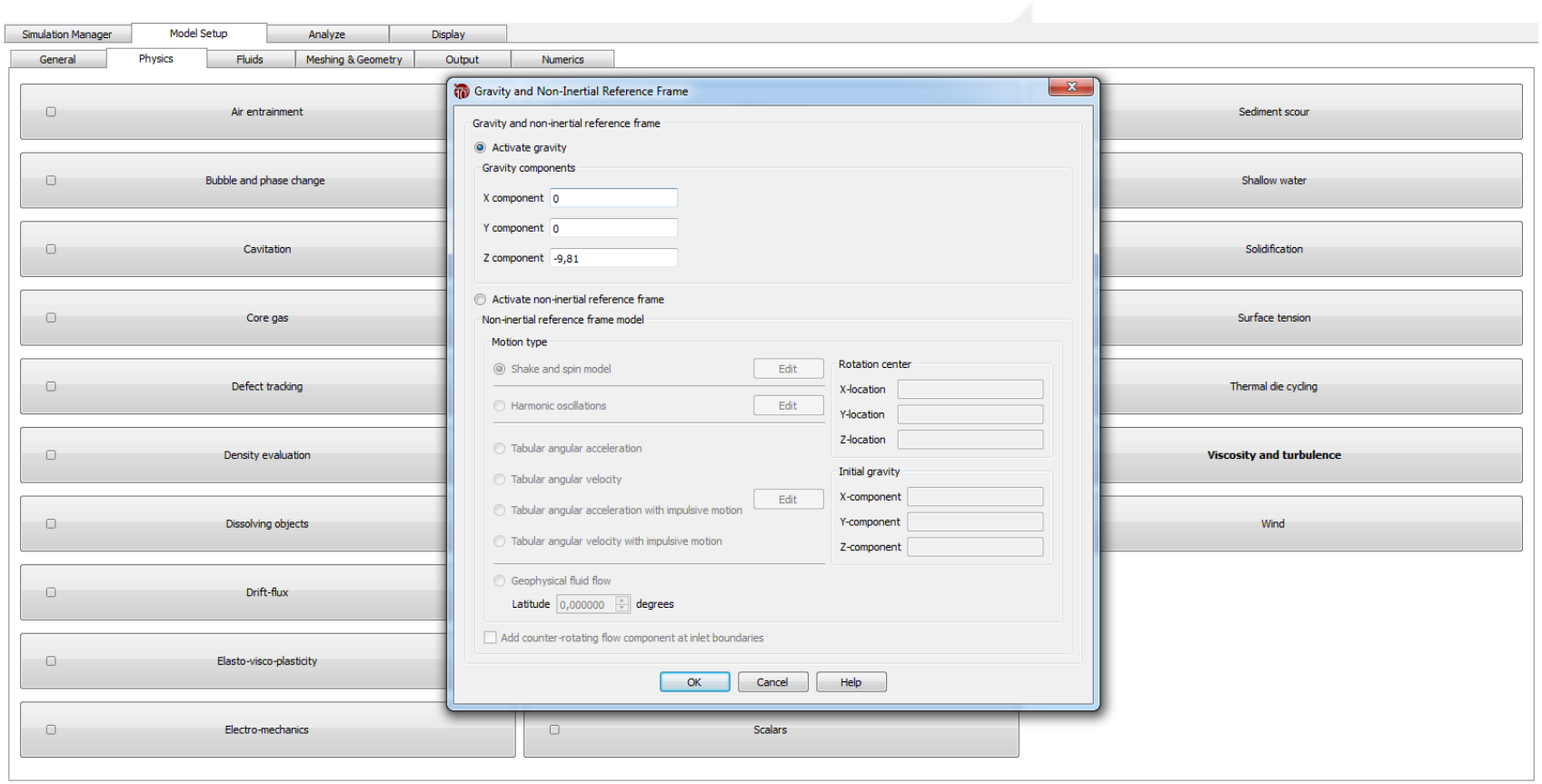

Figure 2.22: Gravity tab

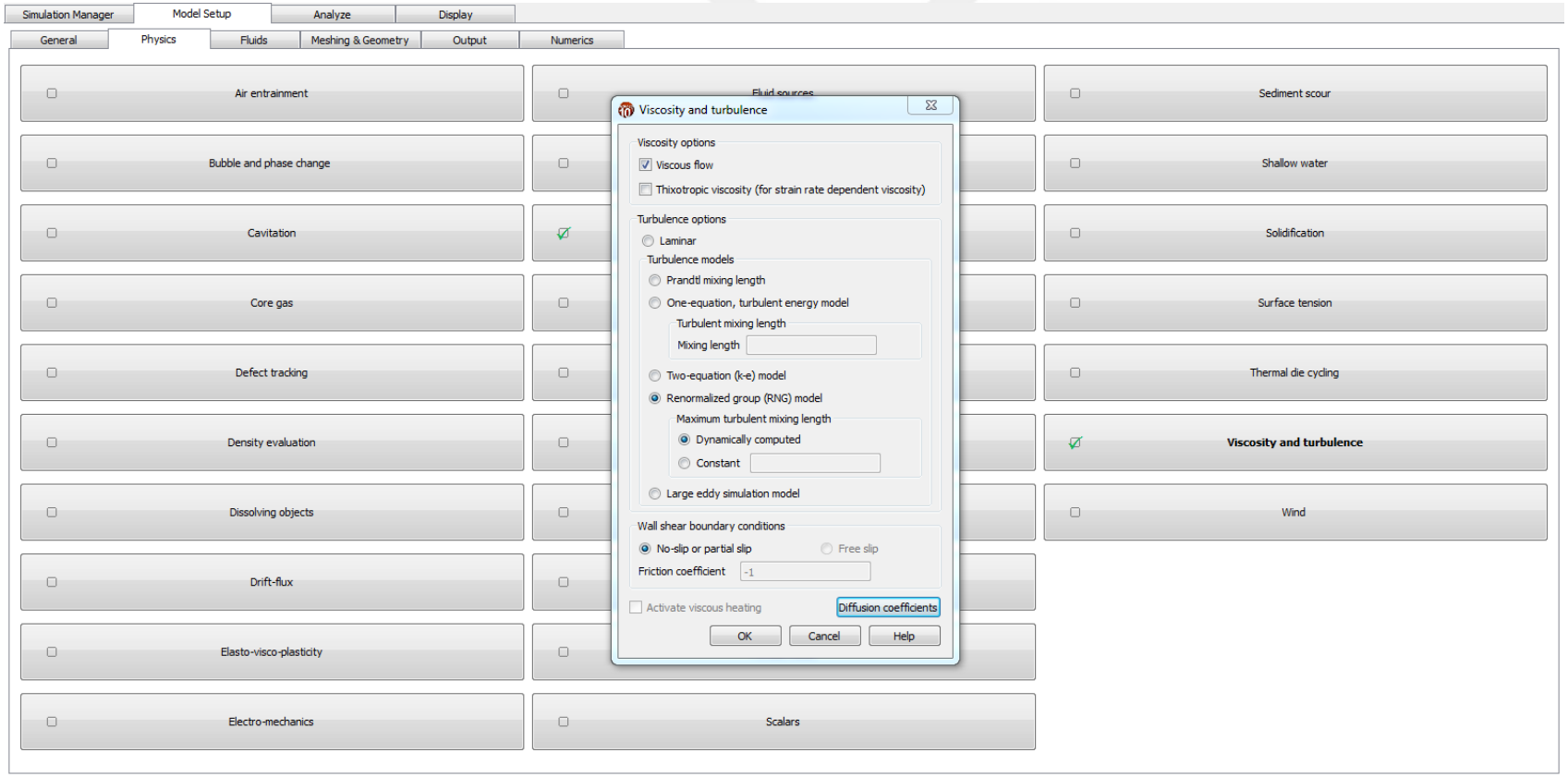

Figure 2.23: Turbulence tab

2.5.1.4 MATERIAL PROPERTIES

'Fluids' tab can be used for definition of type of fluid in Flow 3D. Fluid properties, which are density, viscosity, temperature, etc., can also be defined by using this tab. There is a fluid library in Flow 3D 'fluids' tab which has a lot of common used fluid types such as water. In this study, water is used as a liquid in CFD simulations. Temperature of water is chosen 293 K as default conditions in this tab as shown in Figure 2.24.

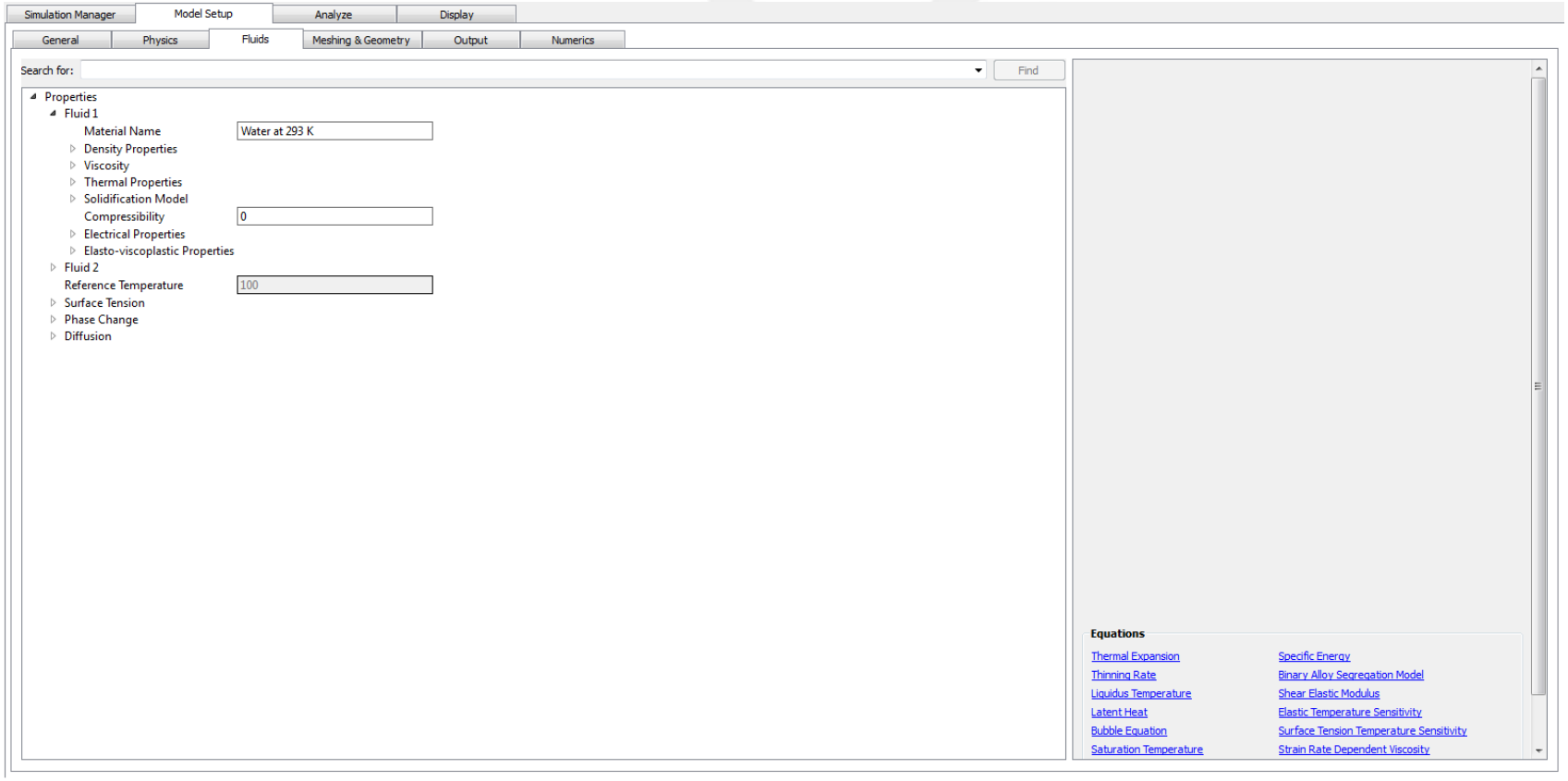

Figure 2.24: Fluids tab

2.5.1.5 SOLVER OPTIONS

Solver options can be defined by using 'Numerics' tab in Flow 3D given in Figure 2.25. In this section, definition of running conditions will influence results and process of numerical analysis. Numerical approximations, time step size, convergence options and solution methods are significant factors that affect the results and time of simulation. In this study, water is used as a fluid. Additionally, fluid is assumed as 'incompressible' and this tab has been activated by using 'Numerics' section. 'Free surface or sharp interface' parameter is defined in terms of 'interface tracking'. 'One fluid' method is defined and 'SI' metrical system is used for CFD simulations. 'Celsius' is chosen as a temperature unit system.

'Implicit' has been identified for pressure solver technique. 'GMRES' tab is activated for algorithms method as default. 'GMRES' is an iterative method for solving pressure. Viscous stress solver is defined as 'Explicit'. 'First-order momentum' solution would be appropriate for free surface flow problems like in this investigation. Because of that reason, this tab is activated during preprocess. 'Momentum and continuity equations' is also selected as fluid flow solver options.

Implicit method requires a final step, which is the testing of the current accelerations and forces for convergence. The convergence test is made on the acceleration, force and torque components of fluid. The change in each acceleration component between iterations must be less than the criterion of convergence. If convergence is not achieved within this limit, the calculation is aborted and an error message generated (Flow 3D Documentation, Release 10.1.0 (2012).

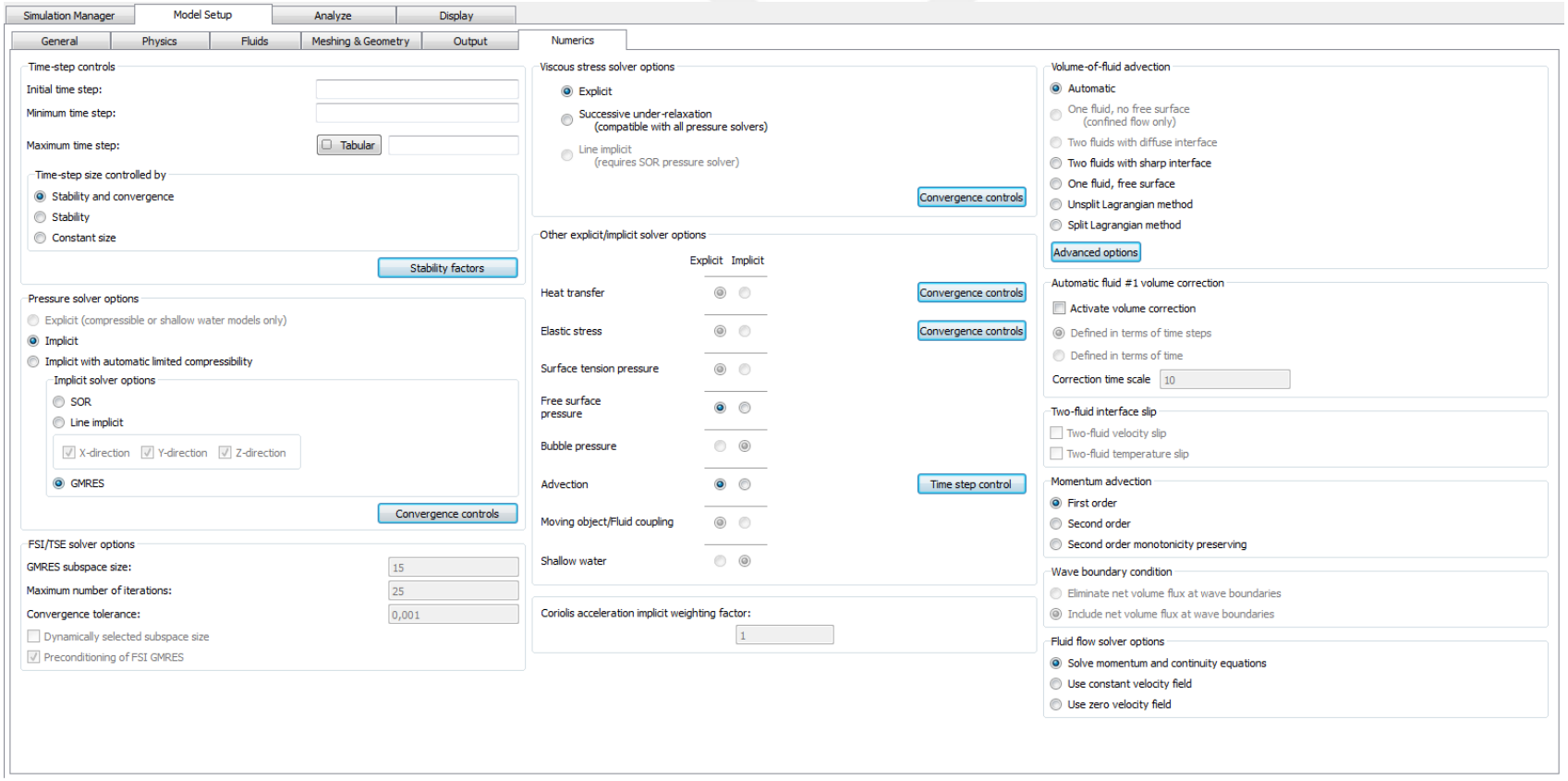

Figure 2.25: Numerics tab

CHAPTER 3

RESULTS

3.1 EFFECT OF SHAPE OF THE PIER ON DRAG (FLOW 3D)

In this part of the study, the piers of different shapes having the same projected area of contraction, b/B=0.33 were simulated for different discharge conditions. b represents width of pier and B represents width of channel, respectively. The shapes are circular, rectangular, elliptical, rhombus, rectangular with triangular nose and tail, rectangular with semicircular nose and tail. Two models of triangular ends having varied lengths of the triangular portion were developed to study triangular-end effect. Numerical investigation is carried out in 4m-long hydraulic flume similar to the one used for the model validation with 0.15 m width. The maximum discharge that is used in this part of the study is 0.006 m^3/s.

In the study Reynolds Average Navier Stokes (RANS) simulations are carried out using Flow 3D. RNG k-ε model is used for the turbulence closure. The free-surface of the flow is tracked using Volume of Fluid (VOF) method. In VOF calculations, the volume fraction in a cell represents how much of that cell is occupied by air and how much of it is occupied by water. The inlet is treated as mass flow inlet and the outflow is treated as mass flow outlet. The bottom and side boundaries are no-slip boundaries. Top boundary is treated as a slip boundary. In the simulations time step is taken as 0.1 s. All simulations are carried out for 60 s.

In Figure 3.1 water surface elevation (in m) is presented as contour plot for circular bridge pier at t=60 s where flow has reached steady state condition. For t>60 s no change in Z is observed for all the simulations considered in the study.

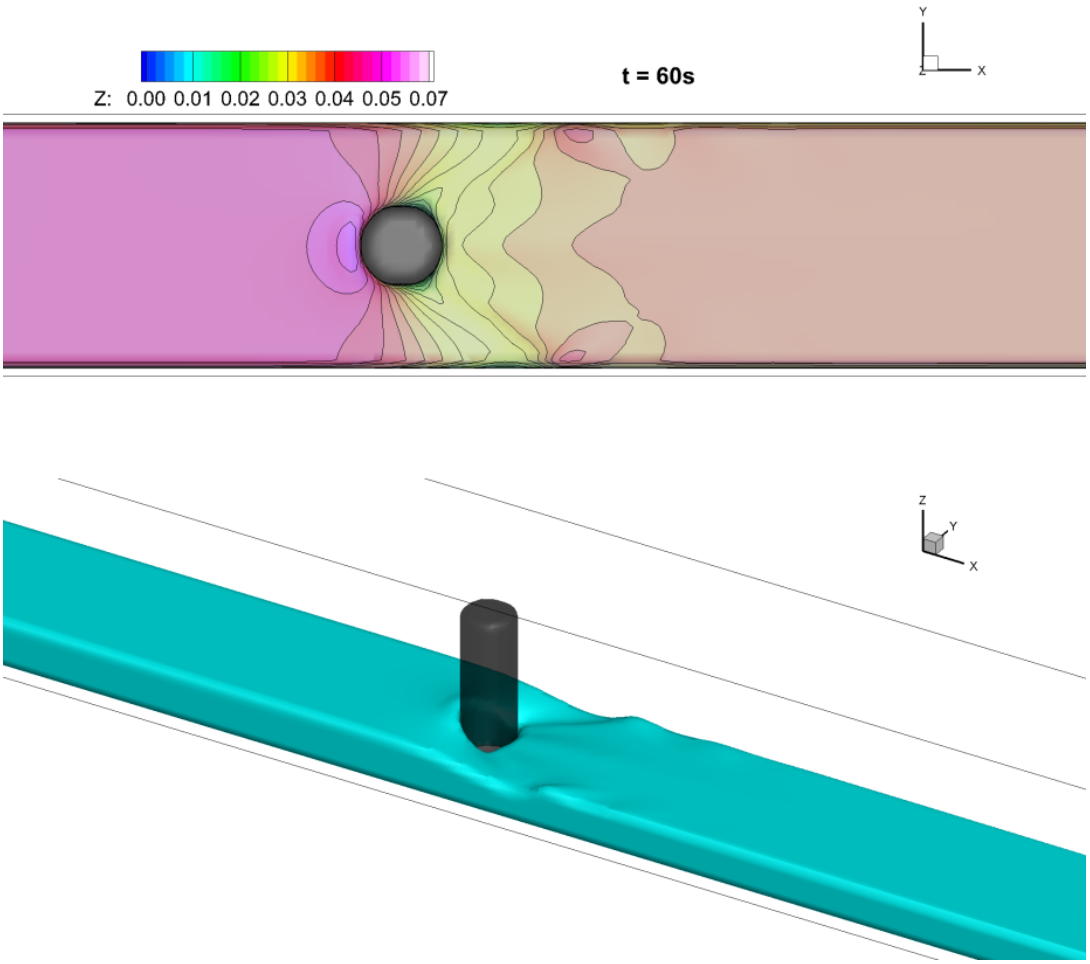

Figure 3.1: Water surface elevation z (m) for circular bridge pier

Three dimensionality of the flow can be seen in the Figures 3.2 and 3.3. In Figure 3.2, the water surface elevation at the back and in front of the pier is shown at t=12 s. At this time in the simulation the flow has already interacted and a backward propagating surge has already leave the vicinity of the pier. Even early on in the simulation, we can observe the difference between the water surface profiles in three cases. At the end of the simulation difference between all three cases in terms of water surface elevation becomes very clear.

Figure 3.3 shows the free surface levels at the end of the simulation time. The raised water surface at the back of the rectangular pier is quite distinct. The shape of the free surface after the pier is also very different in each case. The minimum backwater rise is observed in the circular shaped pier. The impact of the pier penetrates further downstream in the rectangular and rectangle-triangle nose cases compared to the better streamlined circular case. The discharge used in all three cases are identical and equal to 0.006 m^3/s. Even though all the simulations shown in these figures have the identical initial and boundary conditions the effect of the pier shape is clearly observed in the water surface elevation. This has direct effect on drag experienced by the piers.

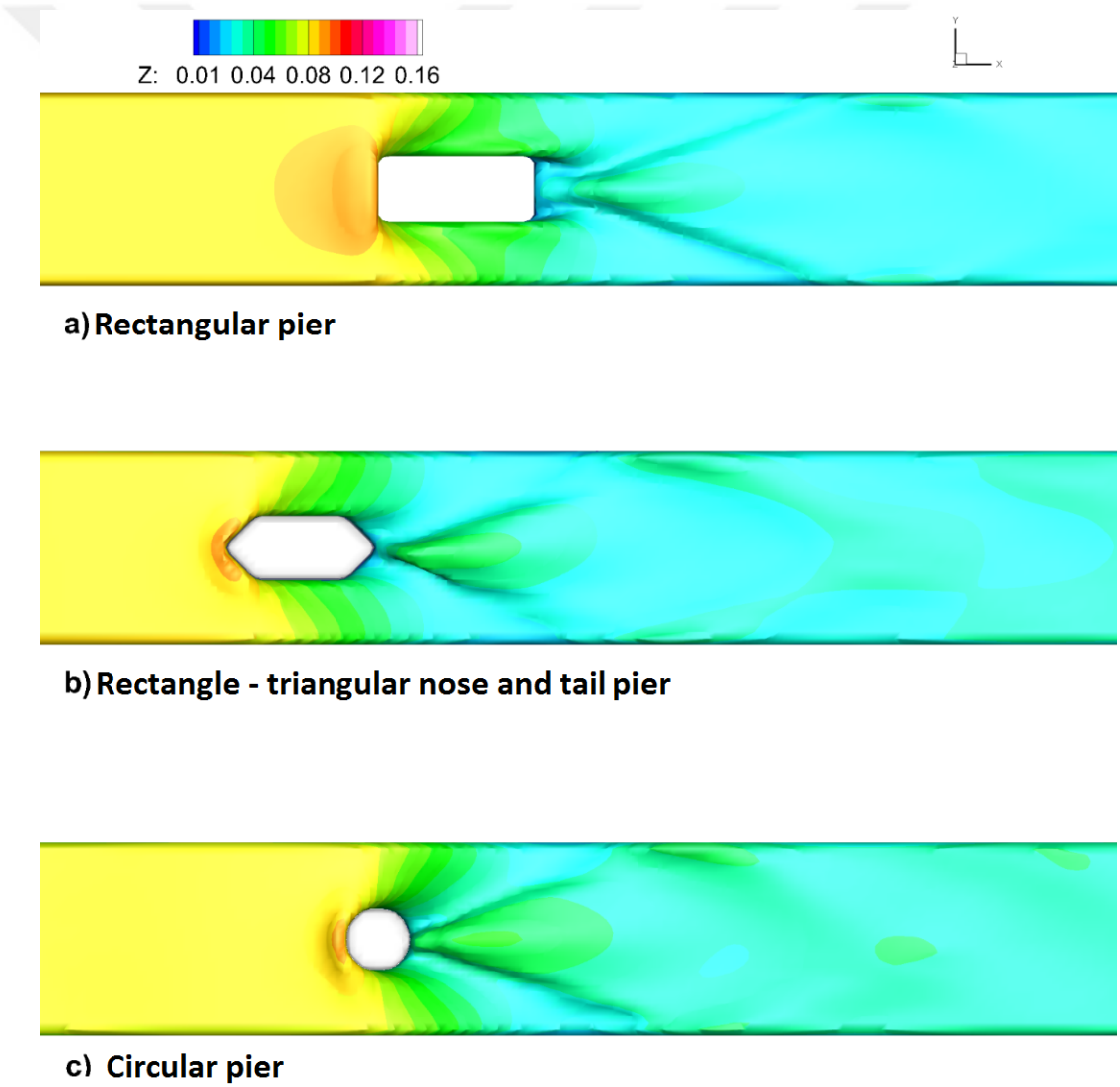

Figure 3.2: Elevation of free surface at T=12 s

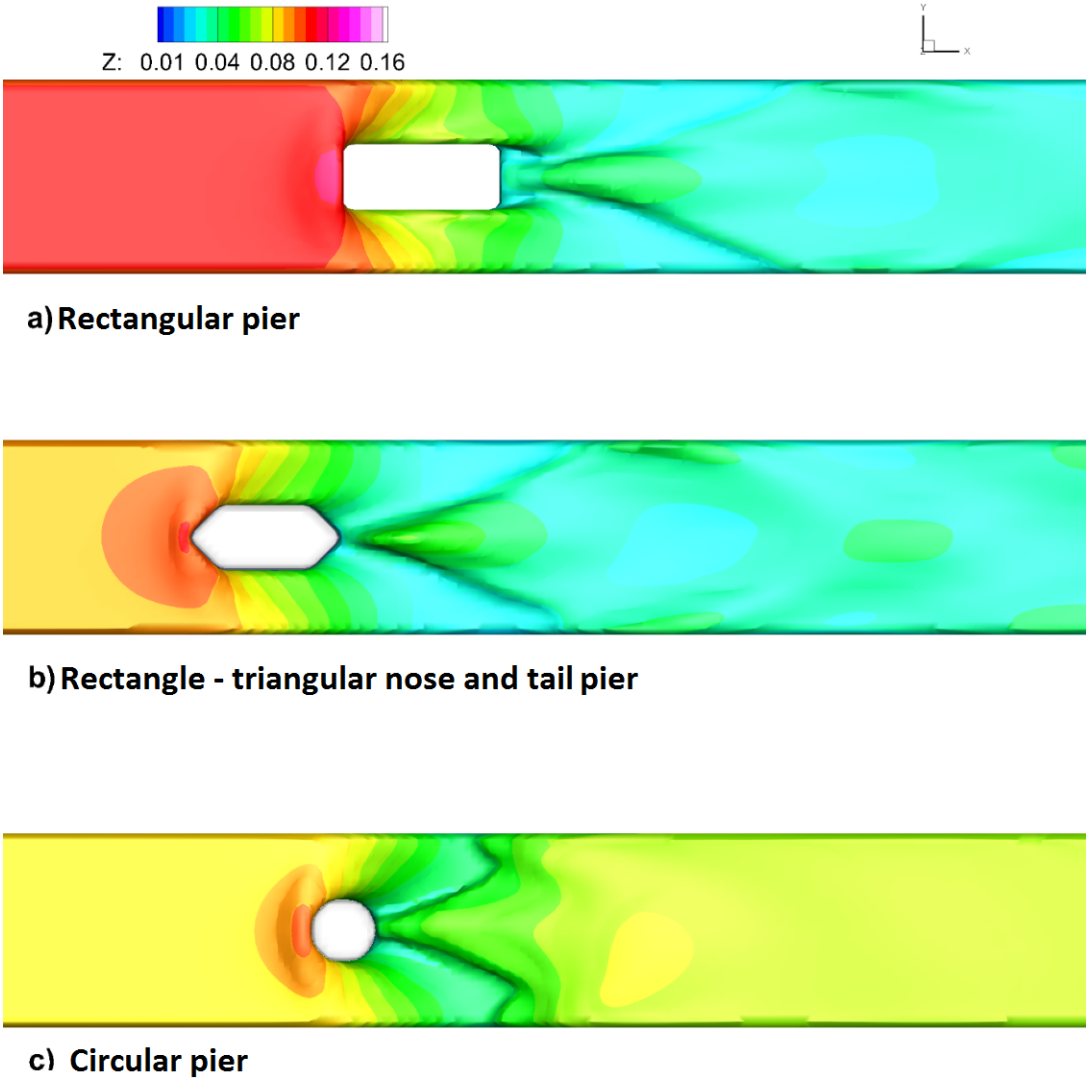

Figure 3.3: Elevation of free surface at T=60 s

Figure 3.4 shows the water surface elevation from the side of the channel. The quick recovery of the free-surface profile in the downstream of the circular pier can clearly be observed in the final frame compared to the other two blunt cases. The backwater level decreases further and further as the bluntness of the shape of the pier goes from rectangular to the circle for the same flow condition.

The chaotic nature of the flow is shown with the streamlines given in Figure 3.5. Especially at the downstream side of the rectangular pier, formation of vortices shows the separation of the flow from the solid boundary as it takes over the pier. Such separation and formation of the vortices in the lateral plane are not observed for more

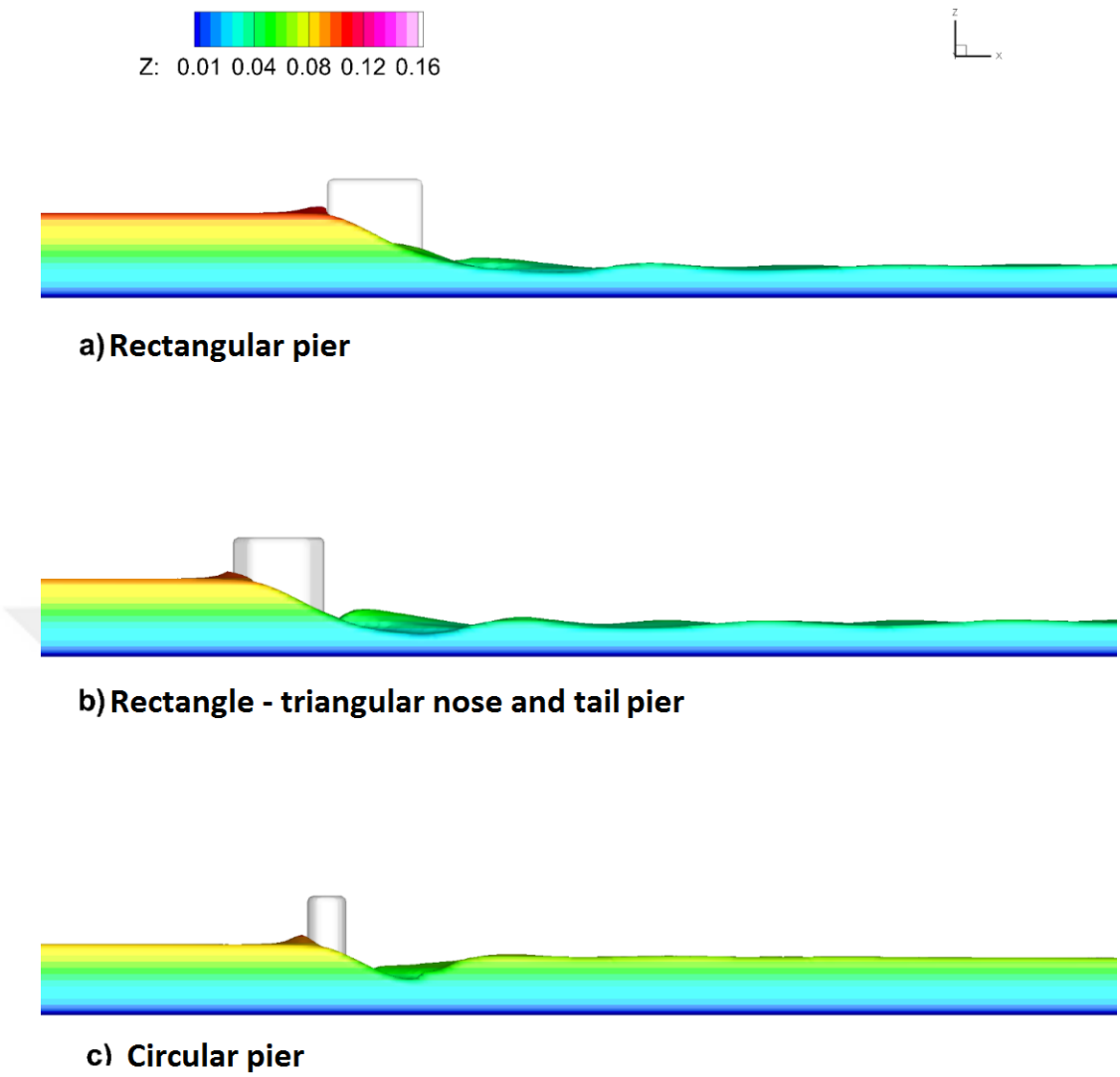

Figure 3.4: Side view of the water surface elevation at T=60 s

streamlined cases as seen in the figure. The yellow streamlines in this figure are based on all three velocity components (u, v, w) while the black streamlines are given on a plane parallel to the channel floor at a 10-cm distance and shows the flow in two dimensions around the pier. However, close to the channel floor in certain flow conditions, one can observe formation of a vortex near the pier wall on the downstream side.

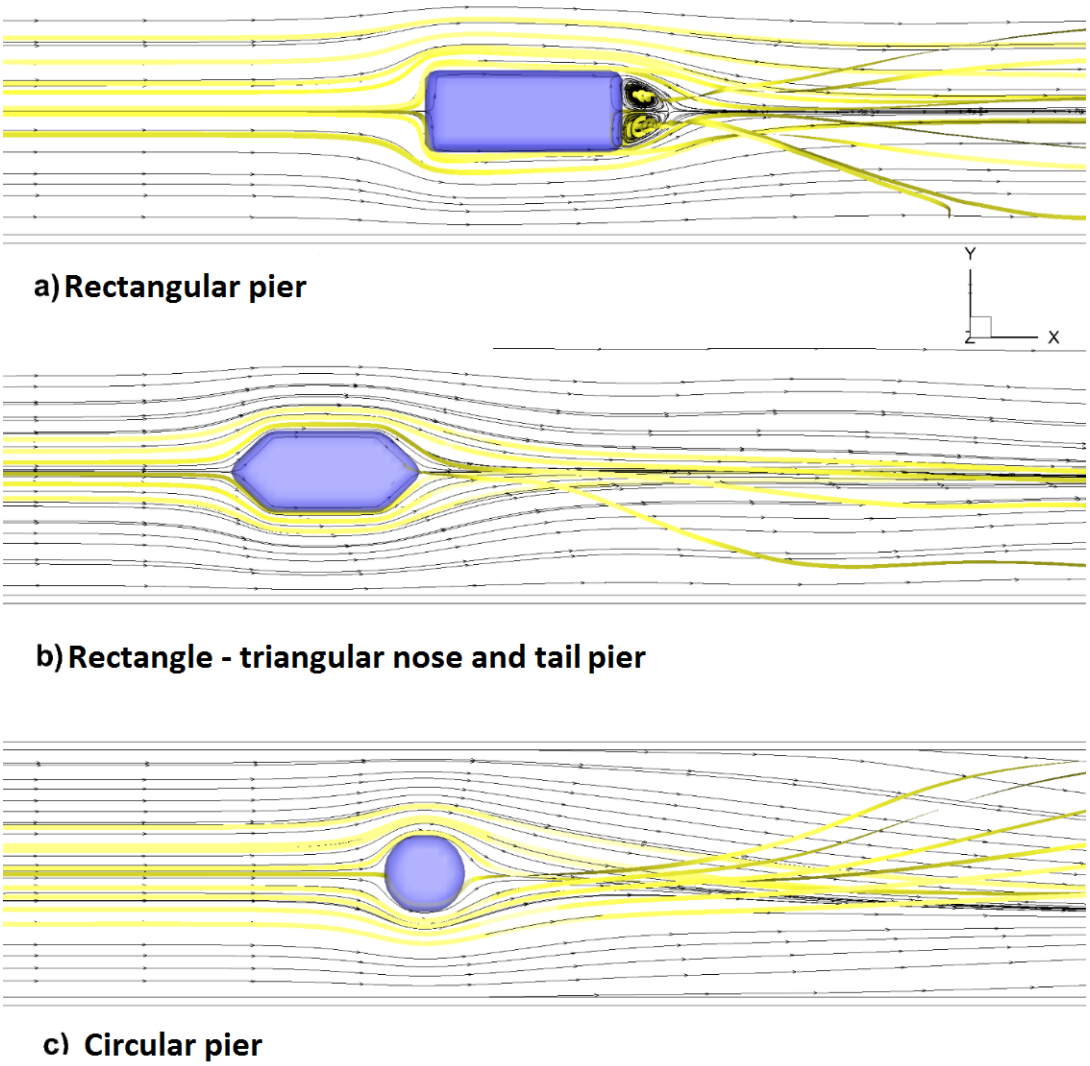

Figure 3.5: Three dimensional streamlines (yellow) and two dimensional streamlines at a surface 0.05 m away from the channel floor at T=60 s

Figure 3.6 shows formation of such vortex near the circular pier. Despite the fact that the shape of the pier is streamlined, the flow around it is still three dimensional and rotational, hence the use of three dimensional model is important in investigation of flow around bridge piers. Even though in this study flow structures are not investigated, their presence and accurate modelling is necessary to calculate the drag coefficient for these piers.

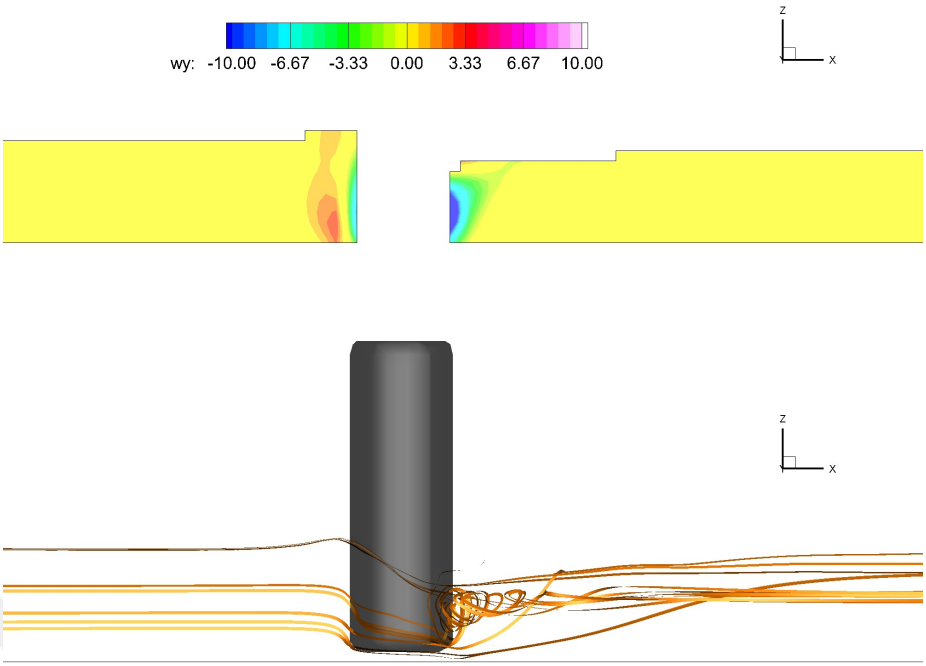

Figure 3.6: Out of plane vorticity 3D streamlines

Table 3.1 shows other pier shapes and discharge values in m^3/s considered in the study together with the drag force values found through these simulations. Figure 3.7 shows the drag force on rectangular, square shaped and rectangular pier with curved ends. These are representative of blunt shaped bridge piers. The highest drag as expected was observed for rectangular pier. Due to bluntness of rectangular pier, the form drag adds on significantly to the total drag foce. As shown in the figure using curved ends instead of sharp ones decreases the drag force on the pier drastically especially for higher discharge values. Even so, a curved end rectangular pier experiences lower drag force compared to a square shaped pier, which has shorter side length compared to the rectangular pier. However, this difference is not as visible for lower discharge values of 0.001 m^3/s and 0.002 m^3/s. For lower discharge drag forces are very close to each other for all three cases.

As the shape of the pier becomes more streamlined, the drag force that it experiences decreases. Figure 3.8 shows the drag forces on rectangular piers with triangular noses and tails, rhombus shaped, circular and elliptical piers. Both rhombus and circular shaped piers have the lowest drag forces acting on them. All piers experience max-

Table3.1: F_d (N) values attained from simulations

Discharges (m^3/s)	**0.006**	**0.005**	**0.004**	**0.003**	**0.002**	**0.001**
Pier Shape	**Drag Force (N)**					
Circular	1.317	1.125	0.803	0.501	0.288	0.095
Elliptical	1.646	1.383	1.094	0.627	0.381	0.209
Rectangle with curved ends	2.356	1.882	1.439	0.985	0.611	0.238
Rectangle with triangular nose and tail 2.5 cm	2.084	1.704	1.361	0.906	0.472	0.182
Rectangle with triangular nose and tail 3.5 cm	1.878	1.634	1.317	0.947	0.462	0.239
Rectangular	2.939	2.390	1.827	1.252	0.586	0.220
Square	2.436	1.967	1.525	1.075	0.541	0.176
Rhombus	1.356	1.005	0.875	0.548	0.368	0.214

imum drag at the highest discharge simulated. The drag force acting on rectangular pier under 0.006 m^3/s discharge is almost 2.2 times higher to the one that acts on a rhombus or circular shaped pier under the same flow discharge.

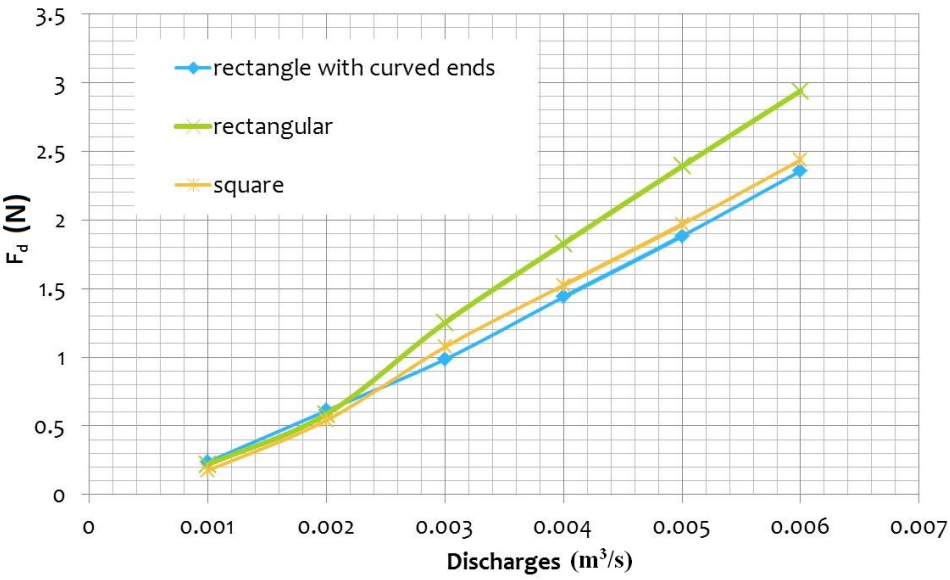

Figure 3.7: Drag force on rectangular pier, square pier and rectangular pier with curved ends for six discharge values

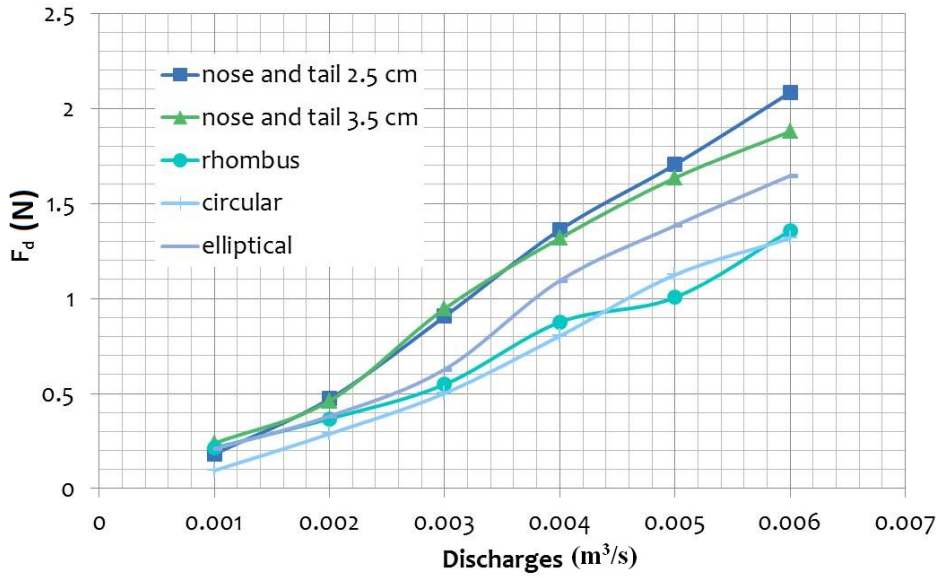

Figure 3.8: Drag force on rectangular pier with triangular nose and tail, rhombus pier, circular pier and elliptical pier for six discharge values

3.2 DRAG FORCE ON CIRCULAR PIER FOR DIFFERENT DISCHARGE A COMPARISON BETWEEN FLOW 3D AND FLUENT

In this part of the study, only circular pier shape is used and it has the same projected area of contraction ratio of 0.33 were simulated for different discharge conditions as in the previous study. Circular pier is simulated using Fluent and Flow 3D. Numerical investigation is carried out in 4 m-long hydraulic flume similar to the one used for the model validation with 0.15 m width (Agarwal et al., 2014). The maximum discharge that is used in this part of the study is 0.006 m^3/s.

In the previous section of the study Reynolds Average Navier Stokes (RANS) simulations are carried out using Flow 3D. RNG k-ε model is used for the turbulence closure. The free-surface of the flow is tracked using Volume of Fluid (VOF) method. In Fluent simulations, SST k-ω model is used for the turbulence closure. Obstacle hugging meshes (hex mesh) are also used in Fluent simulations. Different from Flow 3D in Fluent air phase is also involved in the simulations. The bottom and side boundaries are no-slip boundaries. Top boundary is treated as a slip boundary. In the simulations

time step is taken as 0.01s. All simulations are finished when inlet flow and outlet flow become equal. Additionally, drag forces checked until it reached a constant value.

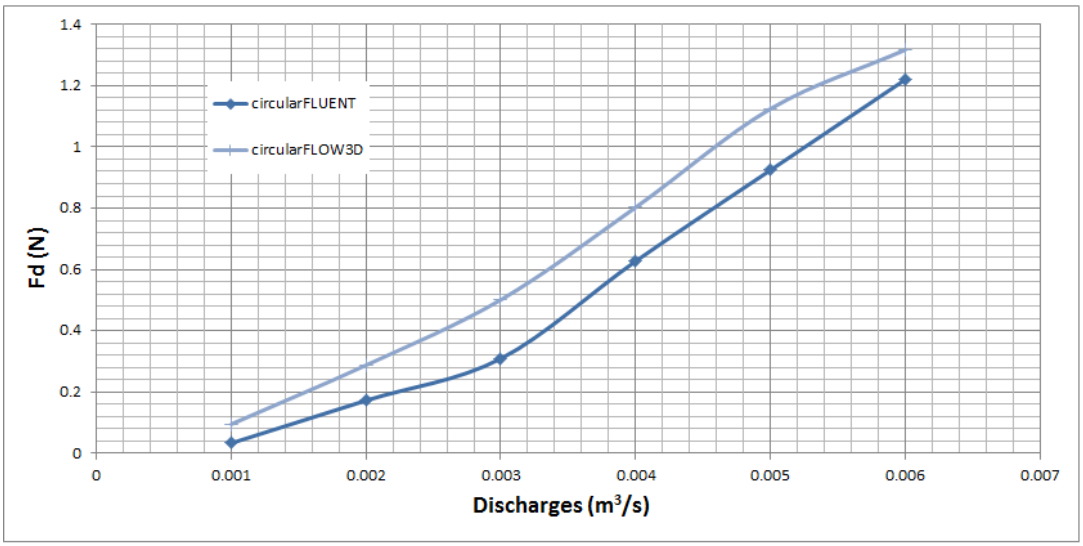

Figure 3.9: Comparison of values of drag force from Flow 3D and Fluent simulations

In Figure 3.9, drag forces which are calculated from Flow 3D, Fluent and analytical method for circle pier are presented. CFD software programs that are Flow 3D and Fluent give very close results.

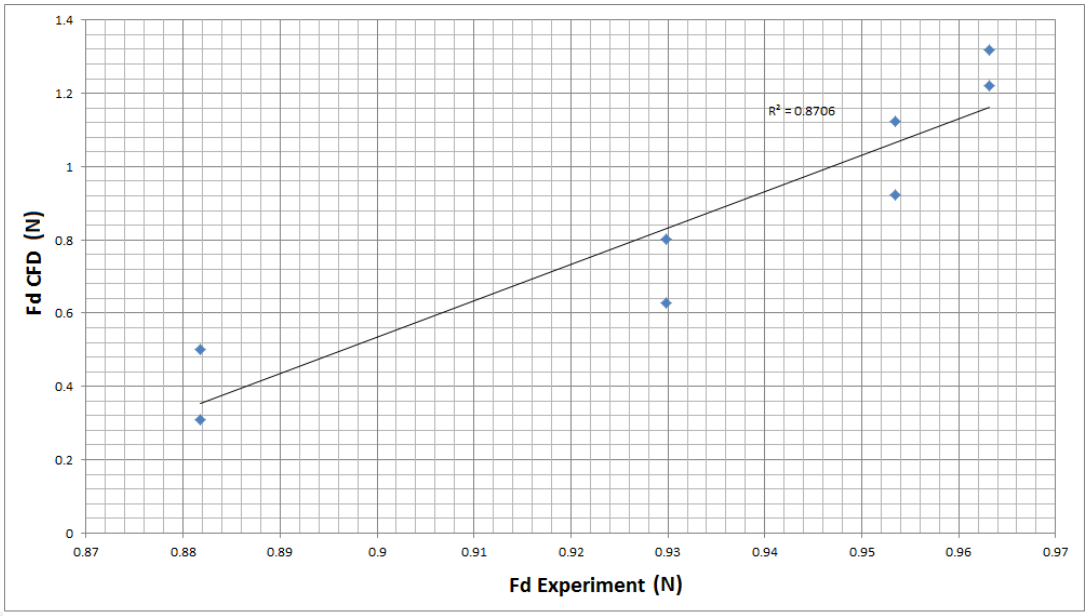

Figure 3.10: Comparison of values of drag force from simulations to ones from experiments of Agarwal et al. (2014)

In Figure 3.10, CFD simulation results and experimental results have been compared. It is observed that the competitive results are similar to the level of 87 percent (R^2). For maximum discharge, the percentage error, e , between numerical solutions of Flow 3D and Fluent is 7.3 %. The error, e is defined as;

$$e = \mid \frac{Fd_{Fluent} - Fd_{Flow3d}}{Fd_{Flow3d}} \mid \times 100 \tag{3.1}$$

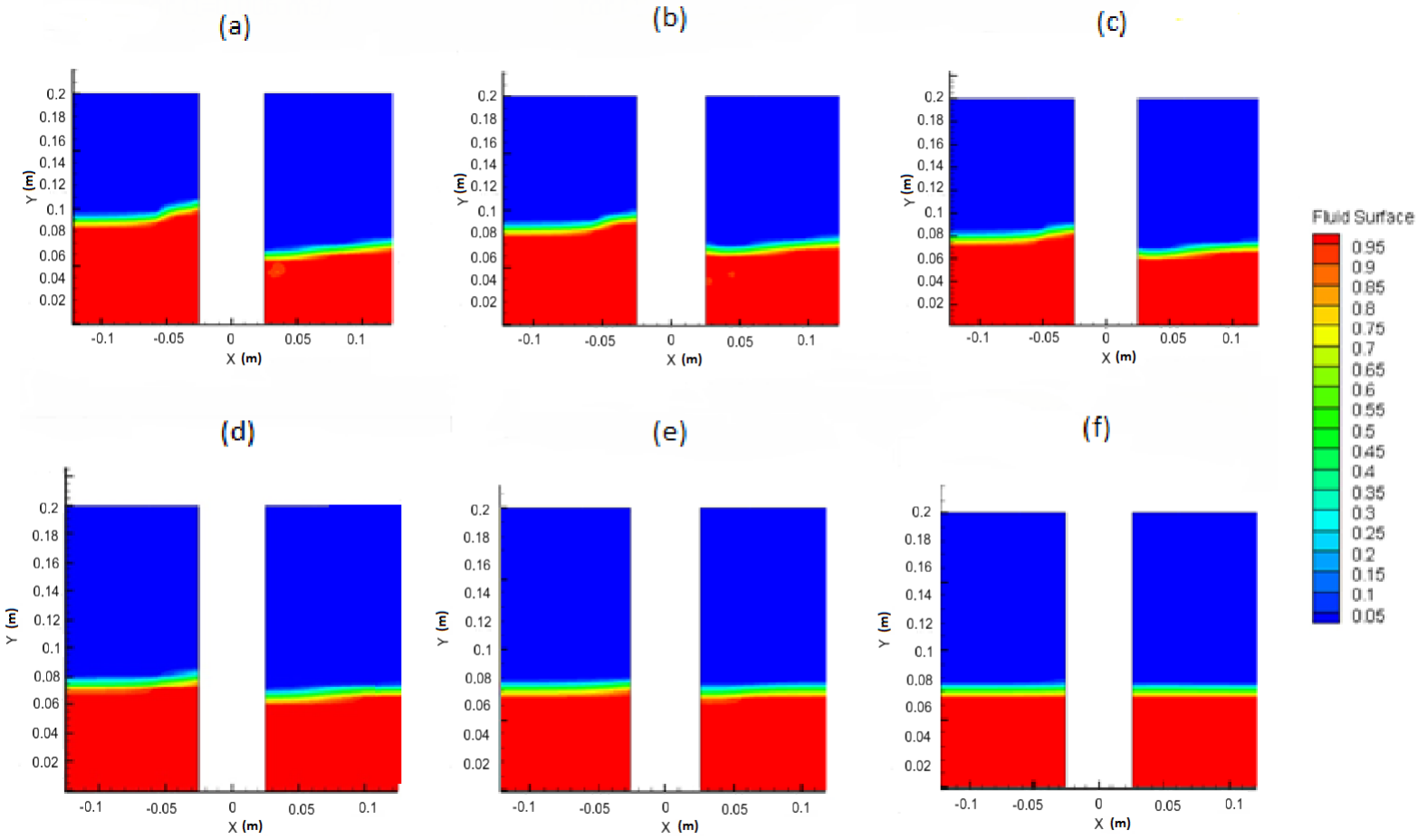

Figure 3.11: Water surface levels both upstream and downstream sides during the steady state conditions (Fluent)

Figure 3.11 shows the results of the simulations using Fluent CFD Software during the steady-state condition.Figures of (a), (b), (c), (d), (e) and (f) represent the discharge of 0.006 m^3/s, 0.005 m^3/s, 0.004 m^3/s, 0.003 m^3/s, 0.002 m^3/s and 0.001 m^3/s, respectively. Profile view of the circle pier, upstream and downstream depths can be seen from that figure. Also free surface profile of water and difference between upstream and downstream flow depths are observed for different flow rates. For maximum flow rate which is 0.006 m^3/s creates maximum difference between upstream and downstream free surface level, while discharge of 0.001 m^3/s compose the minimum difference. It is observed that drag force value increases when difference between upstream and downstream water level increases. Drag force results reduces while flow elevation difference becomes smaller.

Table3.2: Grid dependency for Flow 3D simulations

Mesh Value	**Domain (Geometry)**	**Domain (Volume)**	**Cell Volume**	**Cell Size**
500,000	A=4m	0.12 m^3	0.00000024 m^3	0.0062 m
1,000,000	B=0.15m	0.12 m^3	0.00000012 m^3	0.0049 m
1,500,000	C=0.20m	0.12 m^3	0.00000008 m^3	0.0043 m

Grid dependency calculations that are mentioned in Section 2.5.1.1 not only completed using empirical formulas but also checked trying CFD simulations for different mesh sizes. First to decide cell size, volume of flow domain is calculated. Total number of mesh is assumed. Using those two, cell size of the flow domain is calculated. In Table 3.2, the number of assumed mesh, volume of domain and cell sizes are given. Half million, one million, one and a half million mesh sizes are simulated using Flow 3D CFD software. The results of this analysis are compared and after that a suitable mesh size is choosen for numerical investigation.

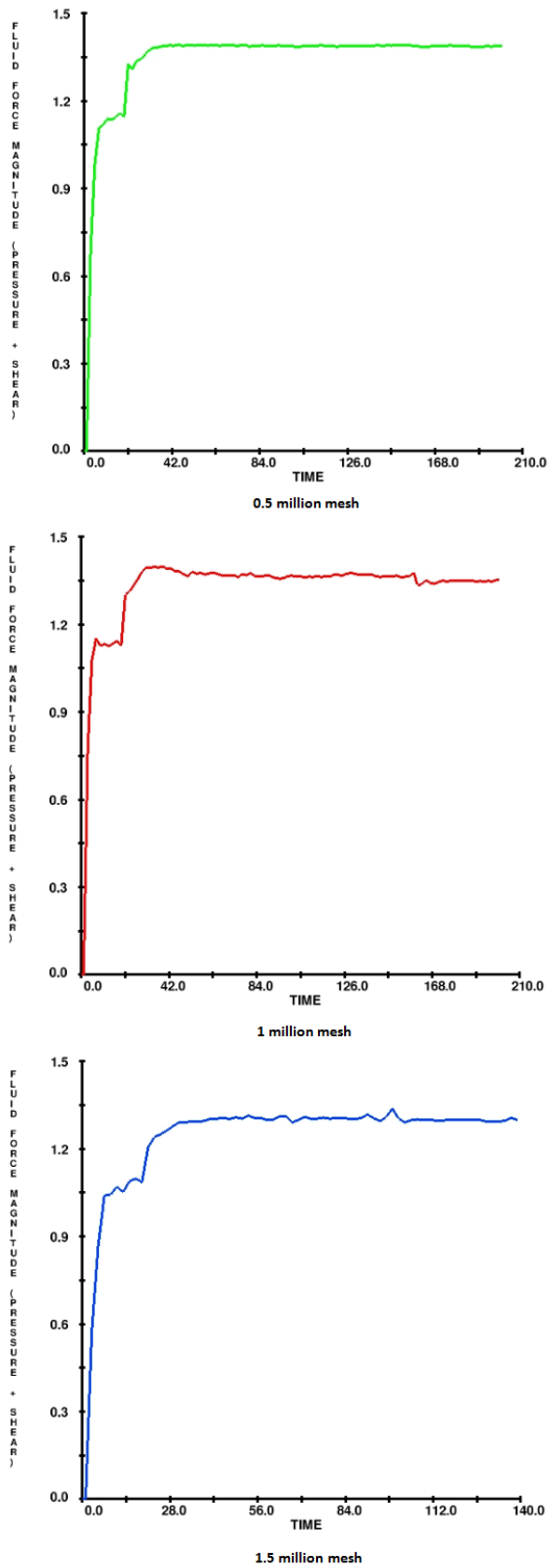

Figure 3.12: F_d values for three different grid dependency attained from simulations (Flow 3D)

In Figure 3.12, drag force results which have half million, one million, one and a half million cell are presented. These simulations are completed using Flow 3D CFD software. Circle pier shape is used in all simulations. All simulations were run until steady-state condition is satisfied. Drag forces computed for different time intervals are shown in Figure 3.12 and Table 3.3. The drag force values computed by using three different mesh size gives very close results.

Table3.3: F_d values for three different grid dependency taken from TecPlot

Mesh Value	F_d **(N)**	**y (u/s) (m)**	**y (d/s) (m)**
500,000	1.31	0.0843	0.0454
1,000,000	1.28	0.0845	0.0452
1,500,000	1.26	0.0839	0.0460

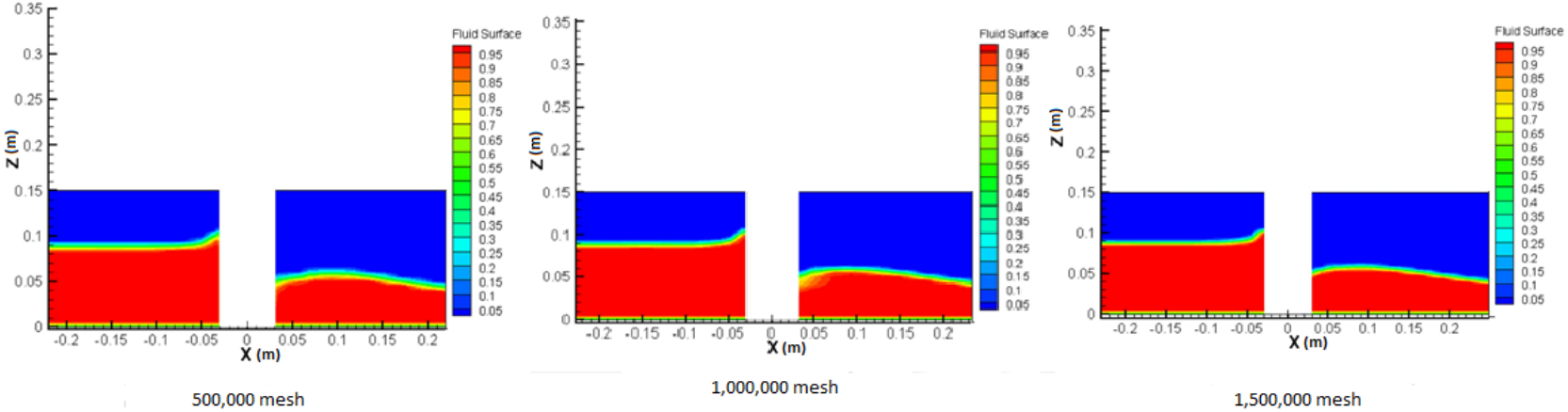

Figure 3.13: Water surface levels both upstream and downstream sides for three different grid dependency during the steady state conditions (Flow 3D)

Flow 3D simulations are imported into the TecPlot. Free surface elevations which belong to upstream and downstream side of the pier are calculated. Comparative values of drag forces and values of water levels are given in Table 3.3. In addition, Figure 3.13 shows that iso surfaces of three different simulations give similar results. As a result, CFD simulations which are Effect of Shape of the Pier, Triangular Nose and Tail Cases - Aspect Ratio Effect and Simulation of flow around Ongözlü Bridge is simulated using one million mesh.

Simulation of circular pier is used to calculate drag coefficient. Result data which are upstream and downstream fluid heights and velocities are taken from TecPlot. Drag coefficient is calculated using Equation 2.17. Drag coefficient is also calculated by Fluent CFD software. Values of drag force and drag coefficient are given in Table 3.4 and Table 3.5. The difference between these values occur due to approximation of calculation method. Pressure distribution has been described as linear in analytical method. The pressure of the water is calculated as the area of the right triangle in the direction of flow. In Fluent 3D CFD simulations, pressure distribution is calculated as integral of the area from bottom to top (real case of pressure distribution) in x,y,z directions and their combinations. Pressure distributions are described both analytical and CFD methods in the Figure 3.14.

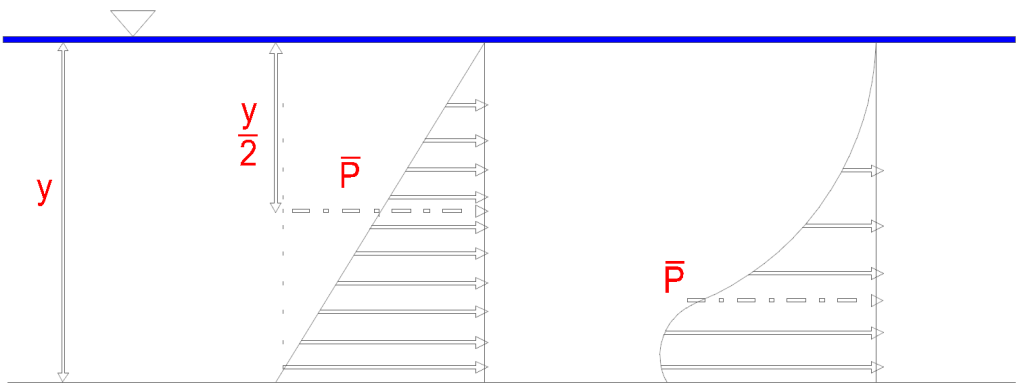

Figure 3.14: Approximations of pressure distribution

Table3.4: C_d values

Discharges (m^3/s)	**0.006**	**0.005**	**0.004**	**0.003**
	Cd			
Analytical	2.62	2.73	2.53	2.24
Fluent	1.83	1.40	0.86	0.44

Table3.5: Comparison of C_d values

C_d	**Average**	**For 2D objects**	**For 3D objects**
Analytical	2.53	1.17	1.42
Fluent	1.13		

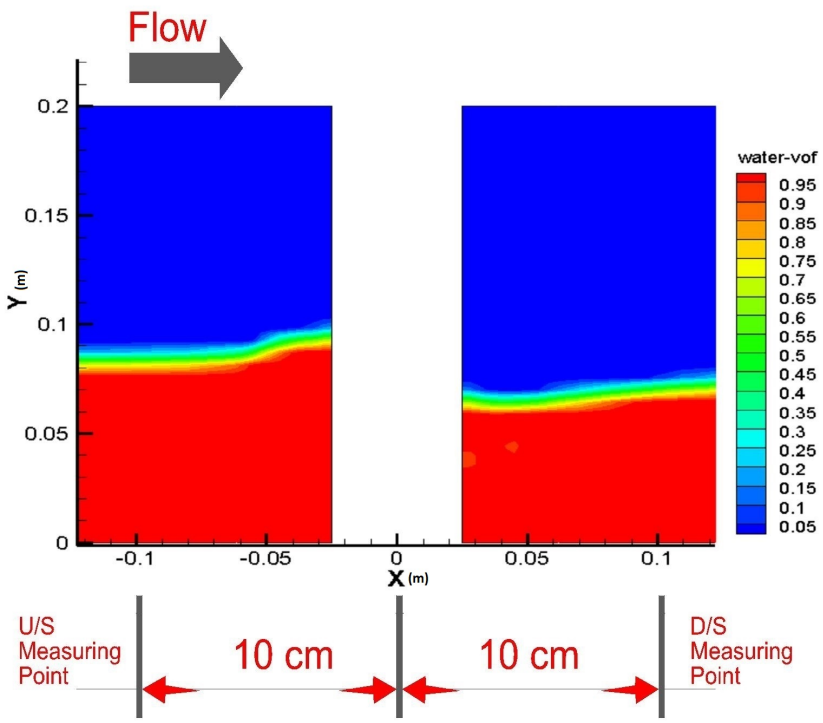

Figure 3.15: Representation of upstream and downstream measuring points

Calculation points on the upstream and downstream side of the pier and flow direction are shown in the Figure 3.15. For calculation of drag force and drag coefficient, water levels and average velocities on the upstream and downstream side of pier are evaluated numerically. These values are used for drag force calculation applying momentum equation as follows:

$$\Sigma F = \rho Q(V_{out} - V_{in}) \tag{3.2}$$

$$\frac{(\rho g B h_1^2)}{2}_{inlet} - \frac{(\rho g B h_2^2)}{2}_{outlet} - F_d = \rho Q(V_2 - V_1) \tag{3.3}$$

F_d represents drag force on the pier, ρ is the density of water, g is the gravitational acceleration, B is the width of the channel, h_1 and h_2 are upstream and downstream water level respectivelty. V_1 and V_2 are average velocities on the upstream and downstream side of the pier.

3.3 TRIANGULAR NOSE AND TAIL CASES ASPECT RATIO EFFECT

In order to validate our simulation approach, experimental study of Agarwal et al. (2014) was recreated numerically. A rectangular pier with triangular nose and tail were simulated. Four different aspect ratios, which is defined as the ratio between pier thickness and pier length, are considered. The thickness of the piers were constant in order to retain a constant contraction ratio of 0.4, however four different pier lengths were selected. The simulations are carried out for five different discharge values that are ranging from 3.73x10^{-4} to 5.06x10^{-4}. The Reynolds number that corresponds to the discharge range considered is given in Figure 3.16. This range is basically for subcritical flow conditions that is given between 300 and $3x10^5$ (Suribabu et al., 2011).

The drag force calculated based on simulation results are given in Table 3.6. As the pier gets longer, the drag force that it experiences gets higher as well. This is due to increase in frictional drag. Similarly, as the discharge increases for all cases, we observed an increase in drag force as expected. This is majorly the consequence of increase of pressure force on the pier with an increase in discharge. These results are shown for all four pier lengths (4, 6, 12 and 16cm) in Figure 3.17.

Table3.6: F_d (N) values attained from simulations

Discharges (m^3/s)	**3.73x**10^{-4}	**4.08x**10^{-4}	**4.48x**10^{-4}	**4.75x**10^{-4}	**5.06x**10^{-4}
Pier Shape	**Drag Force (N)**				
4 cm	0.294	0.331	0.389	0.438	0.493
6 cm	0.338	0.371	0.427	0.451	0.487
12 cm	0.320	0.419	0.452	0.495	0.522
16 cm	0.378	0.442	0.498	0.540	0.585

The drag force values obtained from the simulations are compared to the ones reported by Agarwal et al. (2014). Figure 3.18 shows that the agreement between CFD results and the experiments are quite remarkable with coefficient of determination (R^2) ranging from 0.88 to 0.99. This shows the validity of the model used in the study and encouraged us to apply this model further to other pier shapes and discharge values. Higher aspect ratio causes higher drag force.

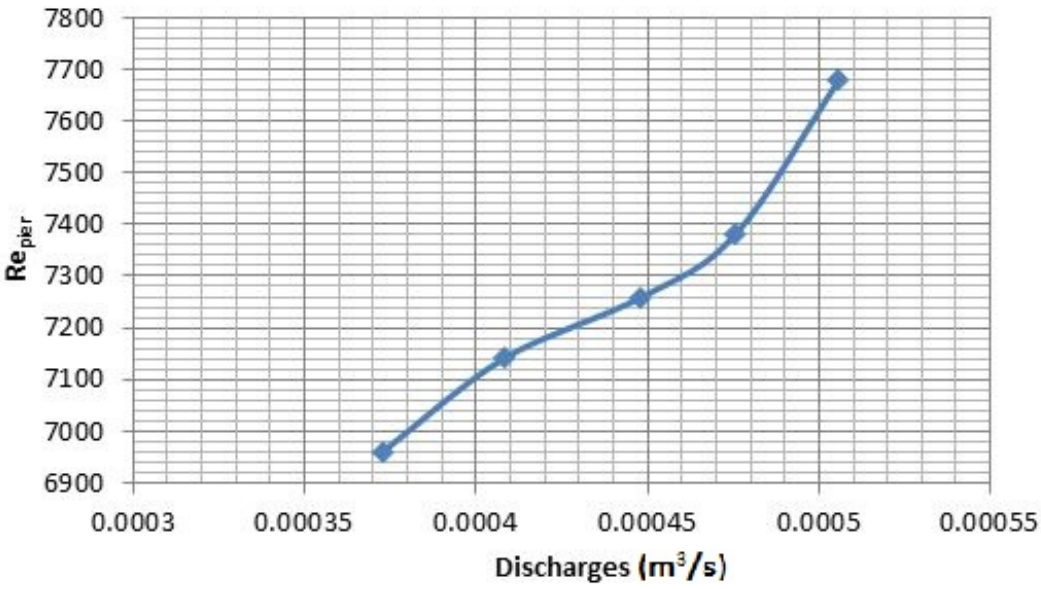

Figure 3.16: The range of Reynolds number ranges from 6.96 x 10^3 to 7.68 x 10^3 (subcritical flow conditions)

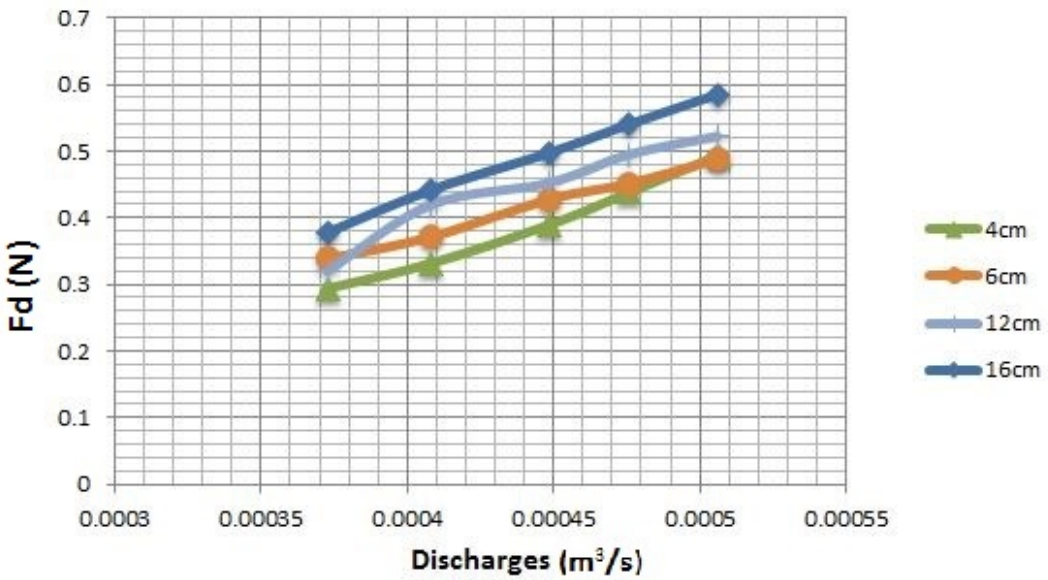

Figure 3.17: Drag force on rectangular piers with triangular nose and tail with constant contraction ratio of 0.4 and length of 4, 6, 12 and 16 cm simulated for five different discharge values

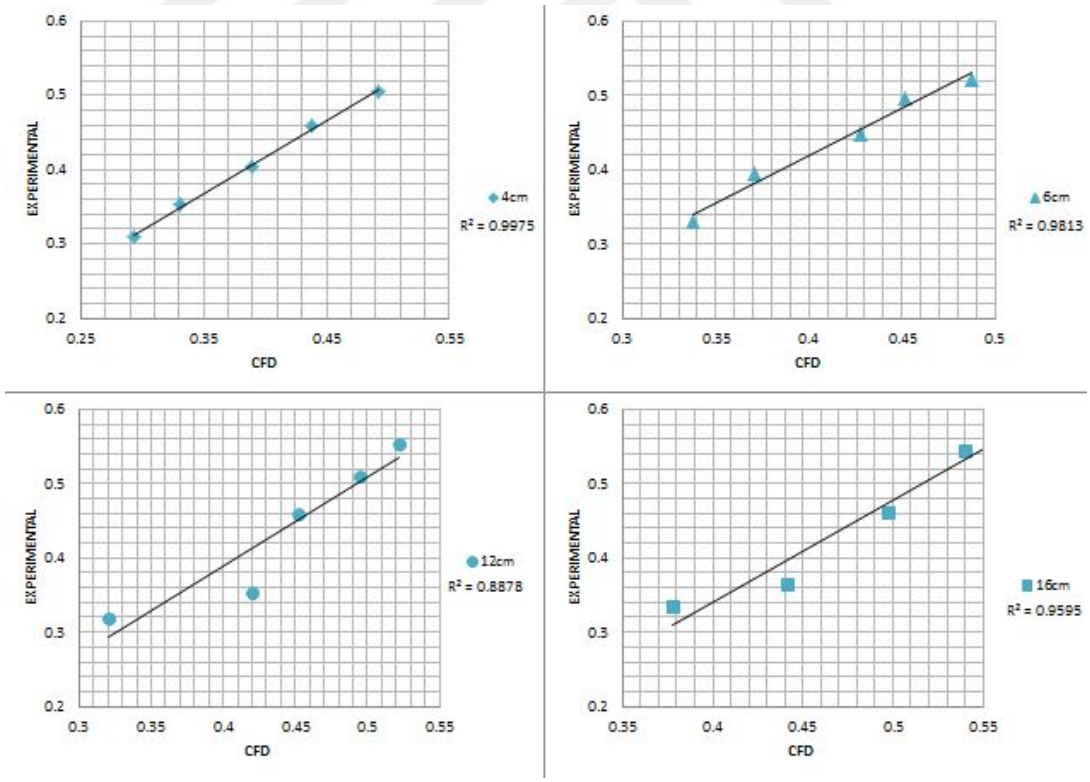

Figure 3.18: Comparison of values of drag force from simulations to ones from experiments of Agarwal et al. (2014)

Yarnell's Equation for Backwater Rise

Yarnell's (1934) empirical equation which is for calculating the increase in the water level due to bridge piers is the most widely used. Yarnell carried out 2600 laboratory experiments about the bridge piers. He investigated the effect of shape of piers, effect of width, length angle and position of the piers under different discharge conditions to improve empirical equation. The equation predicts the water level on the upstream side of the bridge for known water level on the downstream side of the bridge in terms of shape of the piers. The equation calculates for the fluid velocity, pier shape and area obstructed by piers. Yarnell's equation for backwater rise is appropriate at which energy losses are essentially due to the piers.

The ratio of backwater rise to the undisturbed water level under sub-critical flow condition is given by:

$$[\frac{\Delta y}{y}]emprical = K(K + 5F_r^2 - 0.6)(\alpha + 15\alpha^4)F_r^2 \tag{3.4}$$

where;
Δy = Backwater generated by the bridge pier
y =Original (undisturbed) local flow depth
F_r = Froude Number at Downstream of piers
α = Ratio of the flow area obstructed by the piers to the total flow area downstream of the piers
K = Coefficient of the pier shape

Yarnell's backwater rise formula is used in analytical investigation of 'aspect ratio effect – triangular nose and tail pier shape'. Results of Flow 3D simulation is exported into the TecPlot. Values of upstream and downstream fluid height and depth are taken from 3D flow data. First of all, given discharge which is defined as inlet boundary condition in Flow 3D is checked using continuity equation. In addition, upstream and downstream Froude number is calculated based on flow depth and average velocity. Subcritical flow condition is satisfied both upstream and downstream side of the pier. Yarnell back water rise formula is valid for subcritical flow conditions. After subcrit-

Table3.7: Hydraulic characteristics of free surfaces

	Upstream	**Downstream**
Water level (m)	0.022	0.018
Velocity (m/s)	0.144	0.176
Q (calculated) (m^3/s)	4.77x10^{-4}	4.78x10^{-4}
Q (given) (m^3/s)	4.75x10^{-4}	4.75x10^{-4}
Fr	0.31	0.42

ical flow criteria are provided, K number which is equal to 1 for triangular nose and tail case is used. This K value is recommended by Yarnell through his experimental work. (Δy / y) value is calculated using backwater rise formula. y is the undisturbed free surface level in open channel. For obtaining y value, open channel is simulated without pier under the same discharge. Δy value is obtained using y value. Δy replaces the amount of swelling caused by pier. Depths obtained through Flow 3D and analytical results upstream and downstream of pier are compared. It is shown that results are similar to the level of 99 percent. Consequently, CFD simulations which include numerical investigation of aspect ratio give accurate results in terms of flow conditions. Figure 3.19 shows water surface levels in undisturbed and pier case.

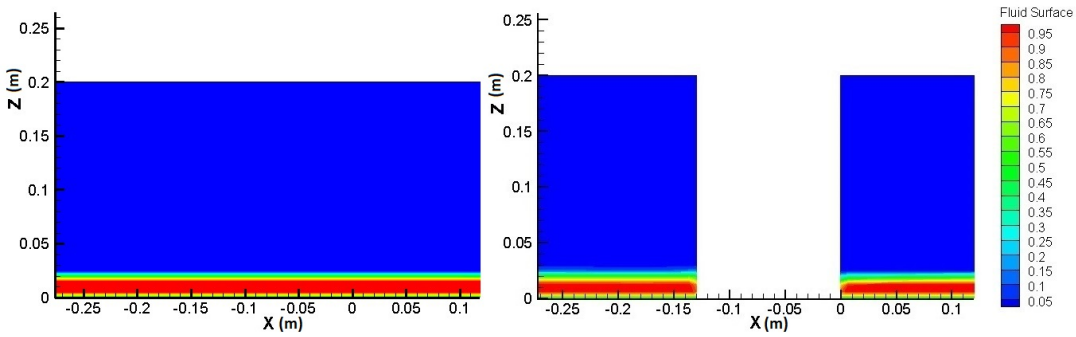

Figure 3.19: Upstream and downstream free surfaces

Table3.8: Values of back water rise calculation

Δy / y	0.191
y (undisturbed flow depth) (m)	0.021
Δy **(m)**	0.004
y (d/s) (calculated) (m)	0.0180
y (d/s) (measured) (m)	0.0183
% Error	0.136

3.4 SIMULATION OF FLOW AROUND ONGÖZLÜ BRIDGE

For a significant physical problem, such as flow over bridge, a submarine moving in the ocean, etc., there are mostly some apparent motion scales. The fewer apparent ones can also be derived by physical evaluation. A problem such as length of the bridge is the obvious length scale L. The time from the start of the flow to become steady state condition or the flood period, can be the time scale T. The speed of fluid is the scale for the velocity U. The gravitational acceleration g can be used as the scale of body force per unit mass if gravity becomes important.

Several dimensionless parameters exist in the momentum equation. Dimensionless parameters are mentioned below;

$$\frac{L}{TU} = Strouhal \quad Number = St \sim \frac{local \quad acceleration}{convective \quad acceleration} \tag{3.5}$$

$$\frac{UL}{\nu} = Reynolds \quad number = Re \sim \frac{inertia}{viscous \quad force} \tag{3.6}$$

$$\frac{U^2}{gL} = Froude \quad number^2 = Fr^2 \sim \frac{inertia}{body \quad force} \tag{3.7}$$

The Froude number is a measurement of the ratio of inertia forces to gravitational forces. Froude number is significant for free surface flows. In open channel flow, it specifies flow regime, which is either subcritical or supercritical. Because of that, for simulation of Ongözlü Bridge, ‘Froude Similarity’ method is used as a dimensionless technique.

Similarity between model and prototype is defined by equation of Froude Number;

$$F_m = F_p \tag{3.8}$$

$$\frac{V_m}{\sqrt{(gh_m)}} = \frac{V_p}{\sqrt{(gh_p)}} \tag{3.9}$$

$$\frac{V_m}{V_p} = \sqrt{(\frac{h_m}{h_p})} \tag{3.10}$$

where F_m and F_p represent Froude Number of model and prototype, respectively. V_m and V_p are velocities of model and prototype, h_m and h_p are water surface levels of model and prototype.

Scale factor of 1/83.33 is applied for Ongözlü Bridge. For comparison, maximum flow rate of 5.06x10^{-4} is examined and then water level and velocity of water is measured from simulation of Ongözlü pier during the steady state condition. These measurements are defined in the simulation of Ongözlü Bridge to create same initial conditions as in the study of Agarwal et al. (2014). Calculation steps of Froude Number is given in Table 3.9. Using Froude Similarity method, discharge is converted from simulation to real case. Also simulation is done for flood discharge of Tigris River.

The minimum and maximum measured discharges of Tigris River are 55 m^3/s and 2263 m^3/s, respectively. Average discharge of Tigris River is also measured as 360 m^3/s. (Onüçyıldız et al., 2016)

Table3.9: Froude number calculation of numerical model

Q=5,06x10^{-4} m^3/s	
h_m (m)	0.0264
V_m (m/s)	0.128
Fr_m	0.251

where h_m, V_m and Fr_m represent water level, velocity of water and Froude number of model, respectively.

Maximum flow rate of 5.06x10^{-4}, which is used in simulation is converted from simulation to real scale and it is found as 356.38 m^3/s. Froude similarity calculations of prototype are given in Table 3.10.

Table3.10: Froude similarity between model and prototype

Q=356.38 m^3/s	
h_p (m)	2.199
V_p (m/s)	1.166
Fr_p	0.251

where h_p, V_p and Fr_p represent water level, velocity of water and Froude number of prototype, respectively.

In this part of the study, one of the piers of Bridge, which Ongözlü has a contraction ratio of 0.33, was simulated for different discharge conditions. Numerical investigation is carried out in 4 m long hydraulic flume with 0.15 m width. In the simulations time step is taken as 0.1 s. All simulations are carried out for 180 s.

In Figure 3.20. water surface elevation (in m) is presented as contour plot for Ongözlü Bridge at t=180 s where flow has reached steady state condition. For t>180 s no change in Z is observed for all the simulations considered in the study.

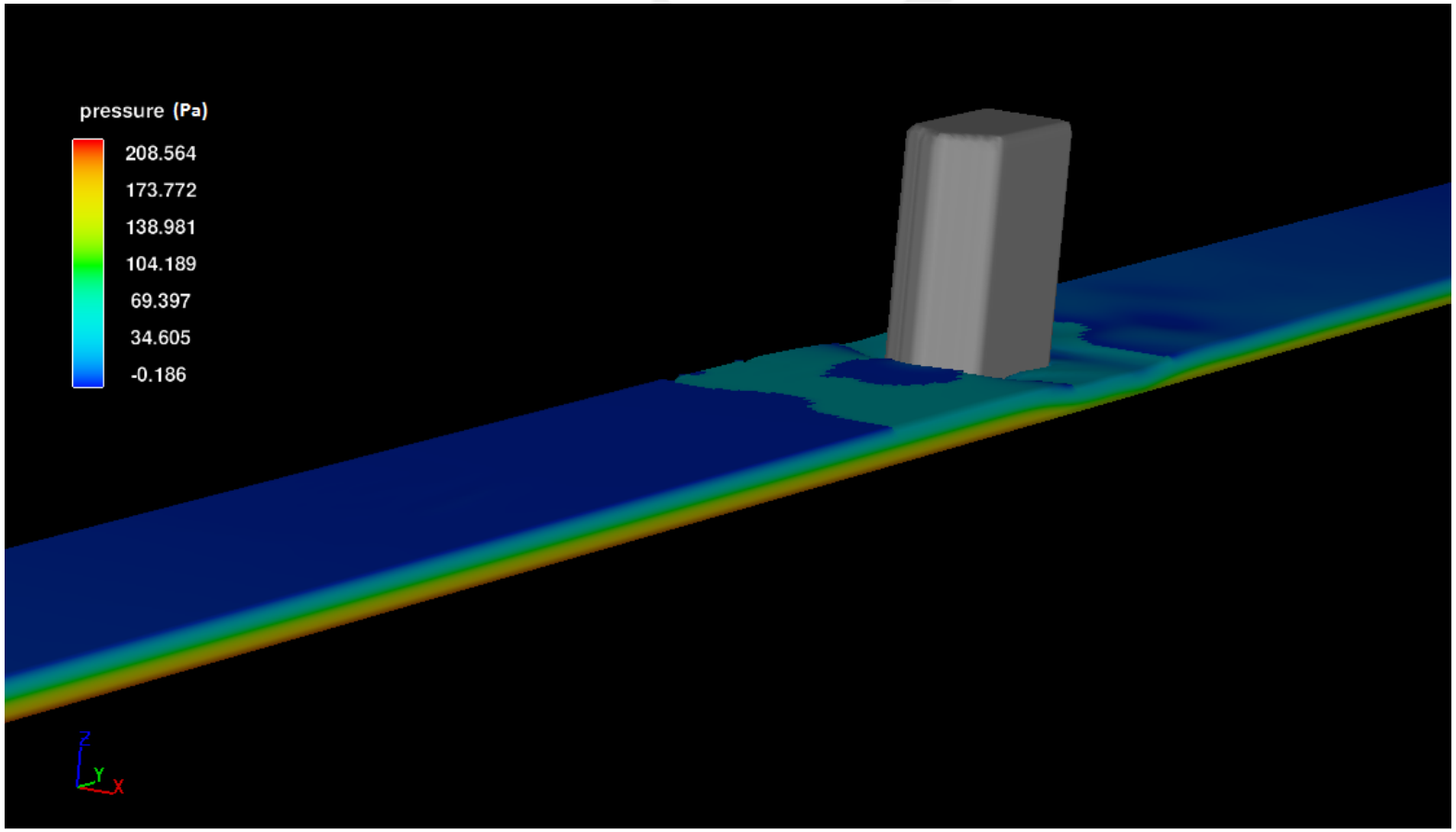

Figure 3.20: One pier of Ongözlü Bridge at T=180 s under discharge of 5.06x10^{-4}

For Ongözlü Bridge, we considered five different discharge given in Table 3.11. The F_d values for one pier of Ongözlü Bridge are approximately 0.240, 0.277, 0.329, 0.349 and 0.373 for the discharges 3.73x10^{-4}, 4.08x10^{-4}, 4.48x10^{-4}, 4.75x10^{-4}, 5.06x10^{-4}, respectively. The geometry of the pier of Ongözlü is similar to a rectangular pier with triangular nose but a rectangular tail. Geometric representation of Ongözlü Bridge Pier is shown Figure 3.21. Dimensions of Ongözlü Bridge are given in Table 3.12. The aspect ratio of this pier is about 6 to 9.95 (or 1 to 1.658). This is in between 6 cm length and 12 cm length validation cases given in section 3.3. The angles of the triangle at the nose of the Ongözlü pier is different from the ones considered by Agarwal et al. (2014), Ongözlü pier experiences far less drag force. The 6cm - 12cm length cases of Agarwal et al. (2014) can be found in Table 3.6.

Table3.11: F_d (N) values attained from simulations for Ongözlü Bridge

Discharges (m^3/s)	**3.73** x10^{-4}	**4.08** x10^{-4}	**4.48** x10^{-4}	**4.75** x10^{-4}	**5.06** x10^{-4}
Pier Shape	**Drag Force (N)**				
Ongözlü	0.240	0.277	0.329	0.349	0.373

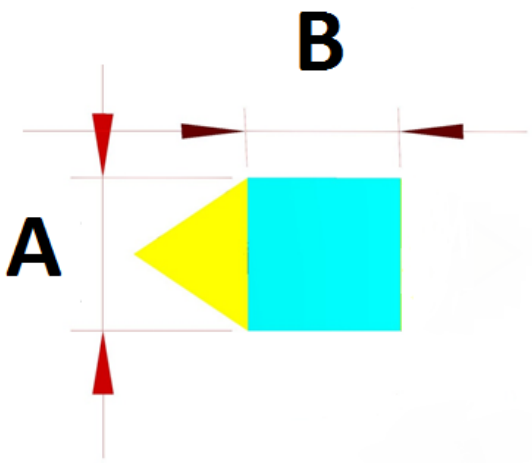

Figure 3.21: Geometrical representation of Ongözlü Bridge pier

Table3.12: Geometrical specification of Ongözlü Bridge pier

Pier Shape	**Ongözlü Pier (for CFD)**	**Ongözlü Pier (actual)**
A	6 cm	5 m
B	9.95 cm	8.3 m

As for the final part of the study, Ongözlü Bridge was simulated as a whole. Additionally, same scale factor (1/83.33) is used for Ongözlü Bridge. To make a comparison, discharges, simulation setup and measurement techniques are used similar to the initial part of the study. Such that, inflow conditions are similar to single pier case where we keep flow depth and average inflow velocity as a constant.

Piers are taken as separate components for the final part of the numerical investigation. Aim of the research is to measure the drag forces on piers separately. 9 piers and 2 abutments are one by one defined in Flow 3D and their coordinates are adjusted to match the original position of Ongözlü Bridge. For comparison maximum discharge of 5.06x10^{-4} is used in simulation.

Results of drag force of abutments and piers of Ongözlü Bridge are given in Figure 3.24. It is shown that abutments experience drag force higher than piers. Representation of abutments and piers of Ongözlü Bridge is shown in the Figure 3.22. Simulation of the Ongözlü Bridge piers and the simulation of the single pier of the Ongözlü Bridge give a minor different results in terms of drag force. Piers affects each other in simulation of Ongözlü Bridge and this situation decreases drag force in small quantities. Results show that value of drag force depends on discharge conditions, span of piers, geometrical features of piers and positions in open channel.

In Figure 3.25, unsteady flow around Ongözlü Bridge is shown. Time of 10 s, 35 s and 120 s are captured from simulation. Time of change of water level and surge formation are also shown in given figures.

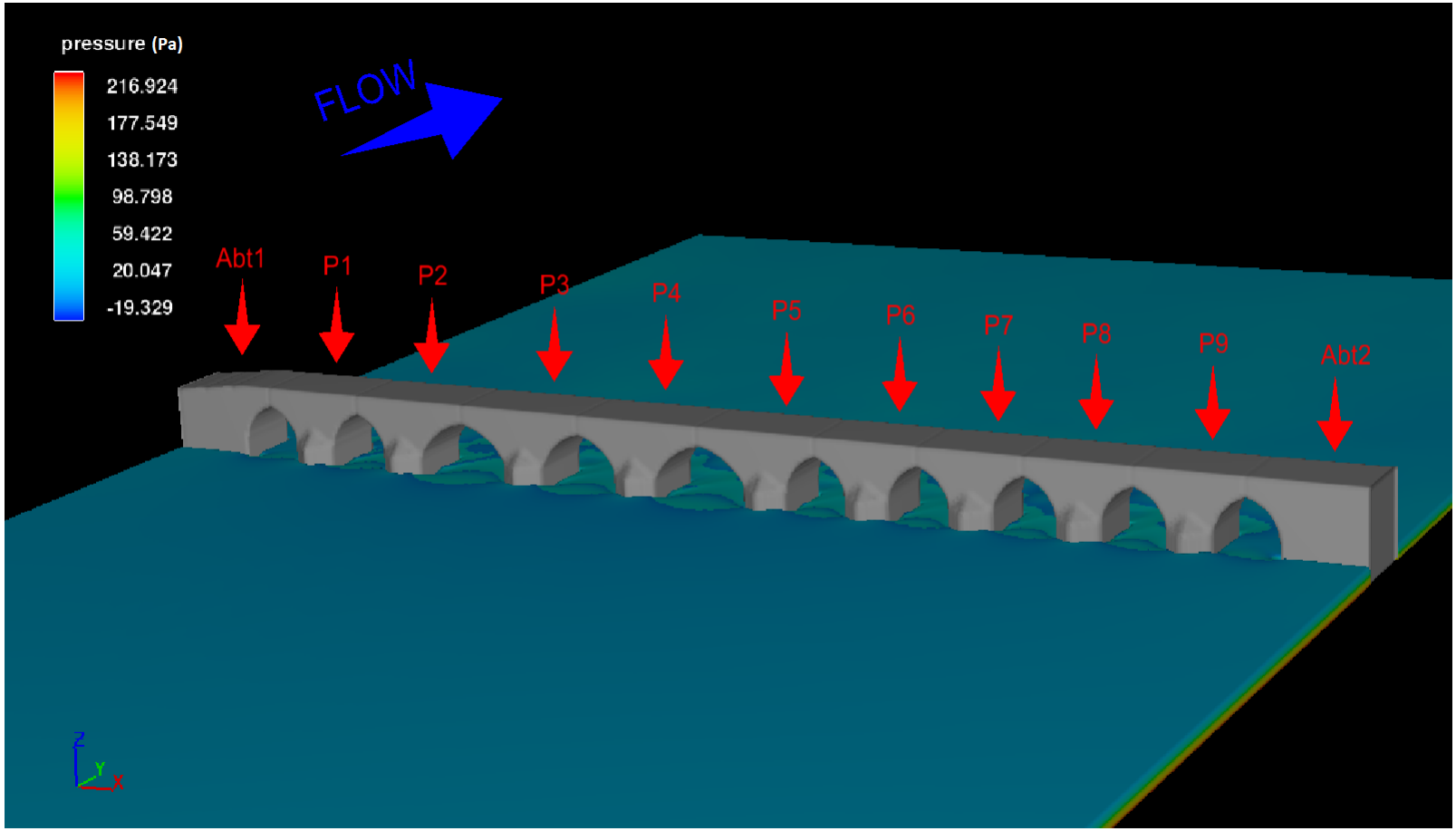

Figure 3.22: Ongözlü Bridge at T=300 s

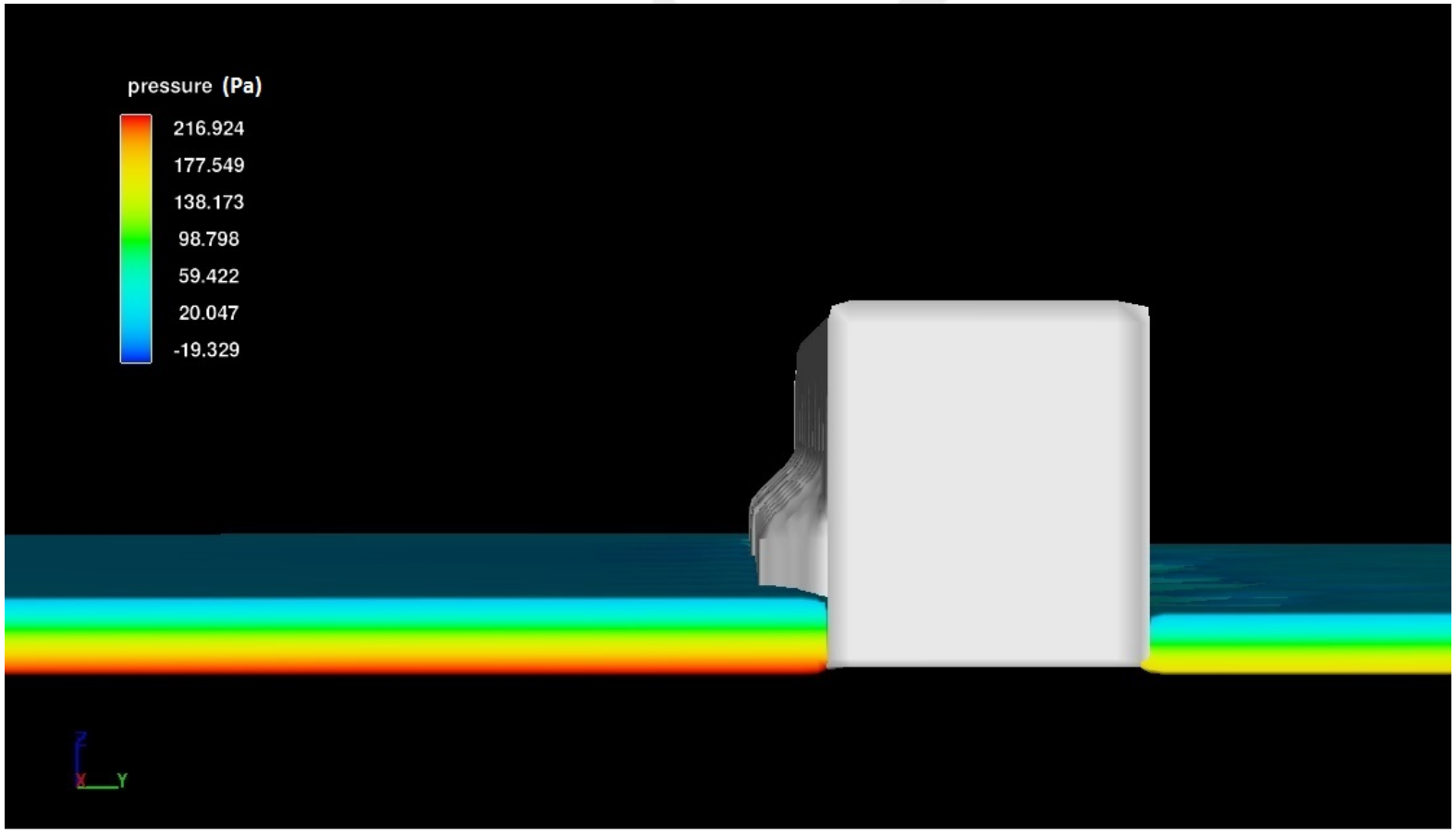

Figure 3.23: Profile view of Ongözlü Bridge at T=300 s

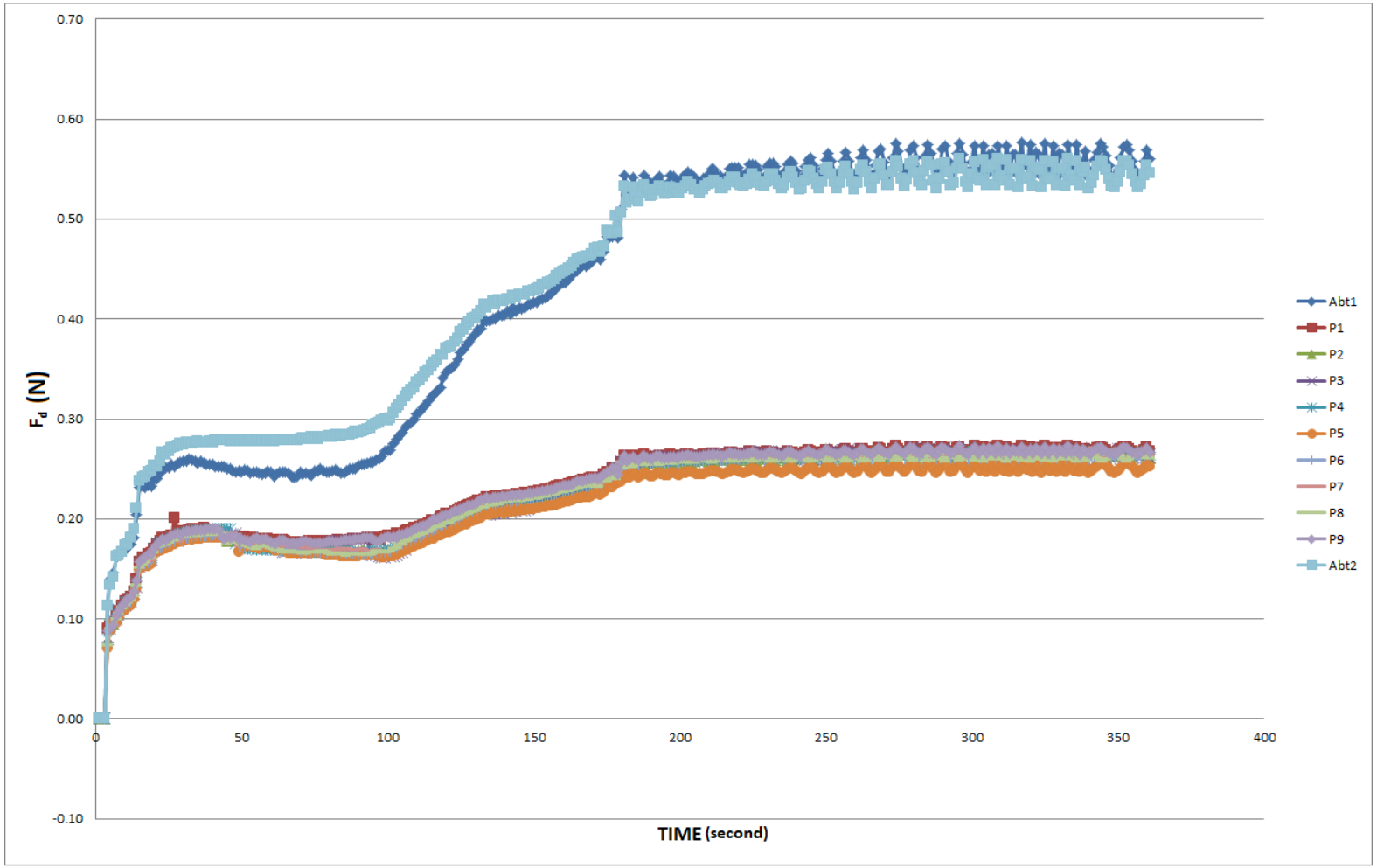

Figure 3.24: Time of change of drag force for abutments and piers of Ongözlü Bridge

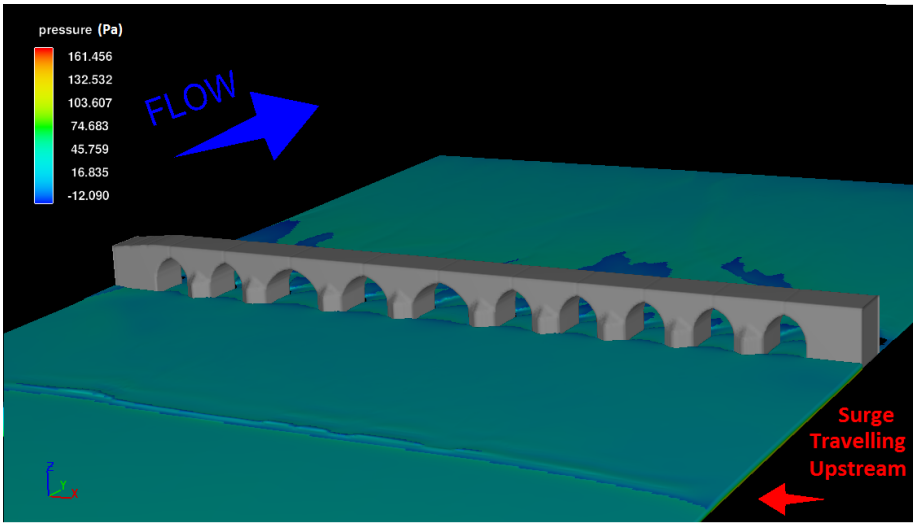

T = 10 s

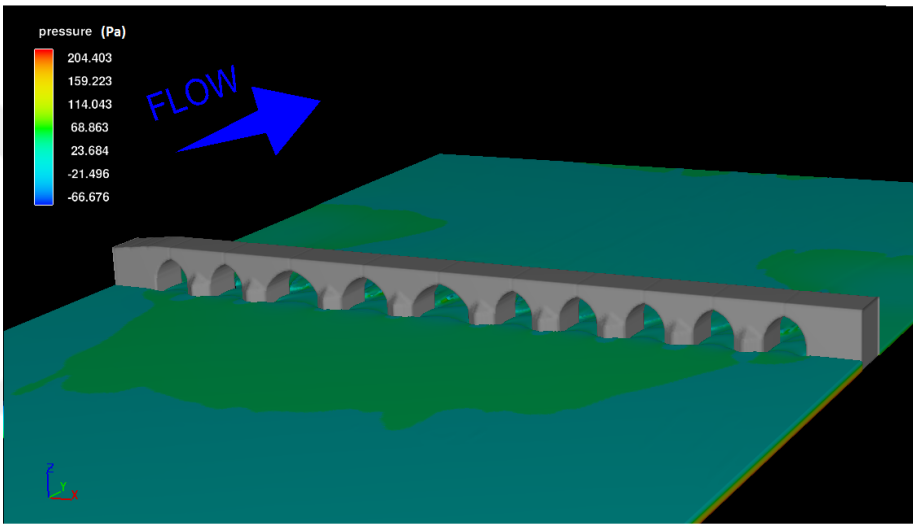

T = 35 s

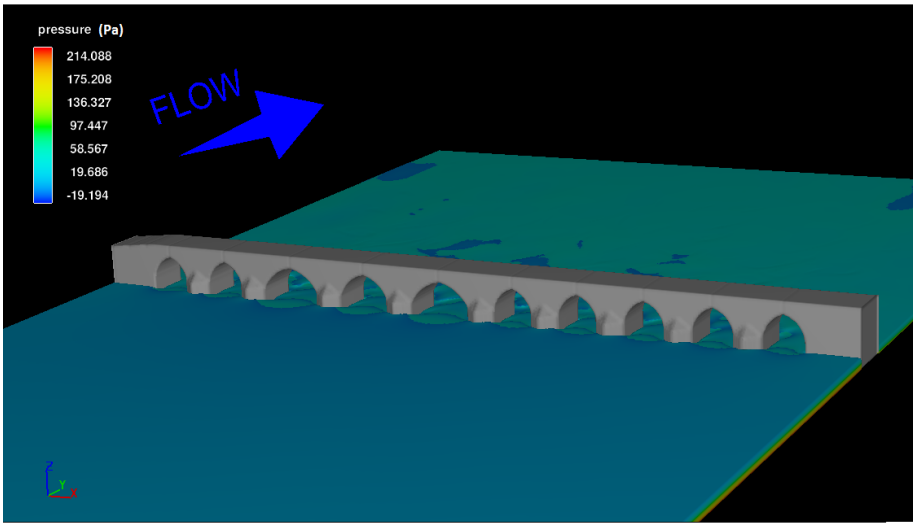

T = 120 s

Figure 3.25: Representation of Ongözlü Bridge at 10 s, 35 s and 120 s

Representation of abutments and piers of Ongözlü Bridge under flood discharge is shown in the Figure 3.26. The depth of the flow is much higher if one compares the flow depth in Figure 3.22. Results of drag force of abutments and piers of Ongözlü Bridge under flood discharge are given in Figure 3.27. The flood discharge is almost eight times that of the average flow rate in the simulations. Similarly, drag forces on the piers are about ten times larger than the ones observed for average flow rate, given in Figure 3.24 and 3.27

In Figure 3.28, unsteady flood flow around Ongözlü Bridge is shown. Time of 5 s, 20 s and 120 s are captured from simulation. Time of change of water level and surge formation are also shown in given figures.

For a final simulation of Ongözlü Bridge, flood discharge of Tigris River which is equal to 2263 m^3/s is used in simulation. Flood discharge is scaled with using 'Froude Similarity' method from real case to simulation.

For Froude number of 0.251, discharge of model is calculated as 0.0357 m^3/s for flood flow rate of Tigris River. This discharge is given as boundary condition to the scaled model in the final simulation. Discharge calculation of model for flood case is given in Table 3.13.

Table3.13: Calculations of flood discharge of Tigris River

	Prototype values	**Model values**
Q (m^3/s)	2263	0.0357
h (m)	7.54	0.09
V (m/s)	2.16	0.237
Fr	0.251	0.251

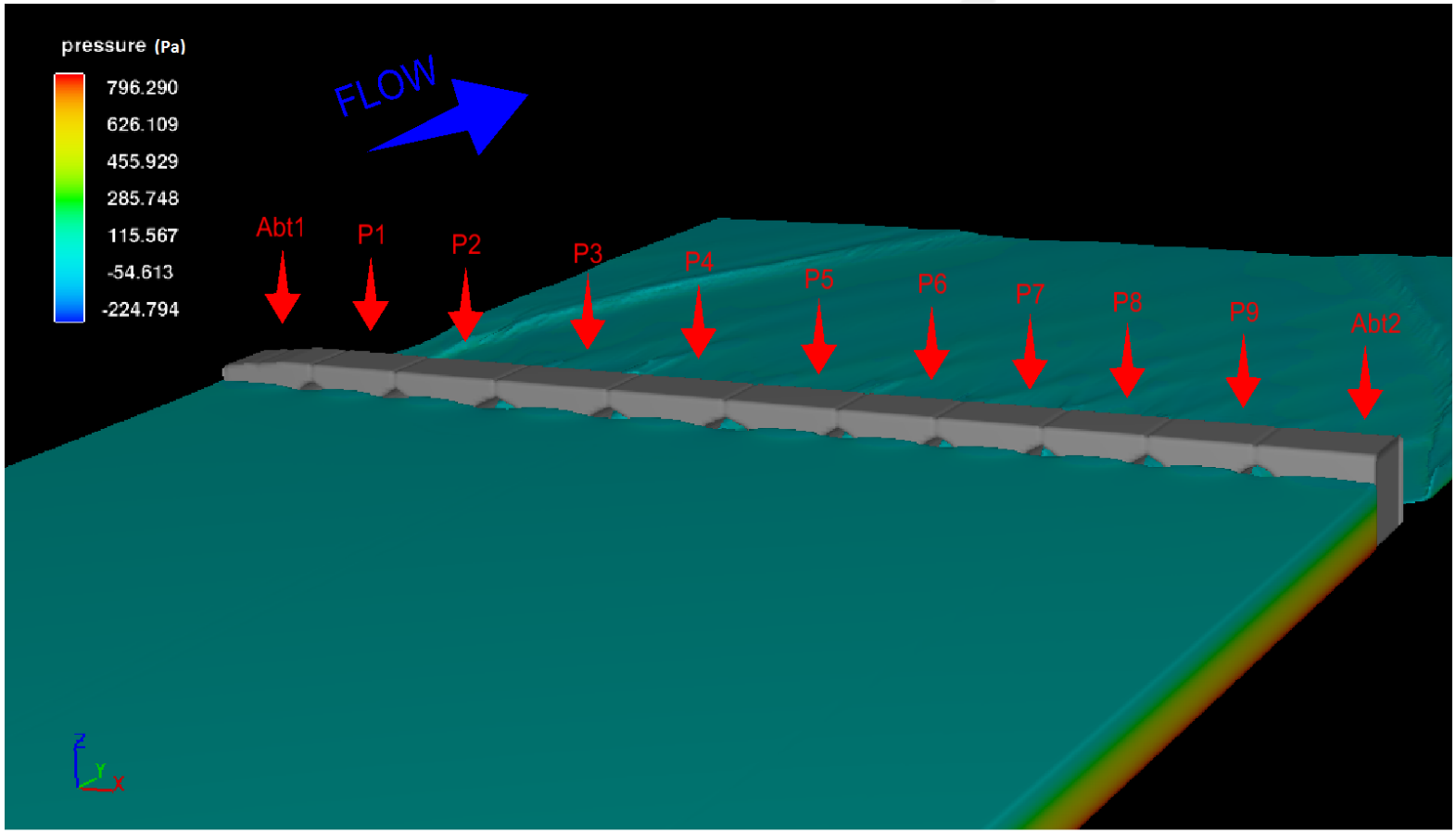

Figure 3.26: Ongözlü Bridge at T=180 s (flood case)

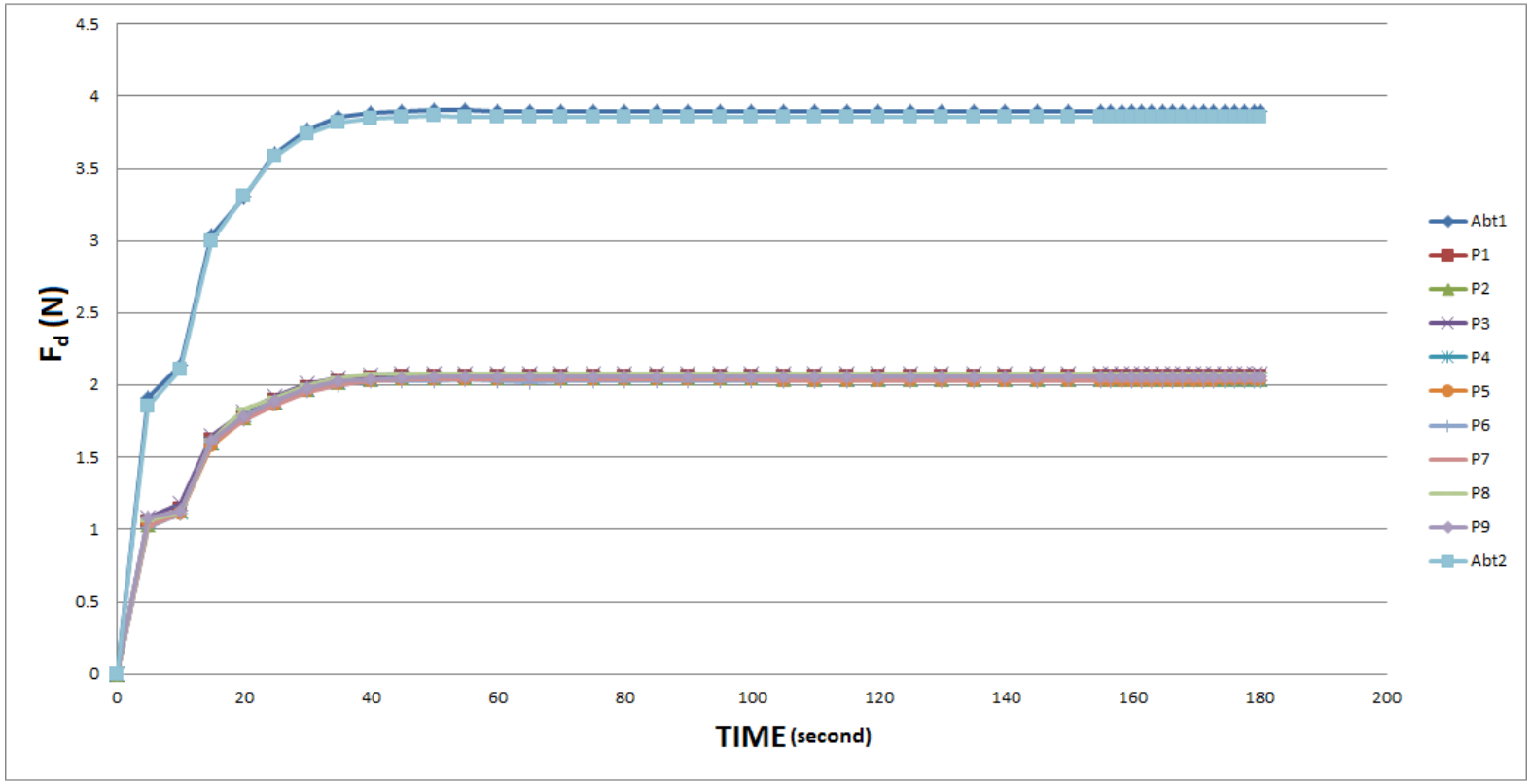

Figure 3.27: Time of change of drag force for abutments and piers of Ongözlü Bridge (flood case)

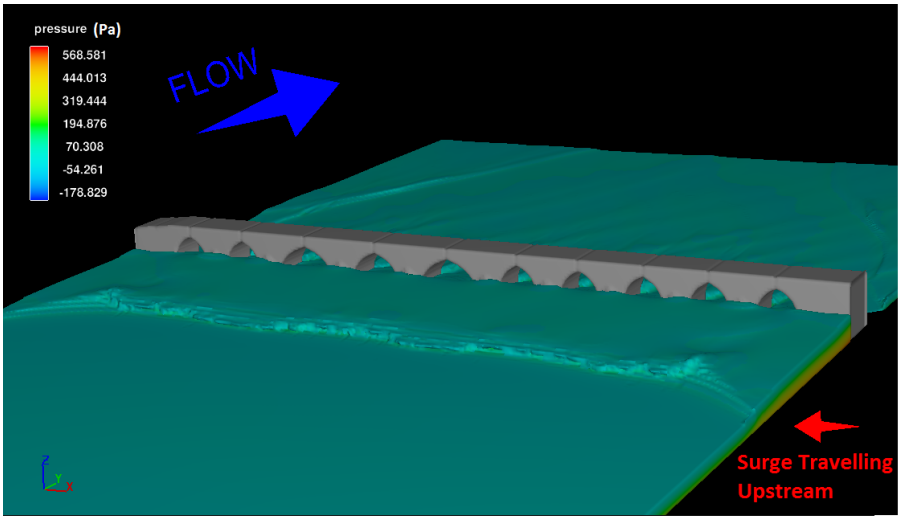

T = 5 s

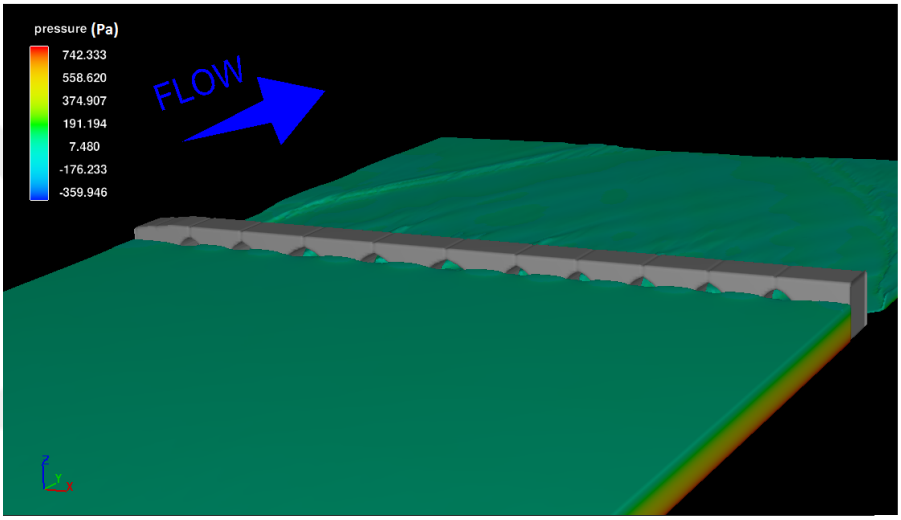

T = 20 s

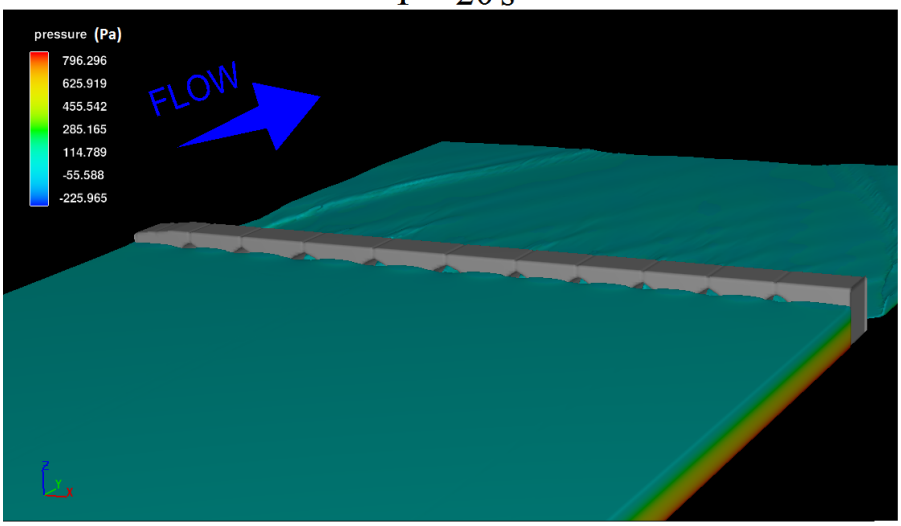

T = 120 s

Figure 3.28: Representation of Ongözlü Bridge at 5 s, 20 s and 120 s (flood case)

CHAPTER 4

CONCLUSIONS

Numerical modelling has a vital role in the design of hydraulic structures. The most important feature of numerical modelling is its cost efficiency. This situation creates an alternative to experimental model tests. However, numerical model results should be confirmed. The confirmation of numerical models is usually ensured by comparison between numerical results and experimental results. CFD software have several restrictions such as long analysis time and limitations in definition of model. However, they provide many details of hydraulic characteristics that would be hard to obtain through physical experiments. Additionally, more investigation could be retested easily with some modifications to the simulation in numerical modelling. For accurate results using numerical modelling, it is significant to define a domain, create numerical grid with coherent boundary and initial conditions.

Flow 3D is chosen as a CFD software to investigate drag characteristics of different pier types, aspect ratio of piers and Ongözlü Bridge as a whole. For comparison numerical model is scaled. The scale factor is selected such that the scaled pier matches with the pier in experimental study of Agarwal et al (2014). The scale factor is 6/500 (1/83.33). In the study, Reynolds Average Navier Stokes (RANS) simulations are carried out using Flow 3D. RNG k-ε model is used for the turbulence closure. The free-surface of the flow is tracked using Volume of Fluid (VOF) method. One fluid method is defined and SI metrical system is used for CFD simulations. Incompressible flow approximation is used in all simulations.

Conclusions attained from the present study are listed:

• CFD technique is an efficient tool to analyse free surface flows around bridge piers. CFD sofwares can be used by engineers to design hydraulic structures. CFD software are alternative design tool with convenient experimental model for validation. Drag related investigations about bridge piers in open channel have been completed.

• The numerical investigations conducted on drag characteristics of bridge piers show that the value of Drag Force depends on discharge, pier shape and alignment, width of the pier and aspect ratios of the pier.

• CFD model results show that values of C_d depends on calculation method. The small difference between these values occurs due to approximation of calculation method. Pressure distribution has been described as linear in analytical method. The pressure of the water is calculated as the area of the right triangle in the direction of flow. In CFD simulations, pressure distribution is calculated as integral of the area from bottom to top (real case of pressure distribution) in x, y, z directions and their combinations.

• Decision of span of piers is an important step in the design of bridges. With this investigation, it is possible to determine the most appropriate span for different types of bridges under different flow conditions. Bridges can be designed with optimum safety conditions using this approach.

• Additionally, the CFD results of Ongözlü Bridge pier were compared with numerical values (Drag Force) of other piers in terms of aspect ratios. Our simulation results show that Ongözlü Pier experienced lower drag force than the rectangular pier with triangular nose and tail with the smallest aspect ratio.

• This has shown that even though the Ongözlü Bridge was designed in early 11th century, its piers are quite streamlined and the Anatolian hydraulicians were quite ahead of their times in terms of their understandings of flow-structure interaction.

CHAPTER 5

FUTURE STUDIES

Drag force on bridge piers are investigated numerically in this study. Numerical simulations can be used for studying other aspects of bridge pier. The transfer of necessary real data is quite important step to obtain accurate results. Definition of 'turbulence model' specifies the flow characteristics of simulation. Simulations of open channel examples, LES (Large Eddy Simulation) models can be used as a turbulence model. This model provides high resolutions in 3D flows. The results which are obtained using LES model can be compared with the experimental results and performance of LES model can be evaluated.

Water surface level changes due to the obstacles in open channel, which in turn changes the flow characteristics. Especially, 'vortex formations' occur on the upstream side of the obstacle. This structure creates scour formations around the bridge pier and damages the stability of bridge. Investigation of flow features in terms of vortices is an important topic to design bridges. Formation of vortices for different shape of piers, effect of span of piers under subcritical and supercritical flow conditions can be studied to determine the stability of bridge.

The instantaneous fluctuations of flow in open channel create increase or decrease of water level. This situation is called as "SURGE" in open channel. A surge is generated in the channel by a sudden change in the cross section, for example, by contraction due to piers. Surge formation can be modelled using CFD software and features of surge can be compared with the experimental and empirical results. With using CFD software, simulations performance and sensibility can be observed.

Impact of sudden pressure change is a quite important topic to design bridges. During the flood, water levels which are above the design levels create forces too much and sometimes it collapses the bridge. Bridges can be modelled under different discharge conditions such as flood discharges of 100 years or 500 years. According to the basin calculations, the performance of reinforced concrete of bridge can be evaluated by measuring forces due to sudden loads while in steady-state condition under the design flow rate.

REFERENCES

Adhikary, B. D., Majumdar, P., and Kostic, M. (2009). CFD Simulation of Open Channel Flooding Flows and Scouring Around Bridge Structures. In Proceedings of the 6th WSEAS International Conference on FLUID MECHANICS (FLUIDS'09).

Agarwal, N., Sreeram, S. and Suribabu, C.R. (2014). Determination of Shape Co-Efficient and Drag Co-Efficient of Triangular Piers Under Sub-Critical Flow Conditions. Asian Journal of Applied Sciences 7 (6): 441-447, ISSN 1996-3343 / DOI: 10.3923/ajaps.2014.441.447, Knowledgia Review, Malaysia.

Ansys, A.F. (2011). 14.0 Theory Guide. ANSYS Inc., 390-1.

Aral, T. (2012). Ongözlü Köprü, Diyarbakır (http://www.fotografturk.com/on-gozlu-kopru-diyarbakir-p269419).

Autodesk, Inc. (2012). User's Guide. Autocad 2013, January 2012.

Burger, M. (2010). Numerical Methods for Incompressible Flow. Lecture Notes.

Charbeneau, R. J., and Holley, E. R. (2001). Backwater Effects of Bridge Piers in Subcritical Flow. Center for Transportation Research, Bureau of Engineering Research, University of Texas at Austin.

Computational Fluid Dynamics Software – Flow 3D from Flow Science, CFD. www.flow3d.com

Department of Transport and Main Roads (2013). Hydraulic Guidelines for Bridge Design Projects. Technical Guideline, State of Queensland.

Dowding, C. H., and Pierce, C. E. (1994, September). Use of Time Domain Reflectometry to Detect Bridge Scour and Monitor Pier Movement. In Proceedings of the Symposium on Time Domain Reflectometry in Environmental, Infrastructure, and Mining Applications, Evanston, Illinois, Sept (pp. 7-9).

El-Alfy, K. S. (2006). Experimental Study of Backwater Rise Due to Bridge Piers as Flow Obstructions. Tenth International Water Technology Conference, IWTC 10, 2006, 319-336.

Elapolu, P. G., Majumdar, P., Lottes, S. A., and Kostic, M. (2012, July). Development of a Three-Dimensional Iterative Methodology Using a commercial CFD code for Flow Scouring Around Bridge Piers. In ASME 2012 Heat Transfer Summer Conference collocated with the ASME 2012 Fluids Engineering Division Summer Meeting and the ASME 2012 10th International Conference on Nanochannels, Microchannels, and Minichannels (pp. 1073-1085). American Society of Mechanical Engineers.

Flow 3D Documentation, Release 10.1.0 (2012). Flow Science, Inc.

Flow 3D Lecture Notes (2013). Hydraulics Training Class.

Flow 3D, Advanced Hydraulics Training, (2013).

Flow 3D, v10.1 User Manuel, (2012).

Hirch, C. (1988). Numerical Computation of Internal and External Flows, Volume 1: Fundamentals of Numerical Discretization.

Hirt, C.W. and Nichols, B.D. (1981). Volume of Fluid (VOF) Method for the Dynamics of Free Boundaries. Journal of Computational Physics 39, 201.

Launder, B.E., Spalding, D.B. (1972). Lectures in Mathematical Models of Turbulence. Academic Press, London, England.

Markatos, N.C. (1986). The Mathematical Modelling of Turbulent Flows. Applied Mathematical Modelling, 10(3), 190-220.

MIT Notes on 1.63 Advanced Environmental Fluid Mechanics. Instructor: C. C. Mei, September 19, 2002 1-9Sca-sim.tex

Nguyen, C. (2005). Turbulence Modeling. MIT Notes (http://www.mit.edu/~cuongng/Site/Publication_files/TurbulenceModeling_04 NOV05).

Onüçyıldız, M., Abdulmohsın, M. S., Büyükkaracığan, N. (2016). Fırat-Dicle Havzası ve Irak Su Yapıları. Selçuk Üniversitesi, Sosyal ve Teknik Araştırmalar Dergisi, Sayı:12,2016, ss. 118-151.

Potter, M.C., Wiggert, D.C., Hondzo, M., Shih T. I-P. (2012). Mechanics of Fluids 3rd Edition. Brooks/Cole, USA.

Rene Garcia, P.E. (2016). Hydraulic Design Manual. Texas Department of Transportation (TxDOT).

Schlichting, H. (1979). Boundary Layer Theory, ISBN 0-07-055334-3, 7th Edition.

Sreelash, K., Mudgal B.V. (2010). Drag Characteristics of Cylindrical Piers with Slots and/or Collars in Subcritical Flow. Journal of Hydraulic Engineering, ISH, 16(2), 75-87

Suribabu, C.R., Sabarish R. M., Narasimhan, R., and Chandhru, A.R. (2011). Backwater Rise and Drag Characteristics of Bridge Piers Under Sub-Critical Flow Conditions. European Water 36: 27-35, E.W. Publications.

Tulimilli, B. R., Majumdar, P., Kostic, M., and Lottes, S (2010). Development of CFD Simulation for 3-D Flooding Flow and Scouring Around a Bridge Structure.

Tănase, N.O., Broboană, D., Bălan, C. (2014). Free Surface Flow in Vicinity of An Immersed Cylinder. Politehnica University of Bucharest, Hydraulic Department, Reorom Laboratory, Romania.

Valiliği, D. (2016). Diyarbakir Valiliği Kültür Turizm Birimi.

Versteeg, H.K., Malalasekera W. (1995). An Introduction to Computational Fluid Dynamics The Finite Volume Method. Longman Scientific and Technical, England.

Versteeg, H.K., Malalasekera, W. (2007). An Introduction to Computational Fluid Dynamics The Finite Volume Method, Second Edition.

Yakhot, V. S. A. S. T. B. C. G., Orszag, S. A., Thangam, S., Gatski, T. B., and Speziale, C. G. (1992). Development of Turbulence Models for Shear Flows by a Double Expansion Technique. Physics of Fluids A: Fluid Dynamics (1989-1993), 4(7), 1510-1520.

Yarnell, D.L. (1934). Bridge Piers as Channel Obstructions. Technical Bulletin, U.S. Dept. Of Agriculture, 442-451.

Zevenbergen, L.W., Arneson, L.A., Hunt, J.H., Miller, A.C. (2012). Hydraulic Design of Safe Bridges. Publication No. FHWA- HIF-12-018, Hydraulic Design Series Number 7, U.S. Department of Transportation, Federal Highway Administration.